

SOLAR-POWERED STEAM GENERATOR HELIOSTAT

FINAL REPORT

J.G. Cottingham
Principal Investigator



December 1978

ACCELERATOR DEPARTMENT

BROOKHAVEN NATIONAL LABORATORY
ASSOCIATED UNIVERSITIES, INC.

UNDER CONTRACT NO. EY-76-C-02-0016 WITH THE
UNITED STATES DEPARTMENT OF ENERGY

BNL 50974
UC-62
(Solar Thermal - TID-4500)

SOLAR-POWERED STEAM GENERATOR HELIOSTAT

FINAL REPORT

**J.G. Cottingham
Principal Investigator**

December 1978

ACCELERATOR DEPARTMENT

**BROOKHAVEN NATIONAL LABORATORY
UPTON, NEW YORK 11973**

NOTICE

This report was prepared as an account of work sponsored by the United States Government. Neither the United States nor the United States Department of Energy (DOE), nor any of their employees, nor any of their contractors, subcontractors, or their employees, makes any warranty, express or implied, or assumes any legal liability or responsibility for the accuracy, completeness or usefulness of any information, apparatus, product or process disclosed, or represents that its use would not infringe privately owned rights.

Printed in the United States of America
Available from
National Technical Information Service
U.S. Department of Commerce
5285 Port Royal Road
Springfield, VA 22161
Price: Printed Copy \$7.25; Microfiche \$3.00
May 1979 375 copies

ABSTRACT

A small-size central-receiver-type solar energy collecting system delivering commercial grade steam is analyzed and a wind avoidance type heliostat designed, built, and successfully tested. The heliostat design effort is described, including reflecting surface materials and measurements, optic considerations and mirror field arrangements, mechanical analysis and fabrication techniques, and economics and cost effectiveness. Measurements of normal incident solar energy at Upton, N.Y., are reported and a method is proposed for estimating this input parameter for other locations proposed.

CONTENTS

<u>Section</u>		<u>Page</u>
I	Introduction	1
II	Heliostat Parameter List	6
	II.A. Parameter List	6
	II.B. Design Error Budget	7
III	Heliostat Design Consideration	8
	III.A. Wind	8
	III.B. Loading	8
	III.C. Mirror Panel Deflection	14
	III.D. Mirror Construction	28
	III.E. Reflecting Specularity	55
	III.F. Mirror Focusing - Facet Shimming	57
	III.G. Motion Control	59
	III.H. Heliostat Assembly	67
IV	Heliostat Performance Thermal Energy Collection	79
V	Reflecting Film Development	83
	V.A. Why Plastic Reflecting Film?	83
	V.B. Reflectivity and Weatherability - Dunmore Subcontract	84
VI	Wind-Solar Insolation Studies	92
	VI.A. Analysis	92
	VI.B. Wind Gusts	94
	VI.C. Operational Scenario	97
VII	Heliostat Optics and Field Configuration	98
VIII	Normal Incident Solar Radiation Measurement	105
IX	Heliostat Production Cost Analysis-- Westinghouse Report	120
X	System Cost and Payback	128
XI	Conclusions and Recommendations	132
XII	Project Personnel	135

ILLUSTRATIONS

<u>Figure</u>		<u>Page</u>
1	Artist concept of roof mounted "power-tower" solar energy collector	2
2	Heliostat design used in motion study	10
3	Heliostat prototype design, side and plan view	16
4	Heliostat dish design	17
5	Drive platform assembly	18
6	Heliostat model, up position	19
7	Heliostat model - folding action	19
8	Heliostat model - stowed position	20
9	Lightweight plastic mirror assembly symmetrical package	22
10	Lightweight plastic mirror assembly symmetrical package, with kraft paper	22
11	Lightweight plastic mirror assembly with Micarta	23
12	Lightweight plastic mirror assembly asymmetrical package	23
13	Deflection test	23
14	Deflection test results	24
15	Computer derived specularity nomograph, copied from Sandia Report SAND-76-5310 by Richard Pettit	56
16	Laser alignment scheme	58
17	Screen from which correction shim values are read during laser alignment	60
18	Laser optical bench showing central alignment procedure	61
19	View looking over the top of laser gun	62
20	Heliostat undergoing laser alignment with only one row of reflecting facets in place	63
21	View of laser optical bench from behind the partially faceted heliostat dish	64
22	Fully faceted heliostat dish undergoing laser alignment, front view	65
23	Rear view of heliostat dish in laser alignment facility	66
24	Bent tubing and U-shaped pieces that form heliostat dish truss assembly	68
25	Heliostat dish support structure	68
26	Heliostat footings	70

ILLUSTRATIONS (continued)

<u>Figure</u>		<u>Page</u>
27	Heliostat base frame	70
28	Heliostat roller assembly	71
29	Rear station stanchion of heliostat assembly	71
30	Movable stanchion of heliostat assembly	72
31	Wedge pivot structure of heliostat assembly	73
32	Heliostat undergoing field assembly - half dish in place on temporary plywood surface	73
33	Field erection - second half of dish moving into place	74
34	Field assembly of heliostat dish - two halves being bolted back together	74
35	Heliostat prototype in face down wind avoidance position	75
36	Heliostat with development team	75
37	Heliostat in working altitude	76
38	Heliostat prototype, front view	77
39	Heliostat prototype in the full up position	78
40	Receiver energy correction characteristic	80
41	Heliostat performance confirmation experimental results	82
42	Reflectivity characteristic of Dunmore film 393	87
43	Reflectivity spectrum for Dunmore material 393 before and after exposure to ultra violet radiation	91
44	Wind-Solar insolation correlation for Upton, NY	93
45	Location of cities chosen for wind-solar insolation study	93
46	Wind-solar insolation history	95
47	Wind-solar insolation history continued	95
48	Wind gust record Upton, NY, and Brookhaven Airport	96
49	Heliostat field performance chart - 51 units design	100
50	Heliostat field performance chart - 53 unit design	101
51	Heliostat field performance chart - 55 unit design	102
52	\bar{K}_H , the ratio of daily average radiation measured on a horizontal surface to that received outside the atmosphere, versus time	107
53	Solar radiation measured on a horizontal surface at Upton, NY, report by various authors and time periods	107

ILLUSTRATIONS (continued)

<u>Figure</u>		<u>Page</u>
54	Measures values of \bar{K}_H versus \bar{K}_L grouped into bins and averaged for Upton, NY, 6/77 through 6/78 with least squares fit polynomial of 3rd order	108
55	Daily values of \bar{K}_H and \bar{K}_L plotted against fit polynomial from Figure 3.	108
56	Curve fit versus data from January 1978	112
57	Curve fit versus data from March 1977	113
58	Curve fit versus data from June 1977 and 1978	113
59	Curve fit versus data from September 1977	114
60	Weighted \bar{K}_H occurrence frequency for Upton, NY, for time period 1950-58 and 1970-78	116
61	Long term weighted \bar{K}_H occurrence frequency for Boston, MA; New York, NY; Sterling, VA; Charleston, SC	116
62	Computed annual normal incident solar radiation received at Upton, NY	118
63	Computed annual normal incident solar radiation received at Greensboro, NC	118
64	Computed annual normal incident solar radiation received at Cape Hatteras, NC	119
65	Computed annual normal incident solar radiation received New York, NY	119

SECTION I
INTRODUCTION

For many years the "flat-plate" solar energy collector has been studied as the collector of choice for building heating and cooling systems. Special absorption-type air conditioning capable of operating with the low temperature thermal output of this collector is being evaluated. Many experiments are underway and others are planned.

The flat-plate collector has economic drawbacks. Its high unit-area cost has made it uneconomical in today's market when seasonal heating is the only load and its low temperature output has made it a difficult energy source to adapt for cooling. Clearly a less expensive, higher temperature solar collector system is desirable.

A concentrating type of solar energy collector has the possibility of fulfilling both the above requirements. Higher temperatures are easily obtained and reflective surfaces have the potential of being inexpensive on a unit area basis. What is required is the development of a concentrating collection system that preserves these advantages.

The central tower collector configuration is proposed and is shown in Figure 1. This type of collector can become economically competitive if suitably developed, and has many technical and economic advantages:

1. More energy is collected per unit area of collector. The projection of a unit area of mirror normal to the incoming solar ray is greater when averaged over the day than that of any stationary or trough-type collector. This advantage outweighs the loss of the diffuse solar radiation.

2. The net energy collection efficiency is very high because of the large concentration ratio. The area from which energy can escape by radiation and convection is much smaller than the area from which energy is collected.

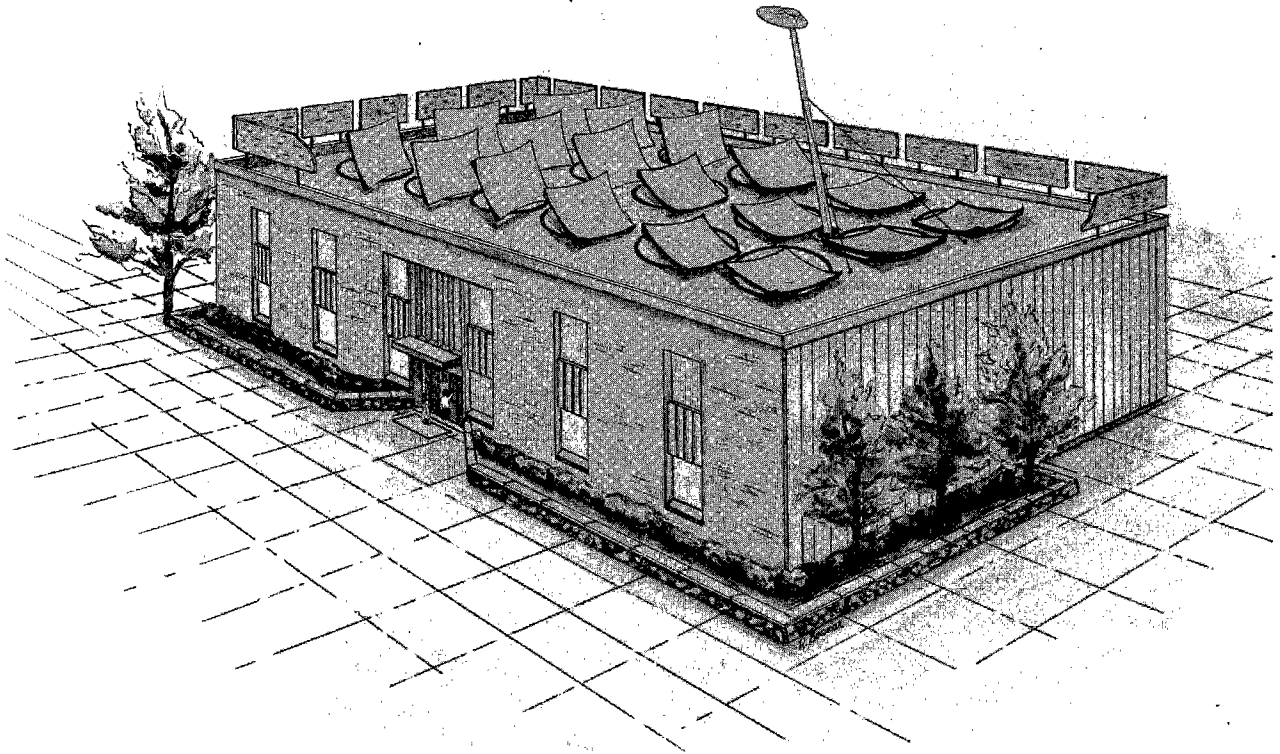


Figure 1. Artist concept of roof mounted
"power-tower" solar energy collector.

3. Cooling loads can be handled with good efficiency and without special cooling equipment. Steam at 125 psig (350°F) can easily be generated and fed to existing one- or two-stage absorption-type chillers.

4. If the collector system is sized to act as an energy supplement to the building rather than to assume the whole load, the cost of energy storage can be avoided.

5. The production cost per unit area of this type of collector should be less than that of other collectors. Less material is required per unit area of reflector than is needed for the flat-plate collector. The cost of the motion mechanism can be minimized by proper use of modern production methods and of the newly developed microprocessor-type computer control.

Solar energy has to date made little impact as an energy source in the world because it has been unable to compete favorably with the costs of other energy sources. If this competitive barrier is penetrated in a form that yields operational cost savings for the user and profit for the solar equipment manufacturer, energy derived from the sun would take its place as a viable energy source.

The solar steam supplement concept is specifically designed to penetrate this competitive barrier in the high energy cost areas of the Northeastern parts of the U.S. Solar energy is captured with a minimum of hardware which is mass producible and in a form compatible with the existing heating and cooling technology of the area. Steam has long been a mode of distributing thermal energy in the Northeast, thus the retrofit market as well as the new construction market is opened to solar energy.

Solar energy collecting systems will first become economically feasible in parts of the country where the product of solar insolation and fuel costs are at a maximum. At the present time, this maximum occurs along the metropolitan Northeastern Seaboard of the U.S. where fuel costs have risen dramatically.

Much of the oil imported into the U.S. is consumed in the Northeast. If solar energy were aggressively and competitively introduced in this region of the country, partly displacing the consumption of oil, it would favorably influence our balance of trade with foreign nations and create an improved, independent atmosphere for international relations.

Solar energy is more abundant in the summer months when building energy loads are dominantly for cooling. If a solar energy collector system is to be competitive with other energy sources, it must handle this cooling load efficiently. Here is where the "power-tower" collector is most effective. The high energy-concentration ratio easily obtained by this configuration generates high temperature (350°F) steam. This high temperature steam can be fed to existing one- or two-stage absorption chillers of conventional design which deliver air conditioning with an excellent coefficient of performance.

The power tower type collector configuration has been widely studied with most of the effort directed toward the generation of electric power on a utility scale. But this efficient collector configuration has many other applications, of which some are easier to engineer and some may be more readily accepted or accepted at an earlier date in a cost-competitive market. All applications must be carefully investigated. The following is a brief list of some of these additional applications for the power-tower collector configuration.

APPLICATIONS

1. Building heating and cooling
 - a. Cluster residential
 - b. Commercial
 - c. Institutional
2. Process heat (300° to 1000°F)
3. Generation of electric power
 - a. Community size
 - b. Institutional size
 - c. Energy feed to photovoltaic arrays

What are the dominant cost factors in the power-tower-type collector? The cost of the field of heliostats represents approximately 70% of the total system cost. It is this cost that must be carefully controlled and reduced to an acceptable value. Wind, more than any other consideration, influences the heliostat cost. Without the wind the heliostat could be nothing more than a wire-supported reflecting foil.

To minimize heliostat costs, Brookhaven has chosen a wind-avoidance concept with a fold-down design which allows the heliostat to be exposed to the wind only under favorable conditions. Energy is lost by folding the heliostats down during sunny, windy hours, but analysis will show that this loss is acceptable. If the heliostats were folded down during all hours when wind speeds are above 15 mph, only 5% of the available solar energy at Upton would be lost. However, the wind-insolation history for other locations is more demanding. Heliostats marketed in the plains states must be designed for higher wind speeds. The heliostat prototype built at Brookhaven has a 20-mph design criterion.

To permit a lightweight support structure the reflecting skin of the heliostat must flex, otherwise a rigid and costly back structure is required. Glass which can be made to flex, if laminated from thin sheets, does not naturally lend itself to this requirement. A good reflecting plastic film would be ideal in this application, if it can be developed.

There are two problems in using reflecting plastic films; specularly and weatherability. Films when bonded to supporting structures often lose clarity and show waves and other small defects. These defects all work to reduce the specular quality of the surface. The development of acceptable reflecting film was a major subtask of this project.

SECTION II

HELIOSTAT PARAMETER LIST

The following is a summary list of input parameters used in this development project and output parameters resulting from this work.

II.A. Parameter List

	<u>Ultimate objective</u>	<u>Present design</u>
<u>Heliostat</u>		
Dish diameter	-	16 ft.
Interference circle, adjacent unit	-	19 ft.
Fold down time	10 minutes	15 minutes
Stall protection	Stallable without damage	Stallable without damage
Start up in snow load	Not specified	6 inches
Dish weight, no skin	200 lbs.	220 lbs.
Skin weight	50 lbs.	75 lbs.
Mechanism weight	850 lbs.	1200 lbs.
Total weight	1100 lbs.	1500 lbs.
<u>Wind</u>		
Image on target	25 mph	20 mph
Wind damage	50 mph	50 mph
<u>Reflectivity</u>		
Coefficient of re- flectivity, solar spectrum	88%	84%
Specularity	0.75 mrad	0.75 mrad
Weatherability	20 years	6 years
<u>Field Design</u>		
<u>Shadowing:</u>		
Worst heliostat		83% annual
Field average, yearly		92% annual
<u>Off-axis optics:</u>		
Field average, yearly		88% annual
<u>Combined shadowing/off-axis and optics efficiency:</u>		
Worst heliostat		66%
Field average, yearly		76%
<u>Current heliostat field design:</u>		
Heliostats		55
Area/heliostat		201 ft ²
Total reflecting area		11055 ft ²
Field area		25,519 ft. ²
Packing factor:		43%

II.B. Design Error Budget

	<u>North corner</u>	<u>Mean</u>
Distance to target	165 ft.	85 ft.
Target size	5 ft. dia.	5 ft. dia.
Aiming precision, total (half-angle)	15.1 mrad	35.0 mrad
	<u>Ultimate objective (half angle)</u>	<u>Present design (half angle)</u>
Reflecting surface specularity	0.75 mrad	0.75 mrad
Skin support flexure with wind	1.5	2.0
Dish flexure	2.0	3.0
Mechanical support flexure	3.0	5.0
Total flexure	7.25 mrad	10.75 mrad
Rms flexure	4.0	6.3
Angle transducer error	1.5	3.0
Digital step	.5	1.5
Total errors	6.0	10.8
Solar width	5.2	5.2
Total (rms-sum)	10.8 mrad	16.1 mrad
Available for off-axis distortion:		
Mean heliostat	24.2 mrad	18.9 mrad
North corner heliostat	4.3	(-1.0)

5'

165

SECTION III
HELIOSTAT DESIGN CONSIDERATION

The design and parameter choices used in this development were influenced by various design considerations. The following is a description of that design process.

III.A. Wind

The action of the wind on the heliostat and its effect on the heliostat design are the major factors governing heliostat costs. If there were no wind, a heliostat could be a simple wire structure covered with reflecting plastic film. Wind loads cause the heliostat disk and support structure to flex, moving the image off-target. To hold the required aiming accuracy, the heliostat must be designed to have the necessary structural strength to withstand specified wind loads. Material added to the disk and upper parts to accommodate increased wind forces in turn increases the load to be carried by the lower supports. This is an amplifying process increasing the material weight and ultimately the production cost.

To produce a lightweight design, it was decided to employ a wind-avoidance concept in which the heliostat was to be folded facedown out of the wind during hours of high wind speed. By so doing, a low wind-speed deflection criterion could be used which would result in material and cost savings.

To test this concept and develop the operational and design requirement the Meteorology Group at Brookhaven was asked to address Wind-Solar Insolation records. The results of this analysis were to determine the heliostat wind speed design criteria and its operation scenario. Favorable results were obtained and are reported in Section VI.

III.B. Loading

The wind-insolation analysis reported in Section VI shows that the heliostat need be operated only during time periods with winds below moderate velocities. This presented an opportunity to cut costs by designing a lightweight support structure.

A motion study of the concept was conducted. The purpose of this study was to proportion the linkage mechanism, locate the pivot points, etc.

Three conditions were considered, as follows:

1. Loading produced by mirrors only (i.e., no wind and no snow).
2. Loading produced by mirror carrying 6 inches of snow up to the vertical position (no wind).
3. Loading produced by mirror with no snow resisting a 50-mph wind force.

Figure 2 shows the pivot point location optimized as a result of this motion study. Tables III.1 to III.3 summarize the forces that result in the optimized configuration.

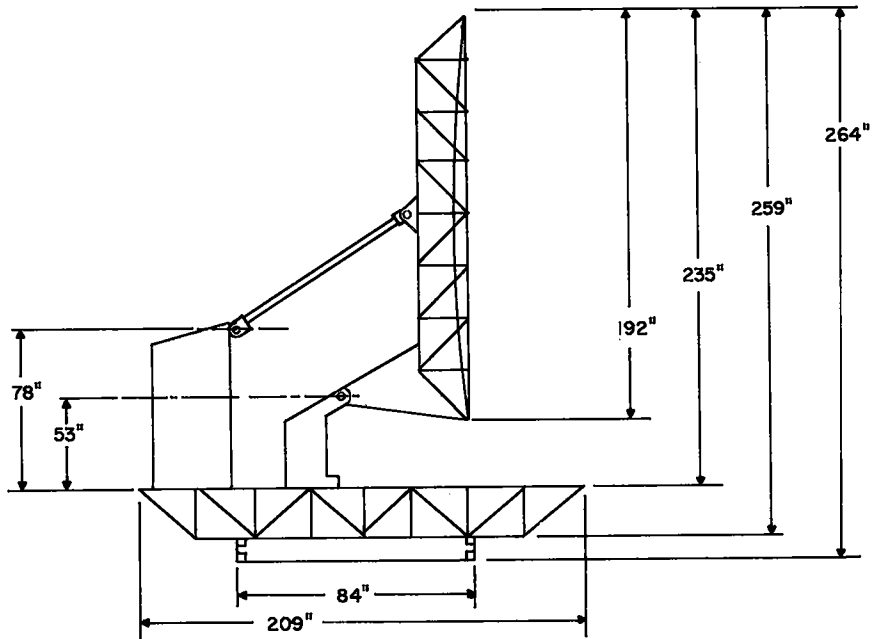


Figure 2. Heliostat design used in motion study.

Table III.1

Condition of Loading: Mirror Weight Only

<u>Mirror Position, degrees</u>	<u>Link Load, lb</u>	<u>Mirror Load, lb</u>	<u>Rider Load, lb</u>
0	1280 T	1045 C	+ 1001
10	1399 T	1250 C	+ 1242
20	1416 T	1357 C	+ 1354
30	1372 T	1400 C	+ 1362
33°-10'	1339 T	1393 C	+ 1335
35	1317 T	1386 C	+ 1315
40	1244 T	1355 C	+ 1245
45	1158 T	1309 C	+ 1152
60	846 T	1107 C	+ 804
90	228 T	657 C	+ 187
106°-35'	0	500 C	0
115	83 C	455 C	- 116
135	456 C	452 C	- 319
160	529 C	643 C	- 516
170	1587 C	1851 C	- 1656
180	2268 C	2359 C	- 2261

C = Compression.

T = Tension.

+ = Force to the right.

- = Force to the left.

Table III.2

Condition of Loading: Mirror + Link + 6-in.-Thick Snow*

<u>Mirror position, degrees</u>	<u>Link load, lb</u>	<u>Mirror load, lb</u>	<u>Rider load, lb</u>
0	3010 T	2455 C	+ 2353
10	3287 T	2938 C	+ 2919
20	3328 T	3188 C	+ 3182
30	3226 T	3289 C	+ 3200
30°-10'	3147 T	3274 C	+ 3138
35	3095 T	3258 C	+ 3091
40	2923 T	3184 C	+ 2922
45	2722 T	3077 C	+ 2706
60	1987 T	2602 C	+ 1890

* Snow density = 6 lb/ft³.

C = Compression.

T = Tension.

+ = Force to the right.

- = Force to the left.

Table III.3

Condition of Loading: Mirror Weight + Link + Wind*

Mirror position, degrees	Total pressure on mirror, lb	Link load, lb	Mirror load, lb	Rider load, lb
0	0	1280 T	1045 C	+ 1001
10	343	2325 T	2018 C	+ 2005
20	623	3138 T	2792 C	+ 2787
30	814	3575 T	3227 C	+ 3138
33°-10'	857	3635 T	3293 C	+ 3156
35	878	3652 T	3314 C	+ 3144
40	914	3618 T	3301 C	+ 3029
45	960	3566 T	3260 C	+ 2867
60	1007	2010 T	1564 C	+ 1136
90	1020	1343 C	282 C	- 80
106°-35'	1017	1228 C	43 C	0
115	1014	1187 C	221 C	- 33
135	960	1158 C	774 C	- 368
160	623	1316 C	1333 C	- 1070
180	0	See Cond.I	See Cond.I	

*Calculations assume wind at 50 miles/hour blowing above the mirror. For the condition in which wind at the same velocity blows below the mirror, the maximum normal pressure is 1.70 times the pressure on the mirror at 90° and acts to raise the mirror rather than depress it.

C = Compression.

T = Tension.

+ = Force to the right.

- = Force to the left.

Using the worst case loads taken from these tables and the allowable deflection assigned via the Design Error Budget (see II.B), an engineering design was developed. The resulting support structure design is shown in Figures 3, 4, and 5.

To aid the design activity, a table model of the heliostat was built and studied. Views of this model are shown in Figures 6, 7, and 8.

III.C. Mirror Panel Deflection

The mirror dish support structure gives edge support to the reflecting mirror facets. Wind forces on these mirror facets will cause the individual facet to alter its focal length and the mechanical strength of the mirror facet must be sufficient to hold this focal length change within limits.

The largest unsupported area in the reflecting dish structure is a set of trapezoidal-shaped regions near the outer edge. For deflection computation, the shape of this region will be approximated by a rectangle measuring 32 x 42 inches.

Using the 2-mrad allowable angular deflection assigned in the Error Budget (II.B) for the reflecting skin, the central displacement (y_m) can be computed.

$$2 y_m = \alpha \times \frac{d}{2} ,$$

where

y_m = central displacement,

α = maximum angular deflection allowed, 2 milliradians,

d = small side of rectangle = 32 inches.

Therefore, $y_m = 16 \times 10^{-3}$ inches.

The equation for deflection of an edge-supported rectangular sheet is given in Mark's Mechanical Engineering Handbook, pp. 5-67, 69, as:

$$y_m = \frac{k_1 w r^4}{Et^3} ,$$

where

$k_1 = 0.0705$ - Mark's handbook, reference above,

w = uniform pressure, psi,

r = smaller side of rectangle,

t = thickness,

E = Young's modulus.

Imposing the following set of parameters, the stiffness quantity Et^3 can be computed:

$$k_1 = 0.0705,$$

$$w = 1.11 \text{ lb/ft}^2 = 7.7 \times 10^{-3} \text{ psi (pressure of wind at 20 mph),}$$

$$r = 32 \text{ inches,}$$

$$y_m = 16 \times 10^{-3} \text{ inches.}$$

Therefore,

$$Et^3 = 3.5 \times 10^4.$$

This quantity is a measure of panel stiffness against which test samples can be measured in a simple point loaded beam test. Deflection of this simple beam is given by

$$f = \frac{Wl^2}{48 EI},$$

where

W = point load, lb,

l = length between supports,

E = Young's modulus,

f = deflection;

and

$$I = \frac{bt^3}{12},$$

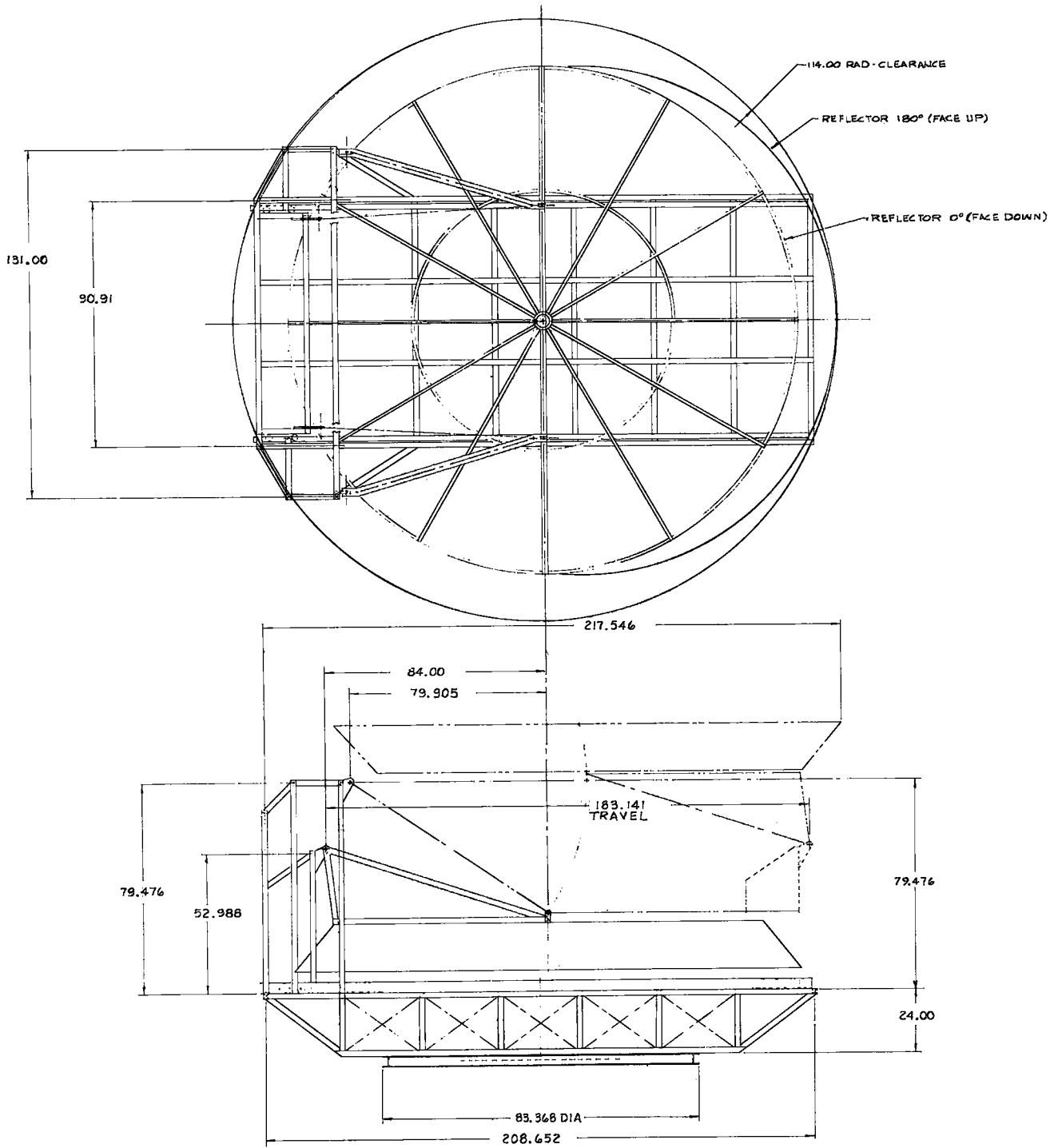
where

b = width of test piece,

t = thickness.

From the above we derive

$$\frac{f}{w} = \frac{l^3}{4b(Et^3)}.$$



BROOKHAVEN NATIONAL LABORATORY
ASSOCIATED UNIVERSITIES, INC.
UPTON, N. Y. 11973
HELIOSTAT
16' DIAMETER
STRUCTURAL CONCEPT

Figure 3. Heliostat prototype design, side and plan view.

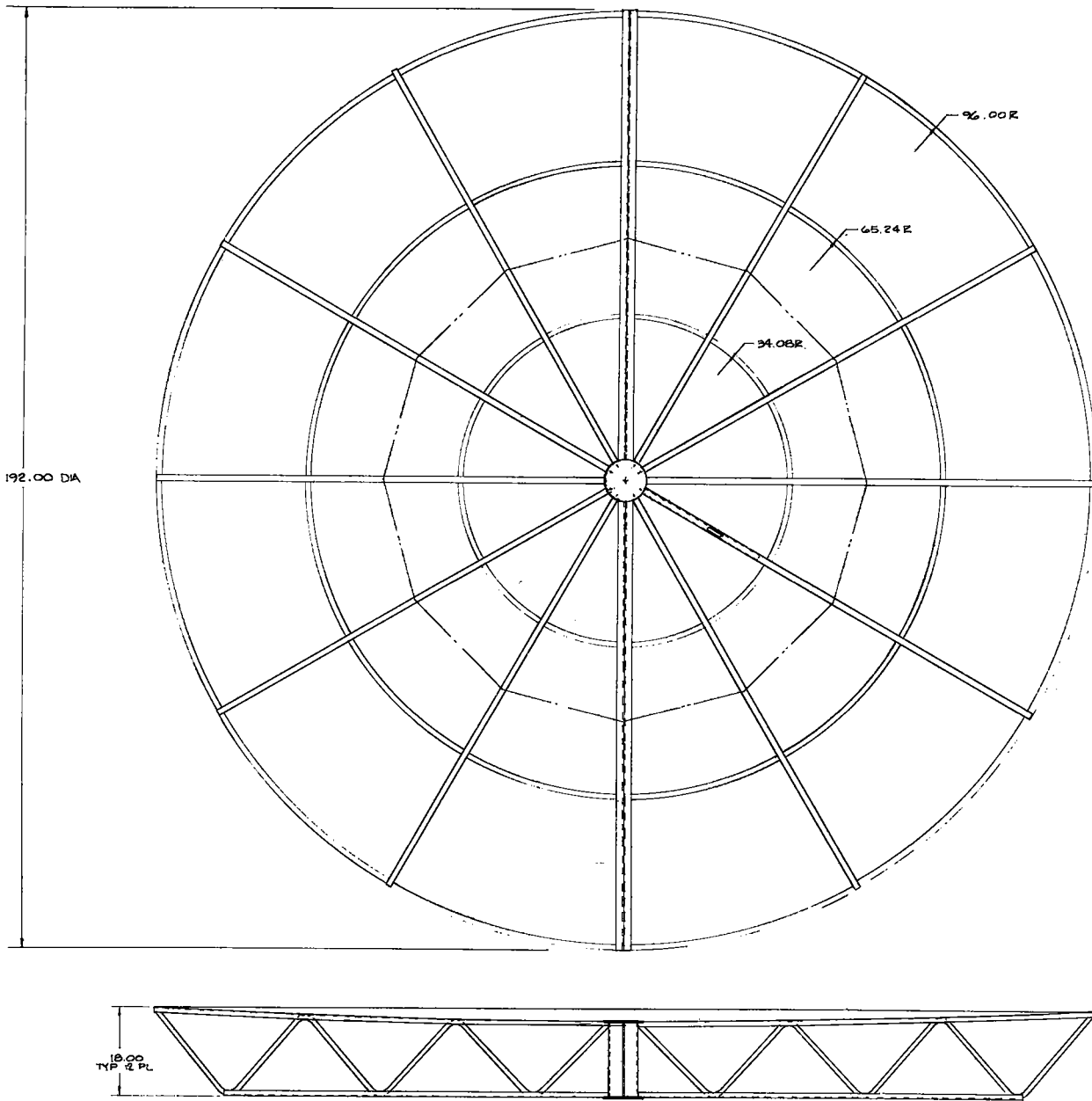


Figure 4. Heliostat dish design.

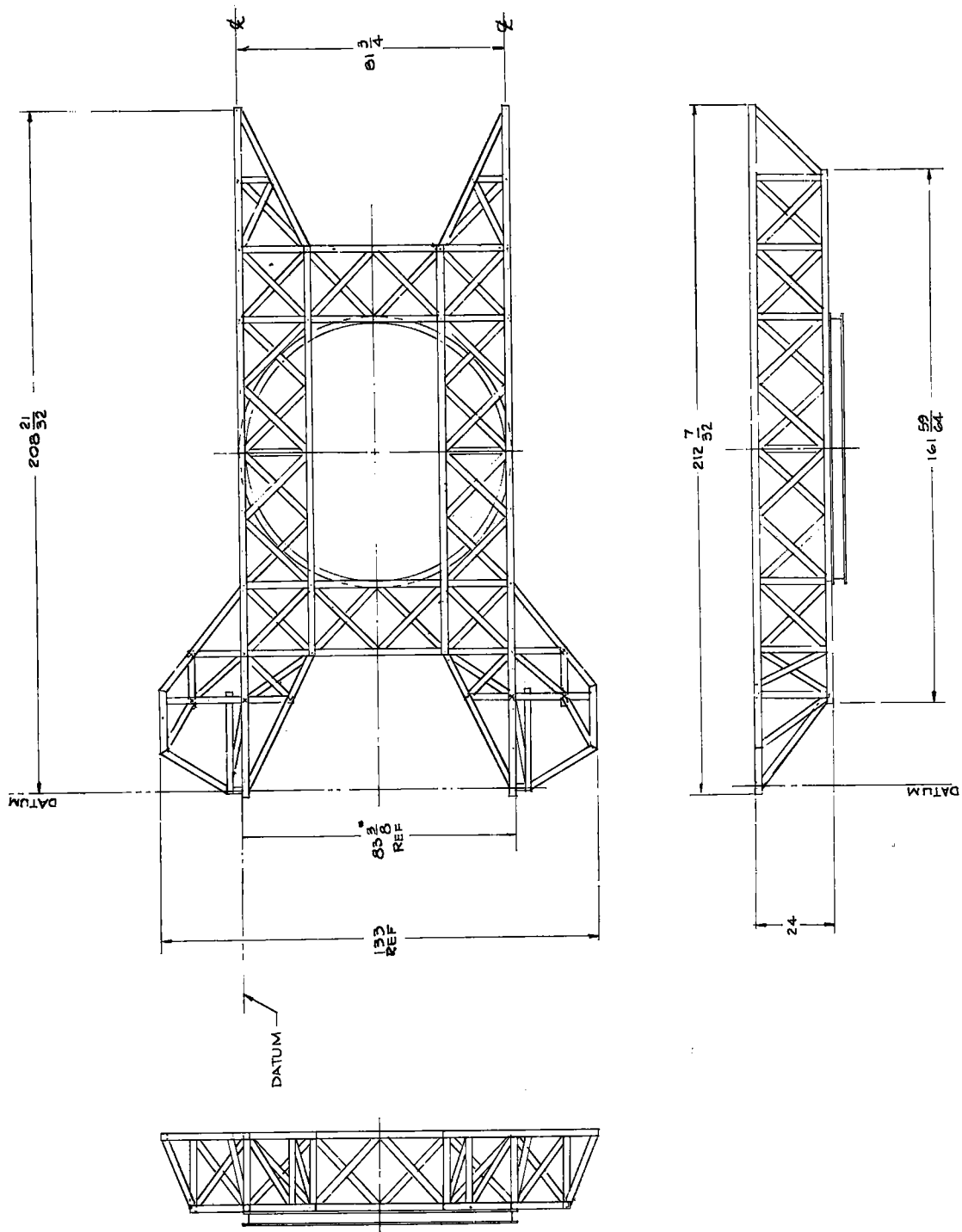


Figure 5. Drive platform assembly.

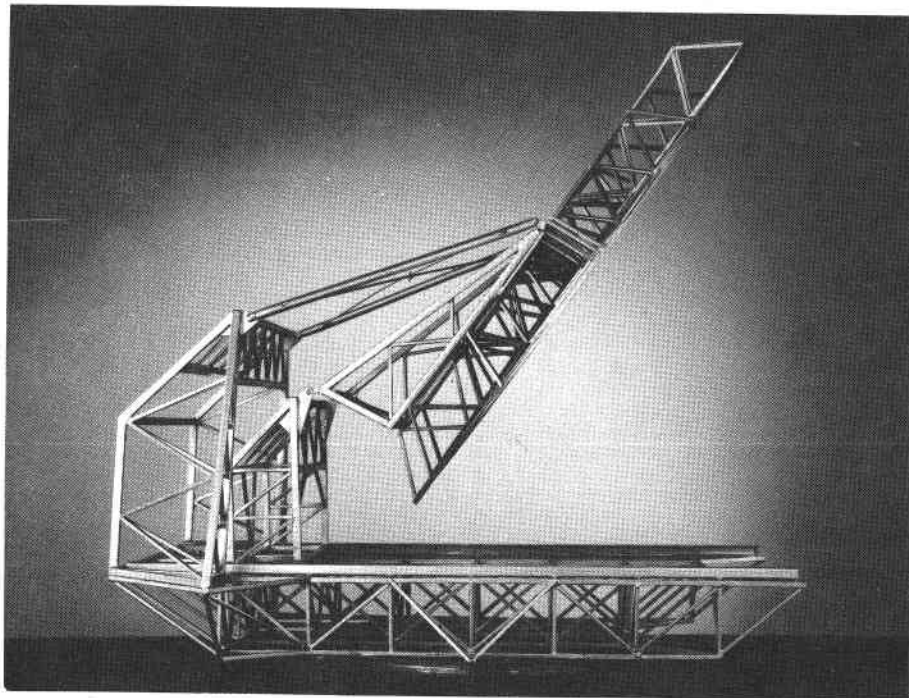
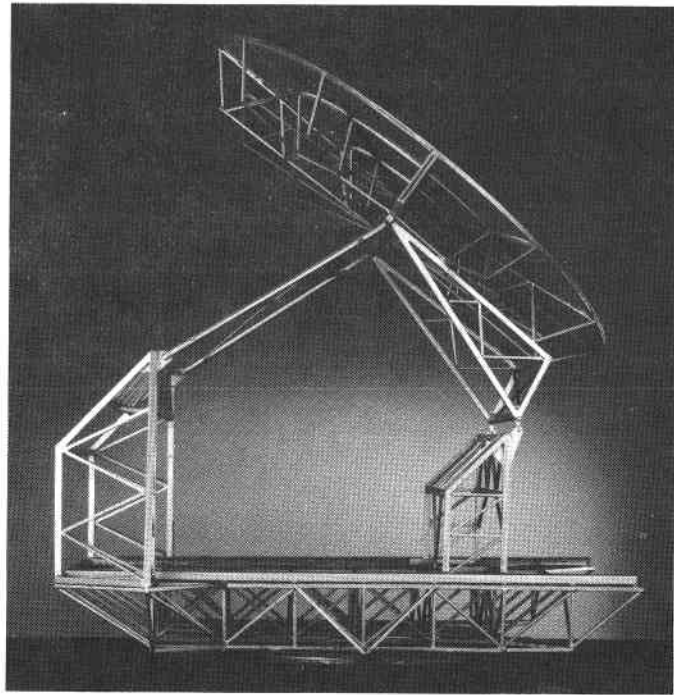


Figure 7. Heliostat model - folding action.

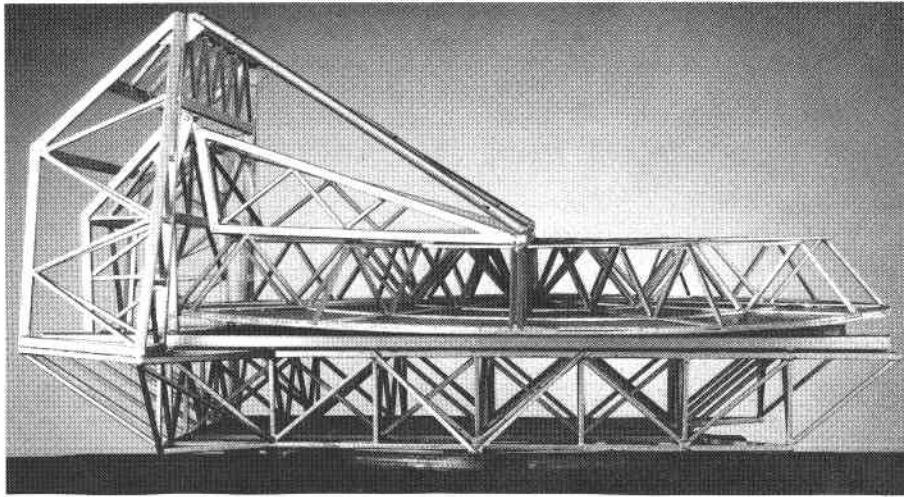


Figure 8. Heliostat model - stowed position.

Setting standard test conditions as follows,

$l = 12$ inches,

$b = 12$ inches,

the deflection/force relationship becomes

$$\frac{f}{w} = \frac{36}{Et^3} \cdot$$

Inserting the previously determined value of Et^3 of 3.5×10^4 , we get

$$f/w = 1.03 \times 10^{-3} \text{ in./lb or } 1.13 \times 10^{-3} \text{ in./500 g}$$

for the elastic deflection of the chosen test samples.

A series of test support packages were assembled and deflection tests made. The interesting candidates from this set are shown in Figures 9 through 12.

These samples were subjected to a simple beam deflection test described above and shown in Figure 13. The deflection was measured with a dial gauge and weights were used to supply the test force. The force was cycled several times and a mean deflection determined.

A force deflection curve was plotted and results were smoothed. Typical results are shown in Figure 14.

A listing of all samples tested and a brief statement of results follow.

1. Sample "A"

Weight is 222.5 grams, size is $12\text{-}7/8 \times 12\text{-}7/8\text{-in.}$ Constructed of 0.013 aluminum on both sides of $1/2\text{-in.}$ Styrofoam. Epoxy mixture was Epon 815 resin and V40 curing agent $2/3$ to $1/3$, respectively. Average deflection at 500 grams is 0.016 inches.

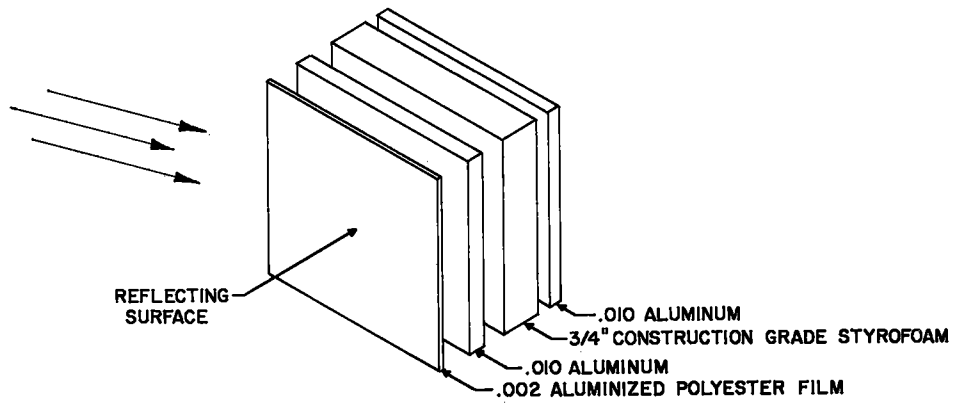


Figure 9. Lightweight plastic mirror assembly symmetrical package.

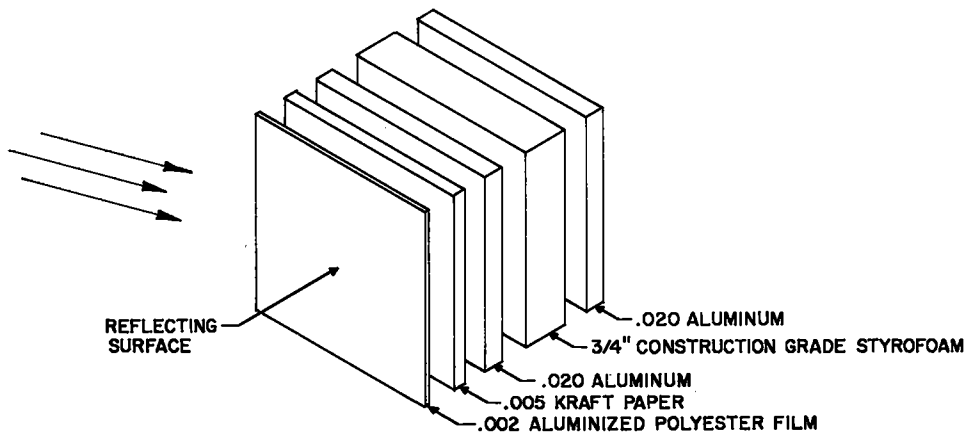


Figure 10. Lightweight plastic mirror assembly symmetrical package, with kraft paper.

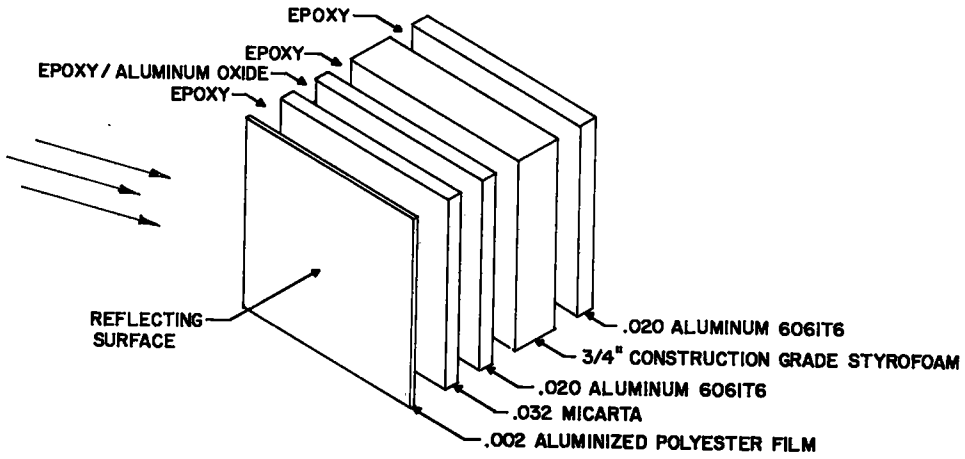


Figure 11. Lightweight plastic mirror assembly with Micarta.

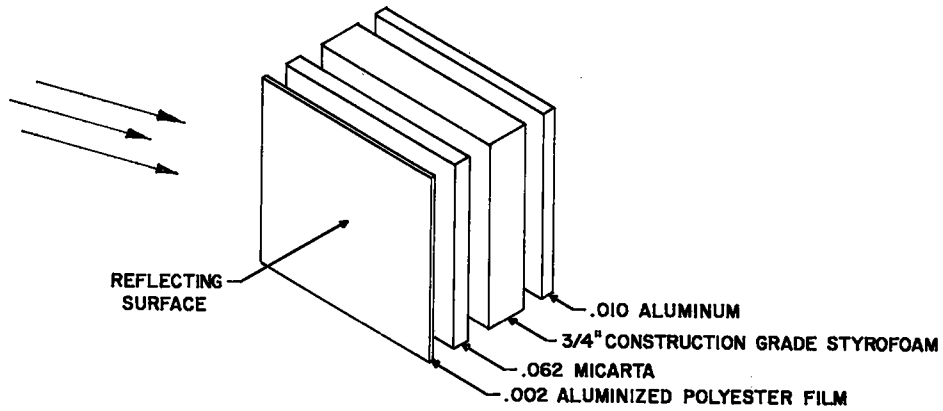


Figure 12. Lightweight plastic mirror assembly asymmetrical package.

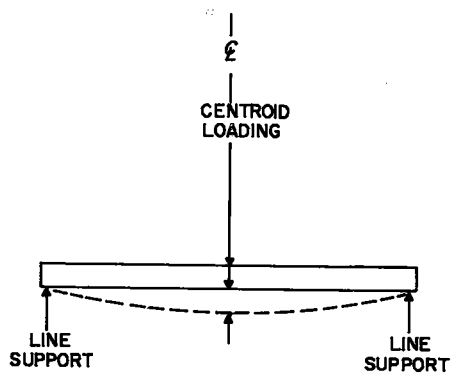


Figure 13. Deflection test.

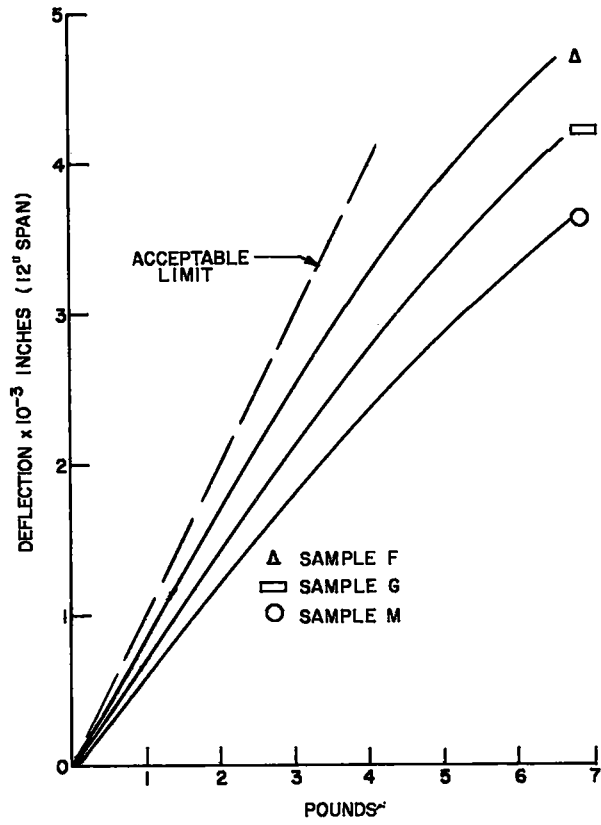


Figure 14. Deflection test results.

2. Sample "B"

Weight is 115 grams, size is 14 x 10 in. Constructed of 1-1/2-in. fiber glass strips bonded to both sides of 1/2-in. Styrofoam with 815 resin and V40 curing agent mixed 60 parts to 40 parts, respectively. Average deflection at 500 grams is 0.0037 inches.

3. Sample "C"

Weight is 141 grams, size is 8 x 12 in. Constructed of 0.005 stainless steel on both sides of 1/2-in. Styrofoam. Epoxy was Epon 815 resin and Epon V40 curing agent. Mixture was 2/3 to 1/3, respectively. Average deflection at 500 grams is 0.0027 inches.

4. Sample "D"

Weight is 74 grams, size is 6 x 14 in. Constructed of 0.013 aluminum on both sides of construction type Styrofoam. Bonded with Epon 815 resin and V40 curing agent with a mixture of 3 parts to 1 part, respectively. Average deflection at 500 grams is 0.0045 inches.

5. Sample "F"

Weight is 286.7 grams, size is 14 x 12 in. Constructed of 0.010 aluminum on both sides of 3/4-in. Styrofoam. Bonded with Epon 815 resin and Epon V40 curing agent mixture of 50/50 with 30% amorphous silica filler added. Average deflection at 500 grams is 0.0018 inches.

6. Sample "G"

Weight is 354 grams, size is 12 x 12 in. Constructed of 3/4-in. Styrofoam with 0.010 aluminum on one side and 0.062 Micarta on the other side. Bonded with Epon 815 resin and Epon V40 mixed 50/50 parts, no filler added. Average deflection at 500 grams is 0.0009 inches aluminum side up and 0.0011 inches Micarta-side up.

7. Sample "H"

Weight is 419 grams, size is 12 x 12 in. Constructed of 1/2-in. Styrofoam, with 0.010 aluminum on one side and 0.062 Micarta on the other side.

Bonded with Epon 815 resin and V40 curing agent 50/50 parts, 30% amorphous silica added to mixture. Average deflection at 500 grams is 0.0012 inches aluminum-side up and 0.001 inches Micarta side up.

8. Sample "I" - Heat Test Sample

Weight is 410 grams, size 12 x 12 in. Constructed of 0.010 aluminum, 1/2-in. Styrofoam, and 0.062 Micarta. Epoxy mixture was Epon 828 resin and V40 curing agent mixed 50/50. Average deflection at 500 grams is 0.0019 inches aluminum side up and 0.0013 inches Micarta side up.

9. Sample "J" - Heat Test Sample (Same as Sample "G")

Weight is 376.5, size is 12 x 12 in. Constructed of 0.010 aluminum, 3/4-in. Styrofoam, and 0.062 Micarta. Bonded with Epon 828 resin and V40 curing agent mixed 50/50. Average deflection at 500 grams is 0.0013 inches aluminum side up and 0.0008 inches Micarta side up.

10. Sample "K" - Destruction Test Sample (Same as Sample "J")

Weight is 372.5 grams, size is 12 x 12 in. Constructed of 0.010 aluminum, 3/4-in. Styrofoam, and 0.062 Micarta. Bonded with Epon 828 resin and V40 curing agent mixed 50/50. Average deflection at 500 grams is 0.0011 inches aluminum side up and 0.001 inches Micarta side up.

Sample K was subjected to very large forces in an attempt to find its destruction limit. Table III.4 is a record of that test.

11. Sample "L" - Destruction Test Sample (Same as Sample "I")

Weight is 407 grams, size is 12 x 12 in. Constructed of 0.010 aluminum, 1/2-in. Styrofoam, and 0.062 Micarta. Bonded with Epon 828 resin and V40 curing agent mixed 50/50. Average deflection at 500 grams was 0.0014 inches aluminum side up and 0.0016 inches Micarta side up.

12. Sample "M"

Same as "F" except 0.020 aluminum was used. Average deflection at 500 grams is 0.0005 inches.

Table III.4

Sample K (Destruction Test)

Sample was edge supported along two opposing sides spanning a 10-1/2-in. gap. A point load was applied to the center of sample.

<u>Load (lb)</u>	<u>Deflection</u>
25	0.009
50	0.015
75	0.020
100	0.025
125	0.030
150	0.035
175	0.040
200	0.045
225	0.050
250	0.055
275	0.060
300	0.063
325	0.067
350	0.071
375	0.075
400	0.080
425	0.085

Note: At 425 lb, sample did not show any signs of destructing. Test was stopped for safety reasons.

III.D. Mirror Construction

III.D.1. Fabrication Method

A model shop type production method for manufacturing reflecting panels evolved through a trial and error process. This process was developed to produce the limited quantity of panels necessary to equip the prototype heliostat (28 panels) and for associated test and evaluation. A history of each panel manufactured is presented in Section III.D.3. The manufacturing method described is simple and readily adaptable to automation.

The first step in the manufacture of a reflecting panel is accomplished in a nominally dust-free environment since dust particles on the outer surface of the plastic film cause small but noticeable imperfections in the reflecting surface. The amount of energy scattered by these blemishes is small, and in general not measurable, but the aesthetic appearance of the reflecting surface is undesirable. This dust free room is air conditioned for heat removal and is separated from the other work areas by a set of double doors.

The film as it arrives from the manufacturer, Dunmore Corp., is relatively dust free and most of the dust accumulated on the film during handling at Brookhaven is probably due to electrostatic attraction. Minimizing the exposure time of the film surface to the environment is effective in reducing dust-caused blemishes. For this reason the roll of reflecting film is located adjacent to the first tool where it can be rolled out and put down rapidly.

The first tool, work station 1, is a sheet of float glass resting on a flat table. This glass plate forms a surface of optical quality against which the reflecting plastic film is held during the bonding and curing process. In preparation for manufacture this glass surface is carefully cleaned and wetted with a liquid soap solution, 9 parts water to 1 part liquid soap.

The outer or overcoated side of the film, which will become the reflecting surface of the finished product, is placed facedown against the glass tool. The film is then carefully squeegeed to remove the excess soap solution. Care must be exercised in this step to remove all excess soap solution since any remaining unremoved excess will cause a wavy appearance in the finished product.

The liquid soap and water solution serves to hold the film firmly and optically flat against the glass surface during the manufacturing process. After completion of the squeegee operation, the film is trimmed to size. The film and glass plate are lifted from work station 1 and moved to another flat table which forms work station 2. A dam made of Styrofoam strips is placed around the perimeter of the mirror to contain any excess overflow of the liquid epoxy bonding agent. The remaining exposed jig surfaces are now coated with an epoxy release agent to facilitate cleaning and reuse.

An epoxy batch compounded of the following material is prepared.

6.8 parts of number 815 Shell Epon resin	375 grams
2.3 parts of number 871 Shell Epon flexerizer	125 grams
0.9 parts of diethylene-triamine hardener	<u>50 grams</u>
Total	550 grams

This epoxy will be used to bond the next layer of the support panel, a Micarta sheet, to the reflecting film. Care must be exercised to prevent air pockets in this bond, since such pockets will produce sizable defects in the mirror product. The air pockets are eliminated by carefully rolling the Micarta sheet into the bonding material. A coat of the epoxy preparation is brushed onto the film surface still being held facedown against the glass tool by the liquid soap solution. This coat is inspected to insure complete wetting. Excess epoxy mix is poured over the "start edge" of the reflecting film and a precleaned and sanded Micarta sheet brought into contact with the reflecting film along this edge. The remainder of the sheet is temporarily held above the work table curving upward. The excess epoxy should form a void free wedge between the reflecting film and the Micarta sheet, if not, additional epoxy is added to produce this wedge. Once the epoxy wedge is formed, the remainder of the Micarta sheet is rolled down slowly advancing and squeezing the epoxy wedge. Again, care is exercised to avoid trapping air into the wedge. Production tooling with controls on the rolling speed should repeatedly produce a good product. At Brookhaven some product was lost because of entrapped air pockets resulting from use of the hand-controlled procedure. With the Micarta sheet firmly in place, the assembly including the glass tool is moved to work station 3.

Work station 3 is a heavy wooden tablelike structure with a 1/4-inch-thick aluminum top that has been shimmed to have a convexed 300 foot radius of curvature. The glass plate carrying the reflecting film and Micarta sheet is placed on this curved jig glassside down. The weight of the glass and assembly is not yet sufficient to force the glass to conform to the jig curvature but will be forced to do so in a later step. The glass is sufficiently elastic in this thickness (1/4 inch) to conform.

The remaining layers of the support package which have been cleaned and sanded are epoxyed and stacked into place. The removal of air pockets is no longer vital, but reasonable care in workmanship should be exercised. The bonding agent used in assembling these last layers contains in addition to the previously listed ingredients 500 grams of aluminum oxide filler to increase the epoxy strength.

After all elements of this sandwich are in place, an epoxy parting sheet (Teflon) and the jig top plate are laid in place. On this top plate, lead weights are placed in a predetermined pattern. This weight and pattern arrangement is engineered to force the entire assembly, glass, sandwich, top plate, etc. to conform to the convexed jig surface. The assembly is allowed to cure for 24 hours after which the mirror assembly is removed and the tooling recycled.

During the course of development, construction details were varied, sometimes in response to observed difficulty and at other times to test different procedures. A detailed history of this development process is presented in Section III.D.3.

From this trial and error two successful product designs evolved. The process described above and illustrated in Figure 11 yields a mirror with better specularly. The mirror package illustrated in Figure 10 is less costly to manufacture and has adequate specularly (<1 milliradian) for the small tower application studied by Brookhaven. To produce this package, the Micarta sheet is removed and replaced by an epoxy-paper layer. The function of this layer is to buffer the reflecting film from the aluminum sheet. Without

the buffering layer imperfections on the aluminum distort the reflecting surface and impair the specularity.

This epoxy-paper layer is formed by carefully wetting all surfaces with epoxy and placing the paper on the reflecting film surface at work station 2. The next package layer, the 0.020-inch aluminum sheet, must be assembled with the same roll-on technique as previously described for the Micarta sheet. All other manufacturing steps are unchanged.

The final manufacturing operation is the sealing of all mirror panel edges. This is accomplished by routing a small groove along the edge of the Styrofoam adjacent to both of the aluminum layers (front and back) and filling this groove with a caulking compound. The following two compounds have successfully undergone a brief life test consisting of 50 freezing-thawing cycles.

1. Silicon Seal manufactured by the General Electric Corporation.
2. Butyle rubber caulking compound made by DAP Inc. An eight hour curing time is required in both cases.

III.D.2. Problems and Solutions

a. Orange Peel Effect

Occasionally a reflecting surface would appear pock-marked, similar in appearance to the surface of an orange. Two causes of this appearance were identified though there may be others. If excess soap solution was allowed to remain between the plastic film and the glass tool surface, it would form into small pockets and make a permanent imprint on the finished product.

The second cause was traced to temperature changes during the epoxy curing process. This mechanism is not completely understood but the observation is clear. When mirror panels were allowed to cure with temperature variations of less than 3°F, as was the case during the winter months when the heating system was on continuously, no orange peel effect was observed. With the arrival of summer the work area heating system was shut down. This allows temperature variation of from 10° to 20°F and serious orange peel effects were often observed. The heating system was reactivated and the problem solved.

b. Package Asymmetry

The earliest production run made mirror panels which were mechanical asymmetric in that the mechanical strength on one side was provided by an aluminum layer and on the other side by a Micarta layer. Warping or changes in the curvature will occur if these two structural members change dimension relative to each other. Samples were cycled in an oven over a large temperature range and the dimensional changes that resulted were found to be acceptable.

However, changes in curvature were observed with age. The Micarta shortened relative to the aluminum piece. This appears to be the result of a interaction between the epoxy, or its solvents, and the Micarta. The curvature change occurs gradually in the first few weeks and then stabilizes. The magnitude of curvature change was not reproducible, but was larger than could be accepted.

The solution was to insert an aluminum sheet between the Micarta sheet and the Styrofoam body. This aluminum piece became the strong element on this side of the package and stopped the dimensional change that was occurring

c. Bonding Failures

Two types of epoxy bonding failures have been observed and their causes identified.

The first resulted from a manufacturing shortcut intended to relieve a short supply of the epoxy flexerizer. This item was omitted in the epoxy mixture used to bond the back side of the support package. When this material is omitted, the resulting cured epoxy is very hard and a larger force is required to stretch this material to conform to the temperature expansion of the adjacent aluminum sheet. When the force required for this stretch exceeds the bonding strength, failure occurs. All panels from which the flexerizer was omitted failed in service from daily temperature cycling.

The second type of bonding failure is similar but caused by a different procedural change. The specularity of the kraft-paper-type support package, Figure 10, is improved if the epoxy layer containing this paper is made thicker. This layer was made very thick, 1/16 in. in some cases, to yield

excellent specularly. These panels were put into service without environmental testing where they failed.

This failure was related to the increased epoxy thickness. As the thickness increased, so did the force necessary to stretch this layer to conform to temperature-induced dimensional changes in the adjacent aluminum sheet. Again, if this force exceeded the bonding strength, failure occurred.

Laboratory tests involving large temperature cycling determined that the epoxy thickness resulting when two layers of kraft paper were used was marginal, and occasionally failure occurred, but no failures were observed in single-layer paper cases. Limiting the epoxy layer to that produced by a single layer of paper became a solution for this failure mode.

d. Bonding Strength

It is clear that improvement of the bonding strength of the epoxy increases product reliability. The epoxy-to-metal interface is the weaker bond. Two primers for the metal surface were found that greatly increased this surface bond:

1. A two-thirds by volume mixture of Duroflex 25-30-9125 polyurethane made by National Adhesive Corporation, a division of National Starch and Chemical Corporation, with one-third Methyl Ethyl Ketone.

2. A one to one mixture of Atprime 100A with Atprime 100B. Materials are made by the ICI United States Inc., Wilmington, Delaware.

e. Electrolysis

To expedite the installation of reflecting panels on the heliostat brass and sometimes stainless steel hardware were used because aluminum hardware was not available. This error produced an interesting effect. Small dark irregular lines in the aluminum reflecting surface radiating from the panel mounting points appeared and grew with time. Later, small (pinhole-size) dots also appeared in the reflecting surface; their density was greatest near the mounting hardware but they extended over the entire panel. These dots and lines were determined by microscopic examination to be missing aluminum plating from the reflecting film which was replaced with foreign material. The pattern suggested electrolysis.

All nonaluminum hardware was removed and replaced with aluminum pieces. The growth of the black line and dot patterns stopped. All panels installed later were exposed only to aluminum hardware and none of them show any signs of this effect.

The frame is also aluminum and thus after the hardware change the reflecting material was exposed only to aluminum material. This like-material condition is essential for the preservation of the reflecting aluminized surface. The dots are believed to be the result of electrolysis over the surface when wet, attacking the aluminum plating through pinhole defects in the plastic protection overcoat.

History of Reflecting Panel Manufacture Cont'd.

No.	Date mfg.	Description of manufacturing	Comments - disposition
57	<p>cont'd 8-27-77</p> <p>completed 8-29-77</p>	<p>The second surface of the film received a thin coating of the epoxy solution.</p> <p>An air hose, held 18 in. away from the surface, was used to even out the epoxy.</p>	<p>Sample separated from the glass form easily. The epoxy unwetting air void seemed to be responding to the two-part 828 - one-part-V40 solution used in this sample. Few unwetting spots were noted. Orange-peel-type craters appeared all over the film surface, because all the soap solution was not worked out from between the film and the glass form.</p>
58	<p>started 9-1-77</p> <p>completed 9-6-77</p>	<p>Procedure 56, modified.</p> <p>Fels soap solution applied to glass. Film rolled onto glass. This was done with a Kodak roller. Rolling was followed up with a plastic squeegee and Kleenex rubdown. An epoxy mix of 150 parts of EPON No. 808 resin and 210 parts of V40 curing agent was used.</p>	<p>The first surface of the film was not cleaned before adhering it to the glass.</p> <p>A ten-minute epoxy curing period was allowed for air bubbles to clear.</p> <p>Epoxy was difficult to spread, probably because of the ten-minute cure period. Glass base cracked.</p> <p>Sample separated from the glass form easily. Sample appeared as follows:</p> <ul style="list-style-type: none"> a) A long distinct line caused by the cracked glass base was seen. b) Numerous voids because of air bubbles. c) Very few dust imperfections.

History of Reflecting Panel Manufacture Cont'd.

No.	Date mfg.	Description of manufacture	Comments - disposition
67	<p>started 10-4-77</p> <p>completed 10-5-77</p>	<p>Dunmore 393 first surface mirror 18-1/2 in. x 52 in.</p> <p>Procedure 56, modified</p> <p>An epoxy mixture of 75 parts EPON 815, 25 parts EPON 871, and 10 parts diethylenetriamine curing agent was used.</p> <p>An aluminum angle bar was secured to the jig plate.</p> <p>Two men held Micarta sheet in "ready to roll" position while one man poured epoxy just ahead of the sheet so as to form an epoxy wave which moved with the rolling action.</p> <p>The 0.060 Micarta was rolled onto the assembly.</p>	<p>The purpose of this sample was to devise a way to prevent air pocket voids between the film and the Micarta.</p> <p>No air pocket voids apparent in surface. Some small indentations appeared, because all of the soap solution was not removed from the center area of the film surface.</p>
68	<p>started 10-6-77</p> <p>completed 10-7-77</p>	<p>Dunmore 393 first surface mirror, 18-1/2 in. x 52 in.</p> <p>Preparation - same as sample 67.</p>	<p>The purpose of this sample was to repeat the method used with sample number 67.</p> <p>Sample had no voids. Specularity was fair.</p>
69	<p>started 10-8-77</p> <p>completed 10-10-77</p>	<p>Dunmore 393 sample, 37 in. x 52 in.</p> <p>Procedure 56.</p>	<p>The mirror surface was excellent, only three small epoxy unwetting air voids appeared. These voids were all within a 3-in.²</p>

History of Reflecting Panel Manufacture Cont'd.

No.	Date mfg.	Description of manufacture	Comments - disposition
69	cont'd. completed 10-10-77		Thus the mirror surface was almost completely free of voids. This mirror was cut and subsequently hung up outdoors to test its weatherability.
75	started 10-22-77 completed 10-28-77	Dunmore 393 sample, 37 in. x 52 in. Procedure 67.	This mirror was also hung up outdoors to test weatherability.
76 CU	started 10-26-77 completed 10-28-77 started 12-1-77	Duplicate of No. 75 except for a 48 hour curing time Step No. 1 a) Procedure 67 was used to assemble the film, epoxy bond and Micarta into a sandwich. b) An epoxy mixture was used for this step, composed of: 375 grams of Epon 815 125 grams of Epon 871 50 grams of diethylenetriamine. c) Sample cured for 48 hours. Step No. 2 a) Standard procedures were used to bond the Styrofoam and aluminum to each other and to the step-1 assembly. b) An epoxy mixture of EPON 815 resin and curing agent V40 in equal parts was used for this step.	No defects were seen in this sample. No defects. <u>Note:</u> All samples with the letter CU in their identification are concave. Previous samples were made flat.

History of Reflecting Panel Manufacture Cont'd.

No.	Date mfg.	Description of manufacture	Comments - disposition
84CU	started 12-8-77	This mirror duplicates sample No. 78, step No. 1, except: 1/8 in. thick glass form was used for the first time.	
	completed 12-9-77	Sample removed.	Good results were achieved with the 1/8" thick glass form. One small air pocket between the film and the Micarta.
	12-12-77	Step No. 2. This mirror duplicates sample No. 76 CU.	84 CU is mounted to the outer perimeter of the heliostat.
	transferred 12-9-77	Sample remains on glass and glass is laid on curve jig.	Good results were achieved with the 1/8 in. thick glass form.
	completed 12-12-77		One small air pocket between the film and the Micarta. 84 CU was mounted to the outer perimeter of the heliostat.
85	started 12-12-77	Procedure 76 CU, step 1.	
	completed 12-13-77	Removed sample from its base glass.	Mirror surface is fair.
86CU	started 12-13-77	Duplicate procedure 76 CU, step 1.	
	completed 12-14-77		Mirror looked good. No air pocket voids.
	started 12-16-77	Step 2.	

History of Reflecting Panel Manufacture Cont'd.

No.	Date mfg.	Description of manufacture	Comments - disposition
86CU	completed 12-19-77		86 CU was mounted to the outer perimeter of the heliostat.
87CU	started 12-14-77	This mirror duplicates sample No. 76 CU, step 1, except: The normal washing was omitted. The virgin material is relatively clean and dust free. Handling and washing could be adding more dust than it removed.	
	completed 12-15-77		Improved results were achieved by this procedure.
	started 12-20-77	Step 2.	Good specularity, no air pocket voids.
	completed 12-22-77		87 CU was mounted to the center of the heliostat.
93CU	started 12-15-77	Procedure 76 CU, step 1.	
	completed		No air pocket voids. Good specularity.
	started 12-22-77	Step 2.	
	completed 12-28-77		93 CU is mounted to the outer perimeter of the heliostat.
94CU	started 12-20-77	Procedure 76 CU, step 1.	The film for this mirror came off a new roll of Dunmore 393.

History of Reflecting Panel Manufacture Cont'd.

No.	Date mfg.	Description of manufacture	Comments - disposition
94CU	<p>completed 12-21-77</p> <p>started 12-28-77</p> <p>completed 12-30-77</p>	<p>Step 2.</p>	<p>No air pocket voids. Good specularity.</p> <p>94 CU was mounted to the center of the heliostat.</p>
95CU	<p>started 12-21-77</p> <p>completed ?</p> <p>started 12-30-77</p> <p>completed 1-3-78</p>	<p>Procedure 76 CU, step 1.</p> <p>Step 2.</p>	<p>95 CU was mounted to the outer perimeter of the heliostat September 26, 1978, when it was removed because of a faulty bond between the aluminum and the Styrofoam. The curve of 95 CU reversed, destroying focus. Flexerizer was omitted from this bond during preparation and caused this failure.</p>
96CU	<p>started 12-27-77</p> <p>completed 12-28-77</p>	<p>Procedure 76 CU, step 1.</p>	<p>Good surface. No air pocket voids.</p>

History of Reflecting Panel Manufacture Cont'd.

No.	Date mfg.	Description of manufacture	Comments - disposition
96CU	started 1-3-78 completed 1-5-78	Step 2.	96 CU was mounted to the midsection of the heliostat. On 8-31-78 it was removed because of bond failure. (See 95 CU)
97CU	started 12-30-77 completed 1-3-78 started 1-5-78 completed 1-9-78	Procedure 76 CU, step 1. Step 2.	Free of air pocket voids. 97 CU was mounted to the outer perimeter of the heliostat. On 9-27-78, 97 CU was removed from the heliostat because of curve reversal, and failure of the bond between the Styrofoam and the back aluminum plate. (See 95 CU.)
99CU	started 1-3-78 completed 1-4-78 started 1-9-78 completed 1-11-78	Procedure 76 CU, step 1. Step 2.	No air pocket voids. 99 CU was mounted to the midsection of the heliostat.
100CU	started 1-4-78 completed 1-5-78 started 1-11-78 completed 1-13-78	Procedure 76 CU, step 1. Step 2.	No air pocket voids. 100 CU was mounted to the outer perimeter of the heliostat.

History of Reflecting Panel Manufacture Cont'd.

No.	Date mfg.	Description of manufacture	Comments - disposition
101	started 1-5-78 completed 1-6-78	Procedure 76 CU, step 1 only. Step 2, never completed.	No voids apparent in surface.
102CU	started 1-6-78 completed 1-9-78	Preparation 76 CU, step 1.	Good specular appearance. No voids.
102CU	started 1-13-78 completed 1-16-78	Step 2.	102 CU was mounted to the outer perimeter of the heliostat.
103CU	started 1-9-78 completed 1-19-78	Procedure 84 CU.	Good specular appearance. 103 CU was mounted to the outer perimeter of the heliostat.
104CU	started 1-10-78 completed 1-23-78	Procedure 84 CU.	
105CU	started 1-11-78 completed 1-25-78		Good specular appearance, one large air pocket void appeared because the corners of the Micarta sheet had turned up during construction. Panel cut up for samples.
106CU	started 1-2-78 completed 1-13-78	Procedure 76 step 1.	106 CU was mounted to the mid-section of the heliostat.

History of Reflecting Panel Manufacture Cont'd.

No.	Date mfg.	Description of manufacture	Comments - disposition
107CU	started 1-16-78 completed 1-27-78	Procedure 84 CU.	Good specular appearance. No voids. 107 CU was mounted to the outer perimeter of the heliostat.
108CU	started 1-19-78 completed 1-30-78	Procedure 84 CU. A 3-qt epoxy mix was used instead of the usual 4 qt mix.	Good specular appearance, no voids.
109CU	started 1-23-78 completed 2-3-78	Procedure 84 CU.	Good specular appearance, no voids. 109 CU mounted to outer perimeter of the heliostat.
118CU	started 2-1-78 completed 2-2-78	Procedure 84 CU.	Good specular appearance, no voids.
119CU	started 2-2-78 completed 2-3-78	Procedure 76 CU.	A few specks, no voids, good specular appearance.
121EX	started 2-9-78 2-10-78 2-10-78 2-13-78	Film placed on glass, glass dammed around edge with Styrofoam. 3/4-gal of std. ratio 815/871/DTA poured into cavity to make a thick epoxy layer between film and support package. Placed sample on curved fixture and loaded it in the normal manner. Removed package from curved fixture	EX means that extra epoxy was added to the interface between the film and the package, as a buffer. Surface generally good, no voids. Bad, bumpy. Generally unsatisfactory condition. Sample was cut to determine problems.
122EX	started 2-10-78 2-11-78	Same as sample 121 EX except: assembly not removed from glass until after curing on curved jig. Removed sample from glass.	Good quality.

History of Reflecting Panel Manufacture Cont'd.

No.	Date mfg.	Description of manufacture	Comments - disposition
123EX	started 2-13-78	Same as sample 122 EX One layer of fiberglass screen submerged in the epoxy pool.	
	2-14-78	<p>Moved sample and glass onto curved plate.</p> <p>Spread a thin layer of 815/DTA mix over the fiberglass mesh partially cured 815/871/DTA epoxy.</p> <p>Coated a sanded sheet of 0.010 aluminum with a thin layer of epoxy.</p> <p>Put aluminum down onto the fiberglass mesh.</p> <p>Coated back of aluminum again and laid down 3/4 in. Styrofoam.</p> <p>Applied heavy coat of epoxy to the Styrofoam.</p> <p>Put a sheet of .010 aluminum onto the coated Styrofoam.</p>	
	2-15-78	Removed sample from curved fixture.	<p>On 4-21-78, 123 EX was cut into a center panel. On 8-31-78 it was removed because of bond failure between the front aluminum sheet and the epoxy.</p>
124EX	started 2-16-78	<p>Film placed on glass base.</p> <p>A dam was built around the perimeter of the glass/film with 2 in. Styrofoam strips.</p> <p>Two coats of Krylon were sprayed on to the film and allowed to dry.</p> <p>A thin coat of epoxy 815/871 & DTA was applied and allowed to cure for six hours.</p> <p>Fiberglass mesh screen was placed on top of the epoxy.</p> <p>A second coat of epoxy 815/871 & DTA was spread over the fiberglass mesh, and allowed to cure for 21 hours.</p>	
	2-17-78	Base glass and assembly moved to curved jig.	

History of Reflecting Panel Manufacture Cont'd.

No.	Date mfg.	Description of manufacture	Comments - disposition
124EX	2-17-78 cont'd. 2-21-78 2-24-78	<p>Liberal coat of 815/871 & DTA was brushed onto .010 aluminum</p> <p>Aluminum added to assembly. Brushed 815/871 & DTA onto exposed side of 0.010 aluminum.</p> <p>Brushed 815/871 & DTA onto one side of 3/4 in. Styrofoam.</p> <p>Added 3/4 in. Styrofoam to the assembly. Brushed 815/871 & DTA onto exposed side of Styrofoam.</p> <p>Brushed 815/871 & DTA onto one side of 0.010 aluminum that will complete the panel.</p> <p>Added 0.010 aluminum to the assembly.</p> <p>Removed assembly from jig.</p>	<p>Appearance good. Mirror cut to size. Adhesive quality is improved.</p> <p>Mirror failed because of air voids. Destroyed.</p>
125EX	3-30-78 4-1-78	<p>Film that had been on glass for 3 weeks is sponged with water. 815/871 & DTA epoxy mix applied to film and allowed to cure for 24 hours.</p> <p>Moved assembly to curved fixture. Added: 0.020 aluminum sheet 3/4 in. Styrofoam 0.020 aluminum sheet.</p> <p>Used standard packaging mix of 815/DTA epoxy.</p> <p>Removed assembly from curved jig.</p>	<p>Film appears to be good.</p> <p>Panel failed - orange peel effect. 123 EX seemed free of voids (March 30, 1978) whereas 124 EX and 125 EX were suffering from void conditions. 125 was the worst of the three, on the basis of this observation.</p>

History of Reflecting Panel Manufacture Cont'd.

No.	Date mfg.	Description of manufacture	Comments - disposition
125EX	cont'd.		<p>Panel failed.</p> <p>Large voids and dents. Epoxy did not bond smoothly to the aluminum - epoxy coat on film was too thin.</p> <p>Poor film-epoxy bond. Krylon spray was not used.</p> <p>After examining samples 123 EX, 124 EX, and 125 EX it was decided to return to the thick epoxy techniques used to build 123 EX, because that particular sample was free of voids. 124 EX and 125 EX both failed at this time.</p>
126EX	3-31-78	<p>Same as 123 EX except as follows:</p> <p>0.020 aluminum sheets were used for this sample.</p> <p>Used 2 qt of epoxy mix 815/871 & DTA instead of 3/4 gal. Omitted fiberglass mesh from the assembly.</p>	Rejected because of specularly.
	4-3-78	Removed assembly from curved jig.	
127EX	5-5-78	Same as 126 EX.	<p>Small amount of orange peel on April 21, 1978. 127 EX was cut to become a panel in the midsection of the Heliostat. Removed because of front bond failure.</p>
128EX	5-5-78	<p>Film on glass.</p> <p>Two coats of Krylon sprayed onto film back.</p> <p>Assembled package now consists of:</p> <p>film Krylon spray, 2 coats one coat of 815/871/DTA epoxy mix 0.020 aluminum 3/4 in. Styrofoam 0.020 aluminum The aluminum sheets and Styrofoam are bonded with 815/DTA, 10:1 mix.</p>	Orange peel, large blotches (4-21-78)

History of Reflecting Panel Manufacture Cont'd.

No.	Date mfg.	Description of manufacture	Comments - disposition
129EX	4-10-78	Same as 126 EX	On 4-21-78 this mirror was cut into a center panel and mounted to the heliostat. It was removed the same day because of a front bond failure.
130EX	4-13-78	Same as 126 EX, except: A new Krylon spray was used. Cure time was reduced from: 48 hours to: 18 hours	Dust became trapped between the film and the glass. Poor specularity.
131EX	4-13-78	Same as 130 EX except: Two coats of Krylon spray were used. Curing time 18 hours.	Better specular appearance than 130 EX, but film leaked epoxy onto glass, causing tearing. Not usable.
132EX	4-13-78	Same as 126 EX, except cure time shortened to 18 hours.	Better specular appearance than 130 EX. Some small pock marks. 132 EX was mounted to the outer perimeter of the heliostat. On July 6, 1978 it was removed because of bond failure between the aluminum and the film. On July 13 the sample was cut up for evaluation, rebonded with 815/DTA and sent to Lawrence Livermore Lab as a sample.
133EX	4-17-78	Same as 126 EX except: Dimensions have been reduced to 37 in. x 45 in. to make use of scrap.	
	4-18-78	Mirror removed from glass.	Failed - air voids.
134EX	4-20-78	Same as 126 EX	There was a small defect near the end of the roll, but specularity was good. On April 21, 1978, 134 EX was cut into a midpanel. Subsequently, it was removed because of strong orange peel effect.

History of Reflecting Panel Manufacture Cont'd.

No.	Date mfg.	Description of manufacture	Comments - disposition
135EX	4-20-78	Same as 126 EX except epoxy mix was 1125 grams of 815 150 grams of DTA. 18 hour cure in curved jig.	On April 21, 135 EX was cut into a midpanel by avoiding the orange peel section and mounted to the midsection of the heliostat. On July 3, 1978, 135 EX's front bond to aluminum failed. This will be the last sample made from Dunmore 393. 2C coated product will be used for future samples instead of 393, because supply of 393 is exhausted.
136EX	4-25-78	Same as 135 EX except: First use of Dunmore film with 2C overcoat.	No void problems. 136 mounted to midsection of heliostat and subsequently removed on August 31, 1978, because of bond failure.
137EX	4-25-78	Same as 136EX except: film was not coated with Krylon for this sample.	Specular appearance is good. Bond not as good without Krylon. On April 29, 1978, 137 EX was cut and mounted to the heliostat midsection. On August 31, 137 EX was removed from the heliostat because of front bond failure.
138EX	4-26-78	Same as 136EX	Specular appearance good. 138 EX mounted to the midsection of the heliostat. On August 31, 1978 it was removed because both aluminum bonds failed.
138EX	4-26-78	Procedure 136 EX - using 2C as 2nd surface mirror, 18 hour cure.	Bond failure 8-31-78
138EX	4-28-78	Procedure 138EX	Specularity fair - small air voids not usable.
140EX	5-1-78	Procedure 138EX	Front bond failed 8/31/78.

History of Reflecting Panel Manufacture Cont'd.

No.	Date mfg.	Description of manufacture	Comments - disposition
141EX	5-2-78	Procedure 138 EX.	Front bond failed 8/31/78.
142EX	5-20-78	Procedure 138 EX.	Used for dust collection experiment.
150EX	5-25-78	Procedure 138 EX.	Herring bone appearance developed after 5 day from removal from jig.
170EX	6-29-78	Procedure 138 EX - extra thick material DL50.	Poor specularity. Orange peel effect. Destroyed.
173S	7-10-78	Procedure 138 EX except a single layer of kraft paper was used to limit thickness of epoxy layer. Material DL-50.	Poor specularity. Sample destroyed.
179	7-13-78	Procedure 173 -DL-50.	Used for dust collection experiment.
180	7-14-78	Procedure 173 - Material DA2C.	Used for dust collection experiment.
181	7-15-78	Procedure 173 -DL-50.	Poor specularity
182	7-17-78	Procedure 173 - double layer of kraft paper.	Good specularity - slight orange peel.
183EX	7-19-78	Procedure 173 - material DL-50 second surface - double kraft paper.	Air void appeared after a few days.
184EX	7-25-78	Procedure 173 - one layer of kraft paper.	Specularity good - single air void - on heliostat.
185S	7-24-78	Procedure 176 CU - sample made flat for shipment to Sandia Lab for test.	Specularity good - shipped to Sandia.
187EX	7-27-78	Procedure 173 - single paper - room temperature was controlled during curing for first time.	Specularity good - temperature control of curing process is key to herring bone and orange peel effects in samples made in June and July.

History of Reflecting Panel Manufacture Cont'd.

No.	Date mfg.	Description of manufacture	Comments - disposition
187EX	7-27-78 cont'd.		Installed, then removed when orange peel effect developed 8/26/78.
188EX	7-28-78	Procedure 173 - material DL-50 second surface, single layer of kraft paper Temperature control of curing processes.	Specularity degenerated in service - exposed to weather on heliostat. Removed from service with orange peel effect 9/78.
189EX	7-31-78	Procedure 188 EX.	Same as 188 EX.
190EX	8-2-78	Procedure 188 EX.	Same as 188 EX.
191PS	8-7-78	Procedure 188 EX. Micarta sheet inserted to replace epoxy - paper layer - temp. controlled curing - made flat.	Specularity good. Held as control on flatness.
192PS	8-9-78	Procedure 191 PS.	Very good specularity - on heliostat.
193EX	8-10-78	Procedure 188 EX. Bondmaster 773A & B used for test.	Specularity good but inferior to 192 PS on heliostat.
194PSN	8-12-78	Procedure 191 PS - except bondmaster 773A & B used as bonding agent	Held for evaluation. Acceptable but no improvement. Bond failed in service.
195PS	8-15-78	Procedure 194 PSN.	Specularity very good - on heliostat Micarta-to-aluminum bond failed in service.
196PS	8-17-78	Procedure 191 PS.	Micarta-to-aluminum bond failed on heliostat.
197PS	8-18-78	Procedure 191 PS.	Micarta-to-aluminum bond failed on heliostat.
198PS	8-21-78	Procedure 191 PS.	Micarta-to-aluminum bond failed on heliostat.

History of Reflecting Panel Manufacture Cont'd.

No.	Date mfg.	Description of manufacture	Comments - disposition
199PSN	8-22-78	Procedure 194 PSN.	Bonding failed in temperature cycling test - freezing/thawing on heliostat.
200PS	8-23-78	Procedure 191 PS - material DL-50.	End of roll film voids appeared on heliostat.
201PS	8-24-78	Procedure 191 PS - material DA-2C.	On heliostat.
202PS	8-28-78	Procedure 191 PS - material DA-2C.	On heliostat.
203PS	8-29-78	Procedure 191 PS - material DA-2C.	On heliostat.
205PS	8-31-78	Procedure 191 PS - material DA-2C.	Spare material.
206	9-7-78	Procedure 188 EX - Klinks Epoxy used as primer on aluminum surface.	Aluminum bond failed - still on heliostat to be replaced soon.
207		Procedure 206.	Aluminum bond failed.
208	9-12-78	Procedure 188 EX - First panel to be edge sealed with butyl rubber compound	On heliostat.
209	9-27-78	Procedure 191 PS - DA-2C second surface.	Air voids - used for small samples
210	10-2-78	Procedure 209.	Also small air voids - used for samples.
211	10-3-78	Procedure 209 - better workmanship.	No air void. On heliostat.
212	10-6-78	Procedure 209.	On heliostat - excellent quality.
213	10-5-78	Procedure 209.	On heliostat - excellent quality.

History of Reflecting Panel Manufacture Cont'd.

No.	Date mfg.	Description of manufacture	Comments - disposition
216	10-25-78	Procedure 209 - except polyurethane use to prime aluminum surface.	Bond test indicates great improvement in bonding strength. Edge sealed and installed on heliostat.
217	10-30-78	Procedure 216.	On heliostat.
218	11-2-78	Procedure 216.	Spare material.
220	11-9-78	Procedure 216.	On heliostat.
221	11-14-78	Procedure 216.	Spare material.
222	11-24-78	Procedure 216.	Spare material.

III.E. Reflecting Specularity

Specularity is a measure of quality of a reflecting surface. An ideal reflecting surface will reflect parallel rays persevering in their parallel relationship. Specularity is measured in terms of the average angular error in this parallel relationship introduced by the reflecting surface and is it measured in angular units, commonly milliradians.

Dr. Richard Pettit, Sandia Albuquerque, has studied this property and built a precision test facility to make specularity measurements. This apparatus and its use are described in a Sandia report, SAND-76-5310. Light emerging from a slit is focused to form an image through two paths, one containing a mirror surface and one without. The illumination distribution of the image is measured and through a computer-derived relationship determined by Dr. Pettit, a measure of specularity is determined. This computer-derived relationship, copied from the Sandia Report, is shown in Figure 15. Lines of uniform specularity are shown relative to the fraction of image light passing through an aperture of known angular size. Measured image illumination plotted over this set of locus curves permits specularity values to be determined.

Brookhaven built a simple but similar arrangement for measuring specularity following the Pettit concept. A tungsten light source was substituted for Dr. Pettit's monochromatic source. Using this test facility to measure specularity, production methods and product quality were monitored. Specularity varied during the course of production but improved as better handling methods were developed. A typical product displayed specularity better than 0.5 milliradians.

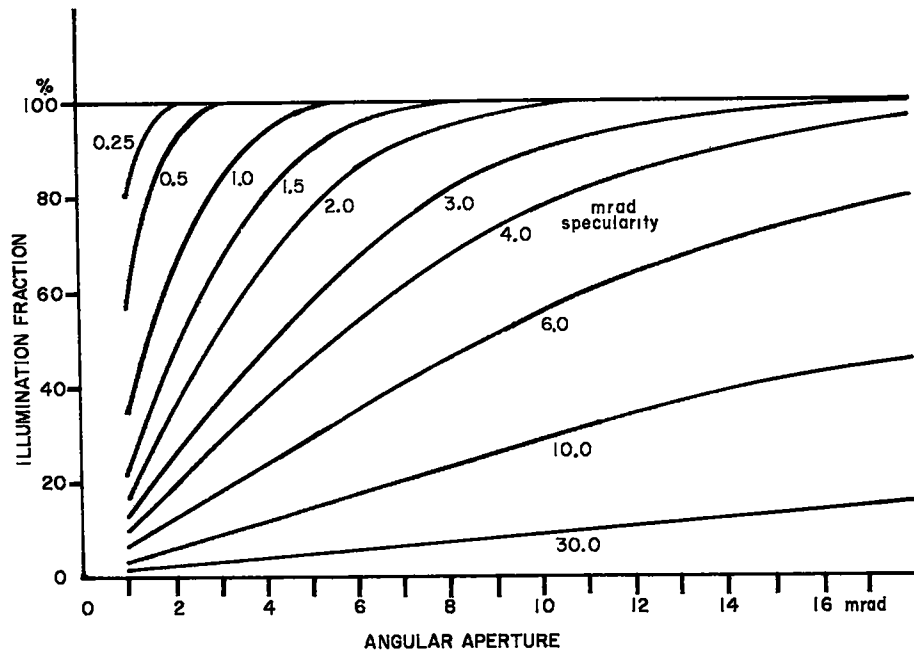


Figure 15. Computer derived specularity nomograph, copied from Sandia Report SAND-76-5310 by Richard Pettit.

BNL sample No. 45 was set aside and used to monitor specularly changes with aging. Over a 10 month period specularly degraded from 0.5 to 0.6 milliradians. Most of the change occurred in the first 6 weeks and no significant changes could be observed during the later months.

III.F. Mirror Focusing - Facet Shimming

The heliostat support dish to which the reflecting facets are attached was not built to the precision required to guarantee focus. The plan was to shim each facet after assembly to obtain proper alignment. While some production engineers have expressed the opinion that the lowest production cost will be achieved by building precision tooling that will fabricate the support dish with the necessary accuracy, this option is left to the future.

The hand-operated facet alignment procedure described here worked smoothly and is adaptable to automation. The setup schematic is very simple and is shown in Figure 16. A laser gun is located on an optical bench over a reference point and aimed to hit the center of the facet, being aligned. These reference points are predetermined marks on a horizontal rigid bar and lie on a line connecting the facet center to the desired center of curvature.

When the facet alignment is correct the laser light reflected from the facet will return and strike the center of the laser gun. For all other facet alignments this returning light beam will fall on a screen placed in front of the laser gun. This screen contains a calibration pattern from which correcting shim thickness values can be read (see Figure 17). When these shims are inserted under the reflecting facet, correct alignment occurs. In general, a one-step shimming produces correct alignment but occasionally operator error makes an alignment iteration necessary.

After a horizontal row of facets is aligned, the heliostat dish is rotated about its optical axis to bring the next row of facets to the horizontal, and then that row can be aligned. This process is repeated until all facets are aligned. The optical axis is defined as the normal to a central reflecting facet which is rigidly fastened to the heliostat dish. Orientation

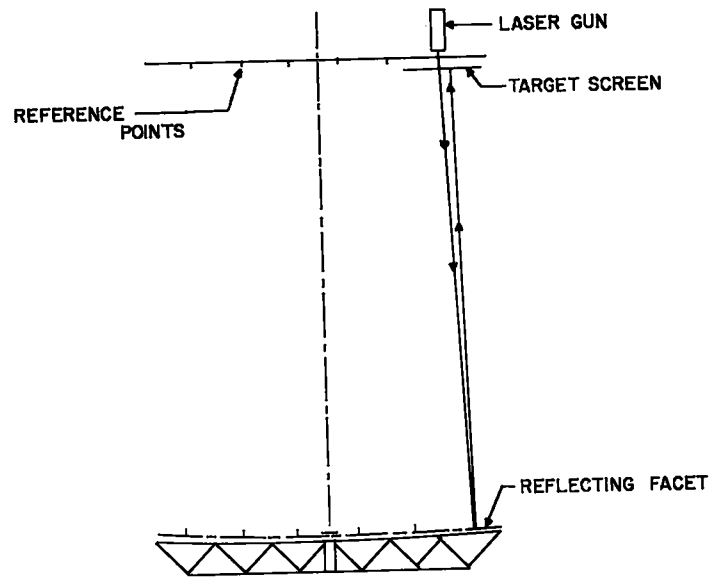


Figure 16. Laser alignment scheme.

of the heliostat frame is adjusted until the laser beam reflected from this central facet strikes the laser target center when the laser is operated from the central reference point.

Alignment results can be repeated, including removal and returning the whole dish assembly to the optical bench. Frame orientation is often rechecked during the alignment procedure as a precaution. An optical sight was erected to facilitate this check. Figure 18 shows an operator viewing through this sight. Also visible in Figure 18 is the laser gun on the optical bench with the target screen removed and placed faceup on the table in front of the optical bench. Figure 19 is a view looking at the heliostat over the laser gun. Only one row of reflecting facets was in place on the heliostat frame when this photograph was taken. Figure 20 is another view of the heliostat at this point in construction.

Figure 21 is a view of the optical bench from behind the partially faceted heliostat frame. The target screen is now in the proper position. Figures 22 and 23 show the front and rear of the finished heliostat dish fully assembled and in position on the laser alignment facility. This dish can be unbolted along a diameter for transport to the final heliostat location where it is reassembled as described in Section III.H.

III.G. Motion Control

The planned heliostat motion is a series of small steps approximating the ideal smooth motion. These steps will be produced by a start-stop action of an electric motor. This action is ideally generated by a stepping motor, but such motors are expensive. A low cost heliostat needs a more economical solution to this stepping problem.

A motor life test bed was constructed in which motors with their control schemes can be given accelerated life and other critical service tests.

The first motor tested was a modified induction motor with an induction "start" windings. The normal centrifugal start switch controlling the "start" winding was removed and its function replaced by a solid state logic package. This switch was removed because there was no chance that it could survive the large number of operations called for by the stepping action. Operation of this motor on the test bed revealed that by limiting the start winding current

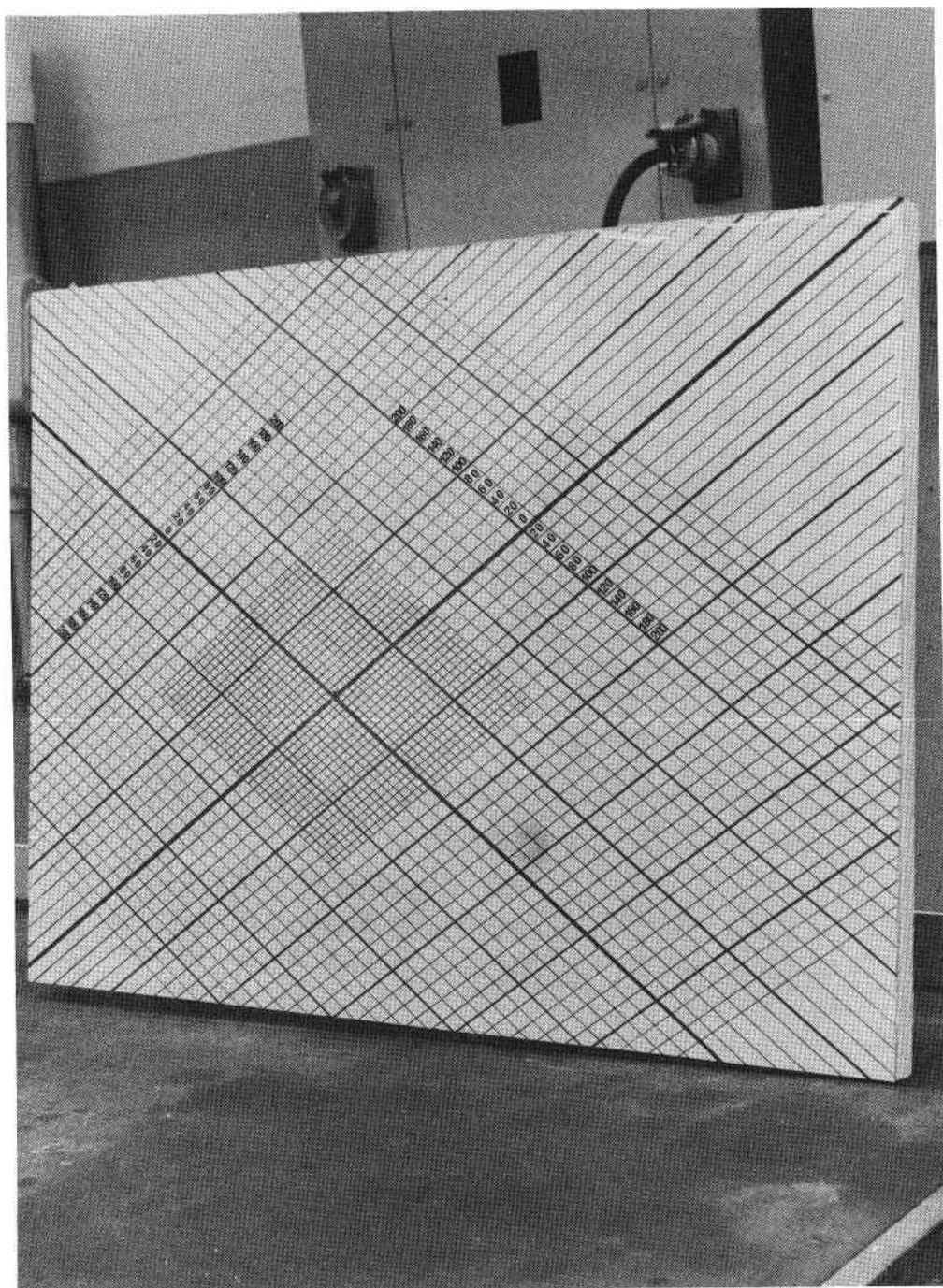


Figure 17. Screen from which correction shim values are read during laser alignment.

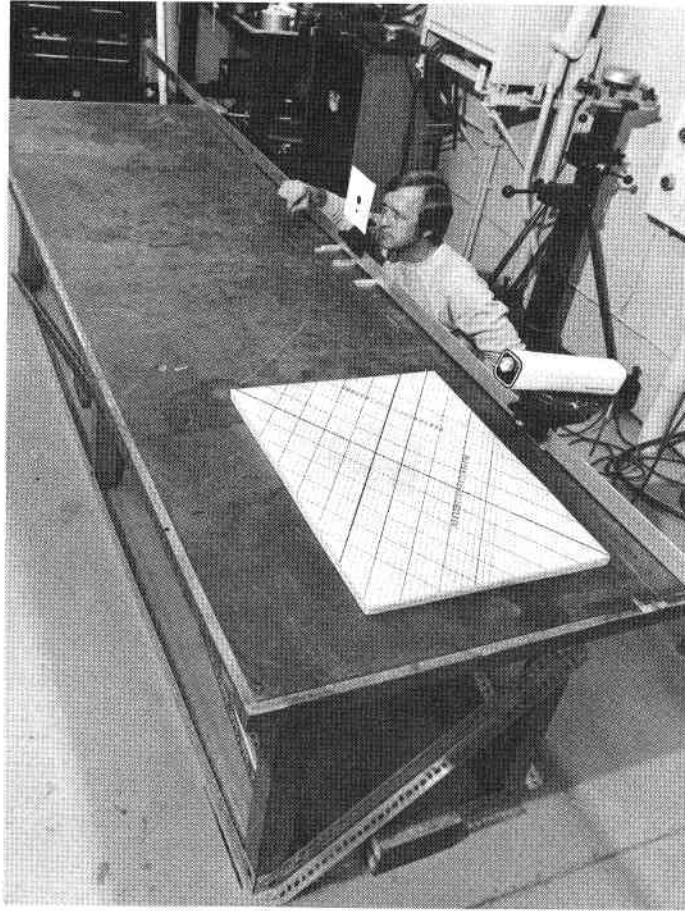


Figure 18. Laser optical bench showing central alignment procedure.

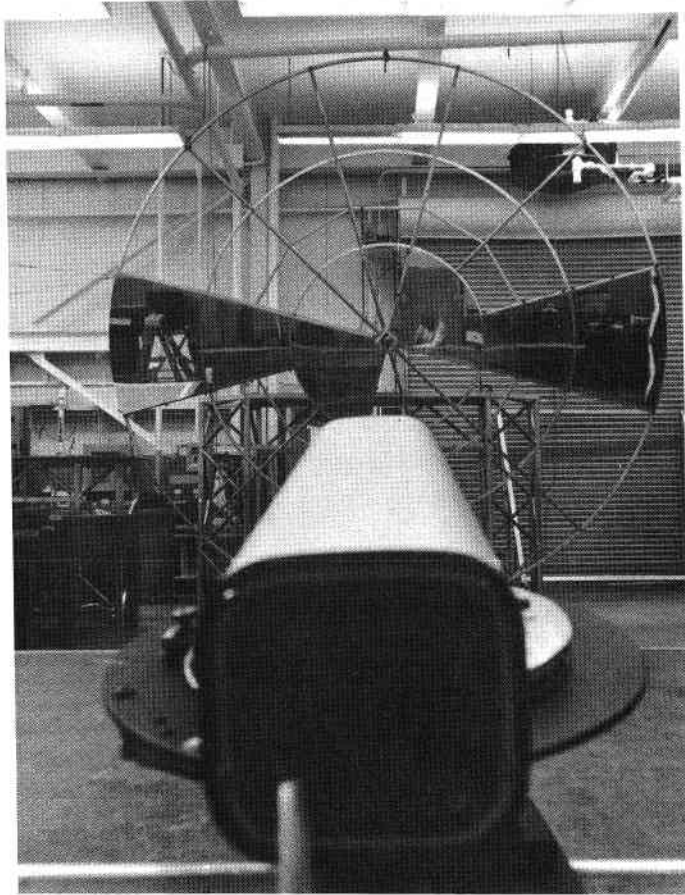


Figure 19. View looking over the top of laser gun.

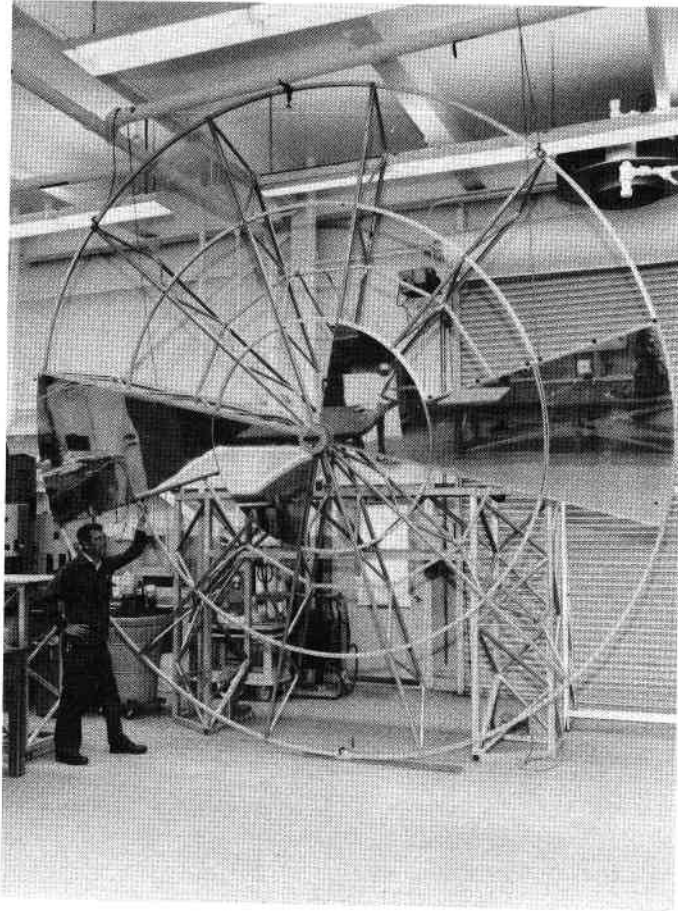


Figure 20. Heliostat undergoing laser alignment with only one row of reflecting facets in place.

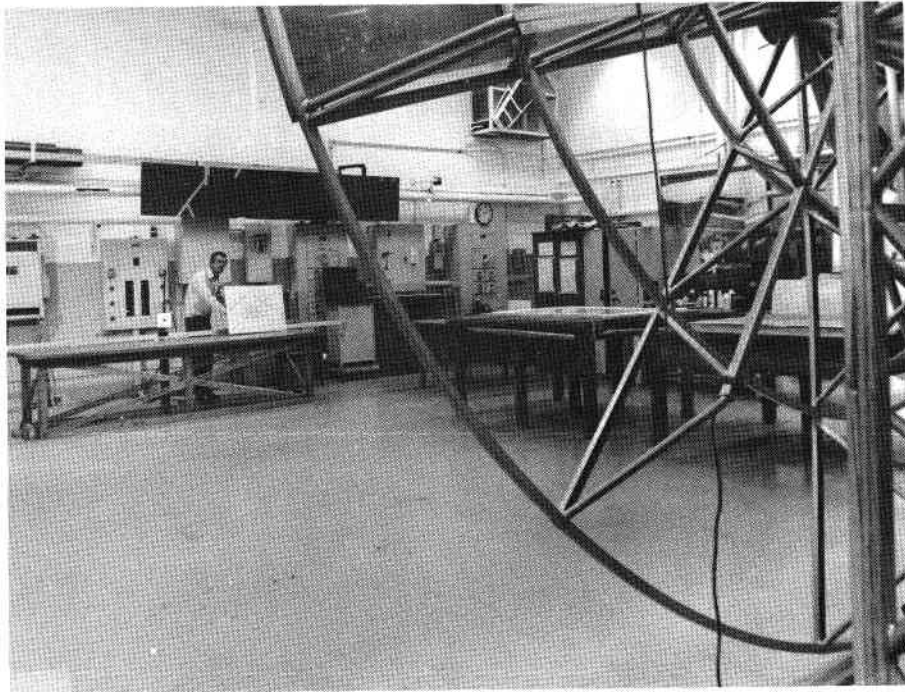


Figure 21. View of laser optical bench from behind the partially faceted heliostat dish.



Figure 22. Fully faceted heliostat dish undergoing laser alignment, front view.

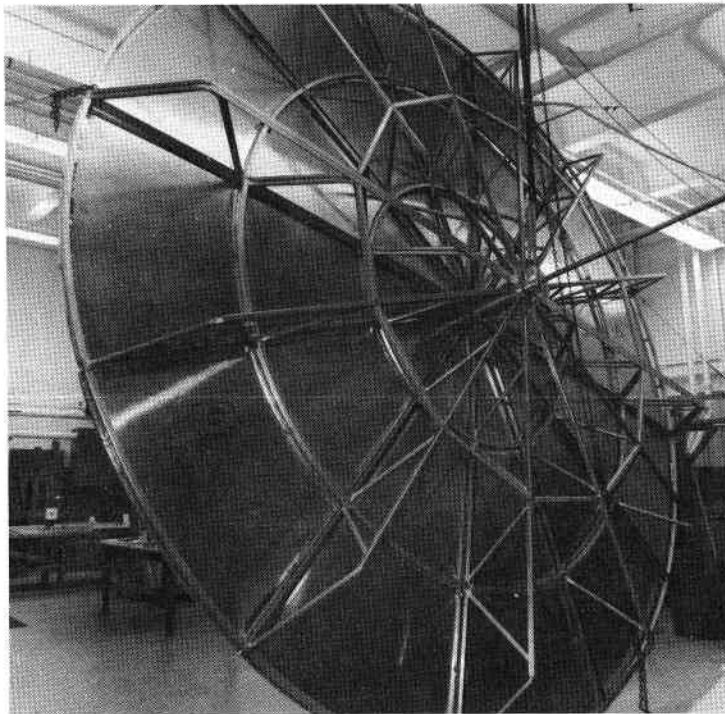


Figure 23. Rear view of heliostat dish in laser alignment facility.

the operating temperature of all winding could be held below design limits for class-B-type insulation (a 40°C temperature rise above a 40°C ambient).

Control of this "start" winding current also provided a very useful way to limit motor torque. This allows the motor to stall without damaging the gear train or other components of the drive system. If the torque is limited in this way, operation under stalled conditions, such as produced by ice, will be safe. The stalled condition can then be sensed and proper action initiated by the computer control system. For example, the motor might be allowed to rest and powering attempted again in 30 minutes. In this way the heliostat returns to normal service when the ice melts. The current in the "run" winding can be used to indicate the stalled condition and provide information to the solid state logic package. Current in this winding drops when running speed is reached.

Further development of the motion control system was stopped because of fiscal limitations. The motor control logic package and the necessary computer interfaces were never developed although this clear path was identified.

III.H. Heliostat Assembly

The design of the heliostat mechanism is a compromise between production methods that are tool intensive and fabrication methods available through the Brookhaven shop system. The Brookhaven shop system is planned and adapted for the fabrication of custom hardware of unusual nature. It is equipped for a wide variety of precision tooling and can accomplish almost any task. It is not geared for production and such work is normally moved to the outside under subcontract.

The frame for the heliostat dish, an important component from a weight consideration, was engineered in considerable detail. This effort resulted in a very low weight design employing aluminum tubing and a U-shaped channel formed by bending. These pieces, shown in Figure 24, are welded together to form truss assemblies which are the strength element of the dish structure. These trusses are in turn welded to other channel pieces to form the dish frame as seen in Figure 25. This frame is fitted with reflecting facets and

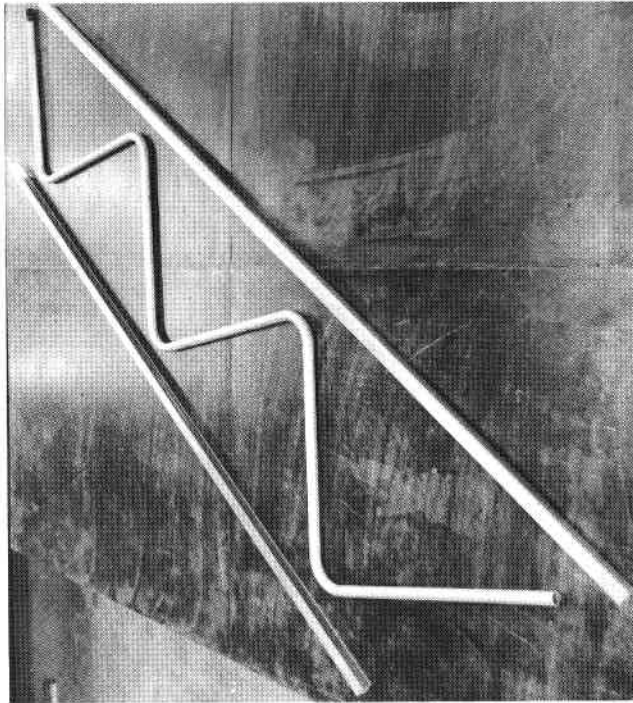


Figure 24. Bent tubing and U-shaped pieces that form heliostat dish truss assembly.

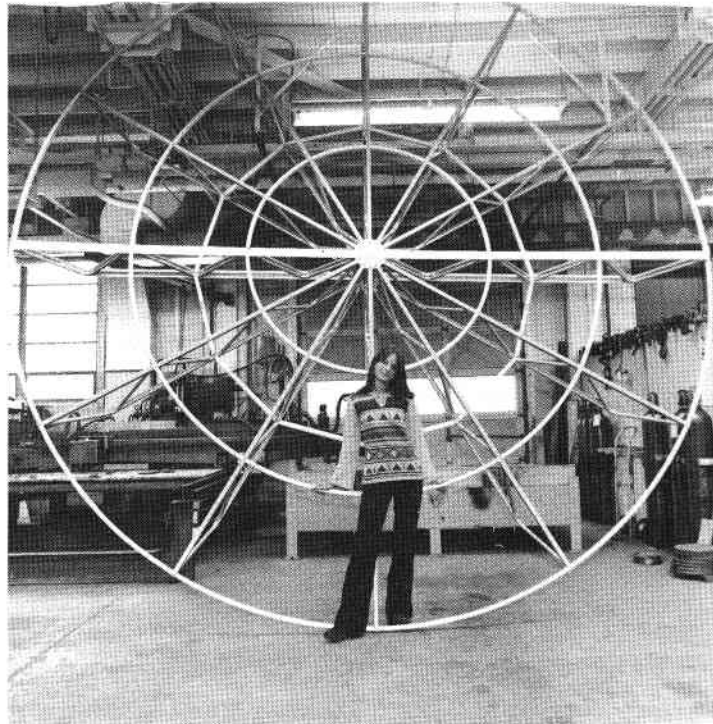


Figure 25. Heliostat dish support structure.

aligned as described in Section III.F. It is then unbolted along a diameter to be moved to the field where it is reassembled.

Field assembly starts with the pouring of six concrete footings as seen in Figure 26 shown with the tubular forms still in place. The anchor bolts were placed in the concrete when wet and were held in place with a wooden alignment jig. When the footings were ready the base frame, shown in Figure 27, was moved into place. This piece, the heaviest item in the field assembly sequence, is secured with the roller hardware shown in Figure 28.

Unlike the heliostat dish the base frame was not carefully engineered; instead it had to be rushed through engineering to meet schedules. It was very conservatively designed and as a result is overweight. It is in this base frame that major design improvements and weight reduction can be made by a careful three-dimensional stress analysis.

After the base frame was in place and the rollers adjusted for free motion the rear stationary stanchion, shown in Figure 29, was set in place and fastened to the base frame. Next the movable stanchion, Figure 30, was set into place and rollers were fitted. The wedge pivot structure, Figure 31, and the spreader arms were assembled to bridge between these two stanchions.

The assembly was now ready to receive the first half of the mirror dish. The base frame was temporarily covered with plywood to provide safe footing for workmen and the bottom dish half was lifted and laid into place on the plywood as shown in Figure 32. This dish half was bolted to the Wedge Pivot Structure. Finally, the second half of the dish was lifted into place, Figure 33, and reassembled to the previous half as seen in Figure 34. The finished assembly is shown in Figures 35 through 39 in various operational positions.

The entire assembly procedure can be conducted by a two-man crew without the aid of a crane although a third man makes the procedure easy. As seen in the figures, additional manpower was used to assemble this first Brookhaven prototype. Experience gained indicates that this was unnecessary.

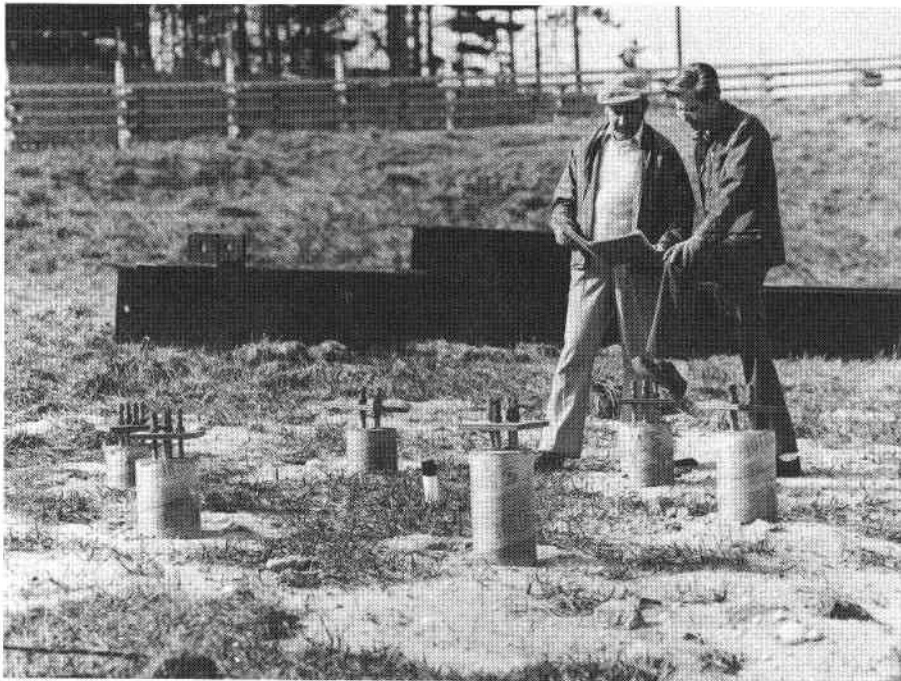


Figure 26. Heliostat footings.

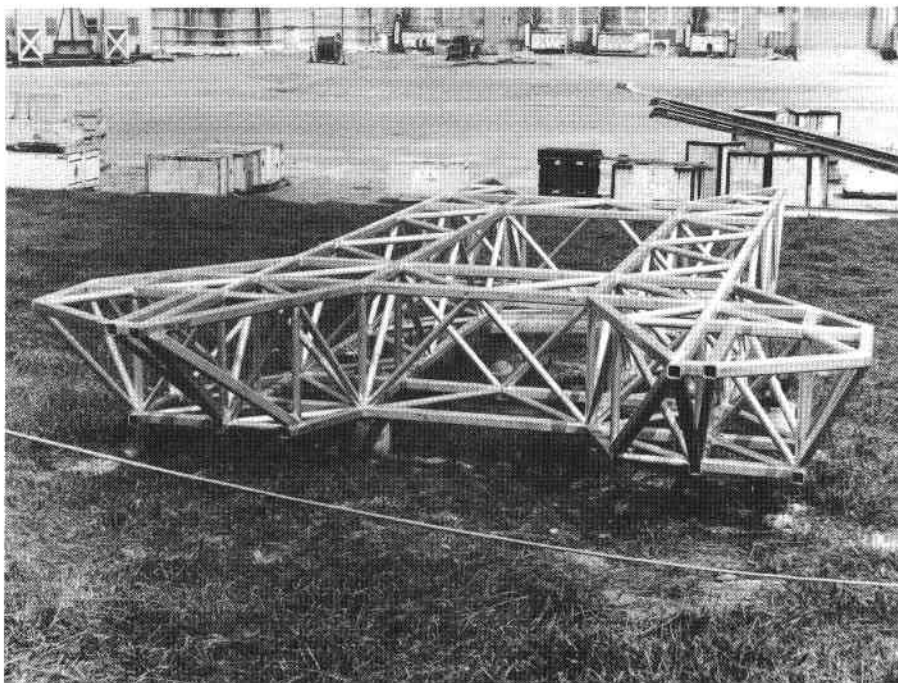


Figure 27. Heliostat base frame.

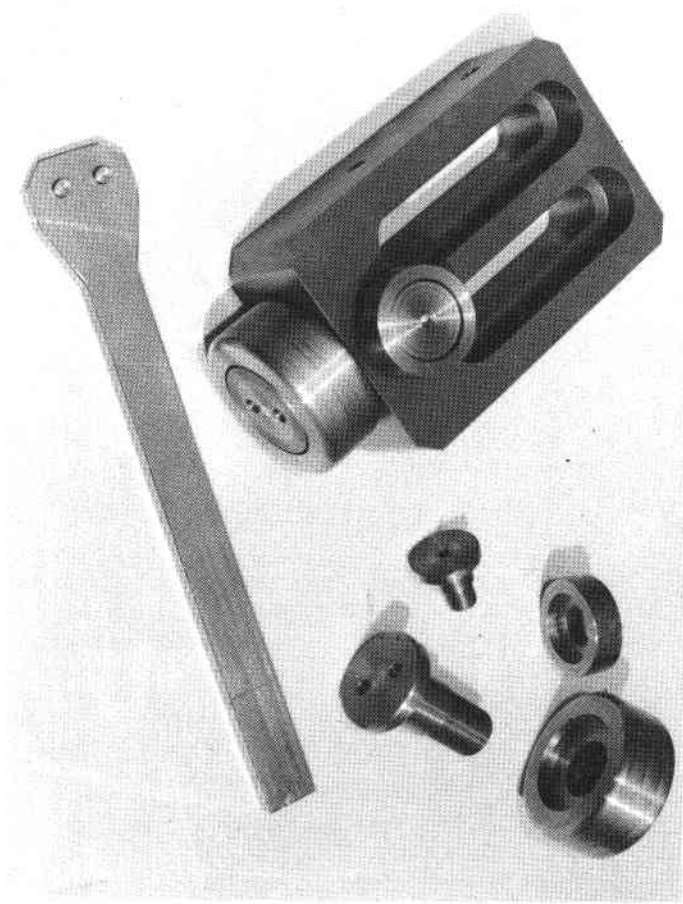


Figure 28. Heliostat roller assembly.

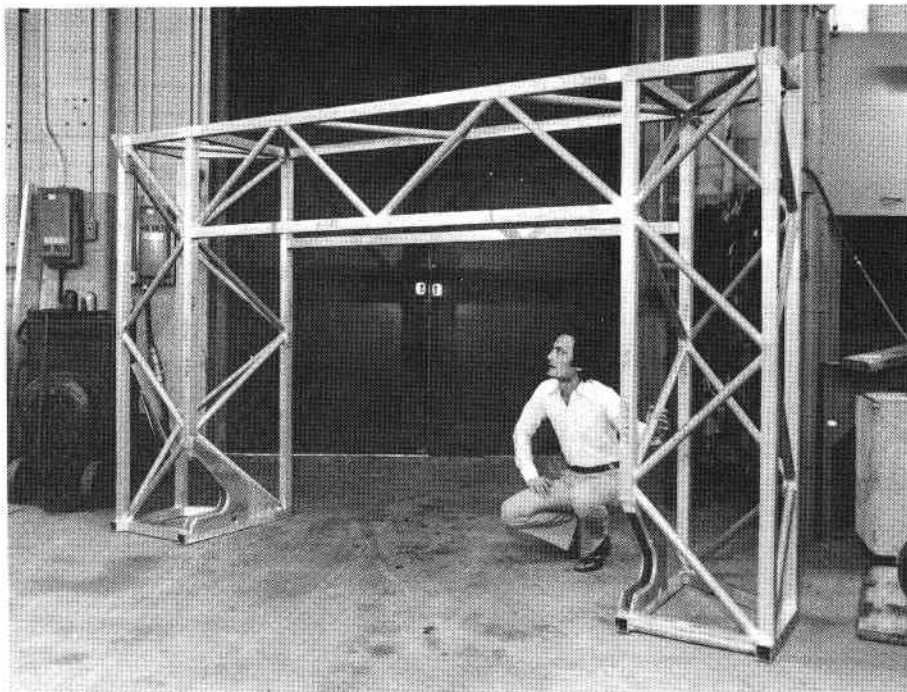


Figure 29. Rear station stanchion of heliostat assembly.

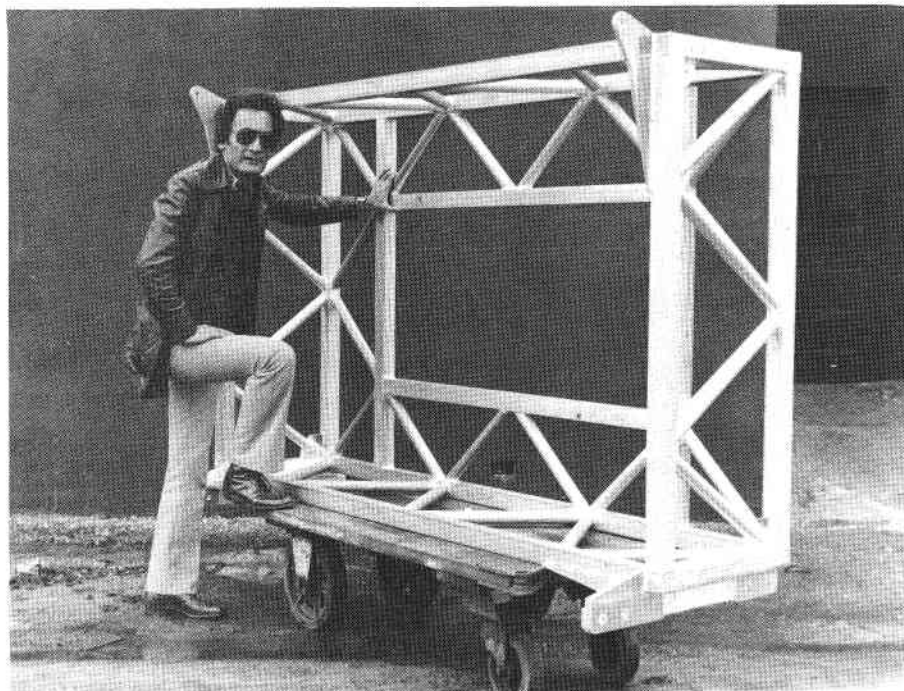


Figure 30. Movable stanchion of heliostat assembly.



Figure 31. Wedge pivot structure of heliostat assembly.

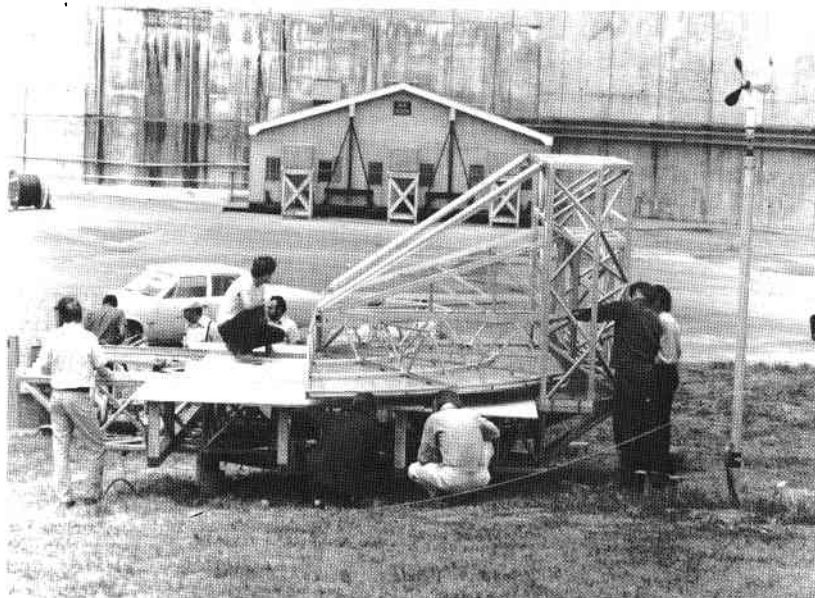


Figure 32. Heliostat undergoing field assembly - half dish in place on temporary plywood surface.

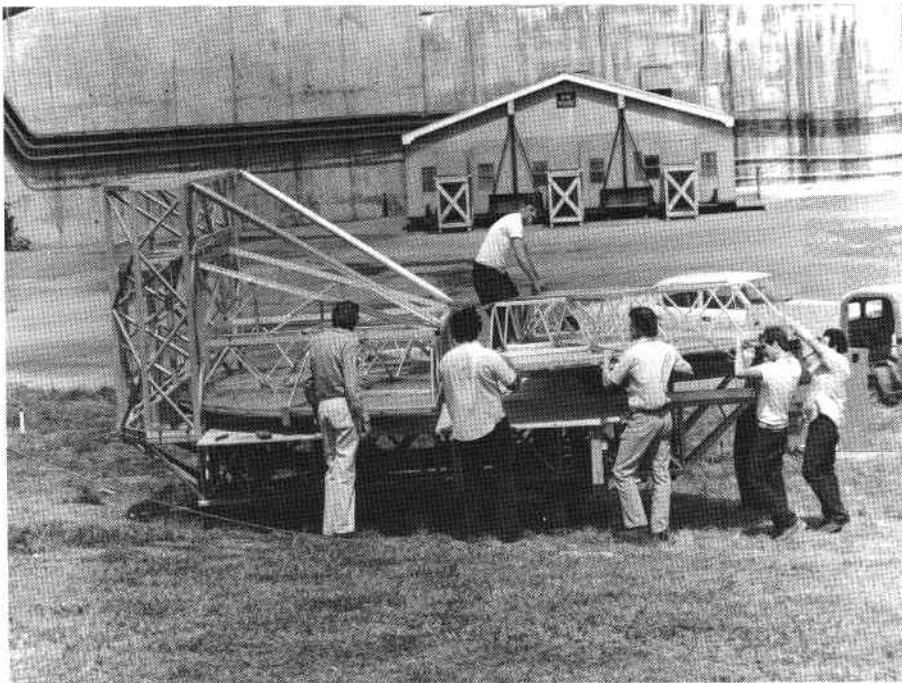


Figure 33. Field erection - second half of dish moving into place.



Figure 34. Field assembly of heliostat dish - two halves being bolted back together.

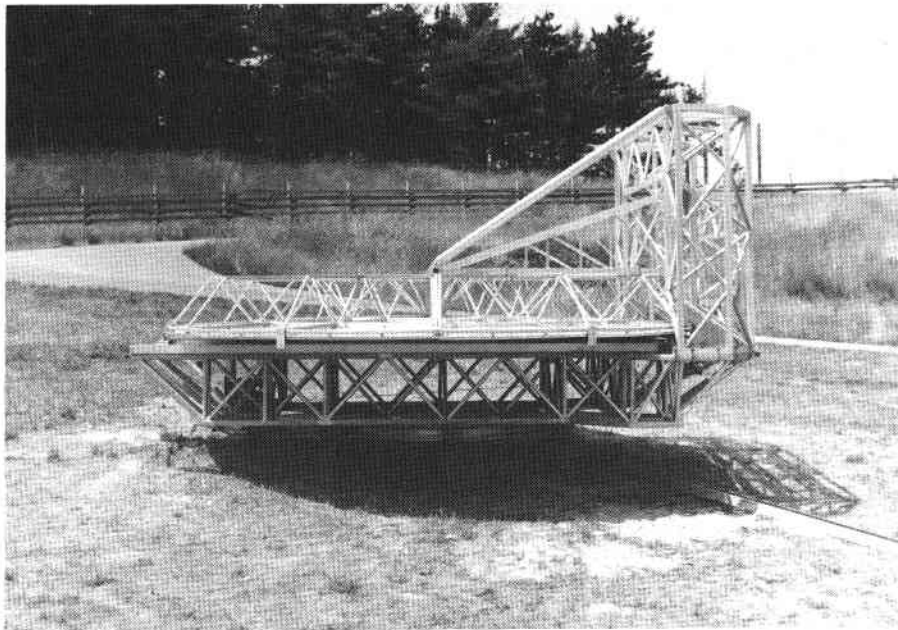


Figure 35. Heliostat prototype in face down wind avoidance position.

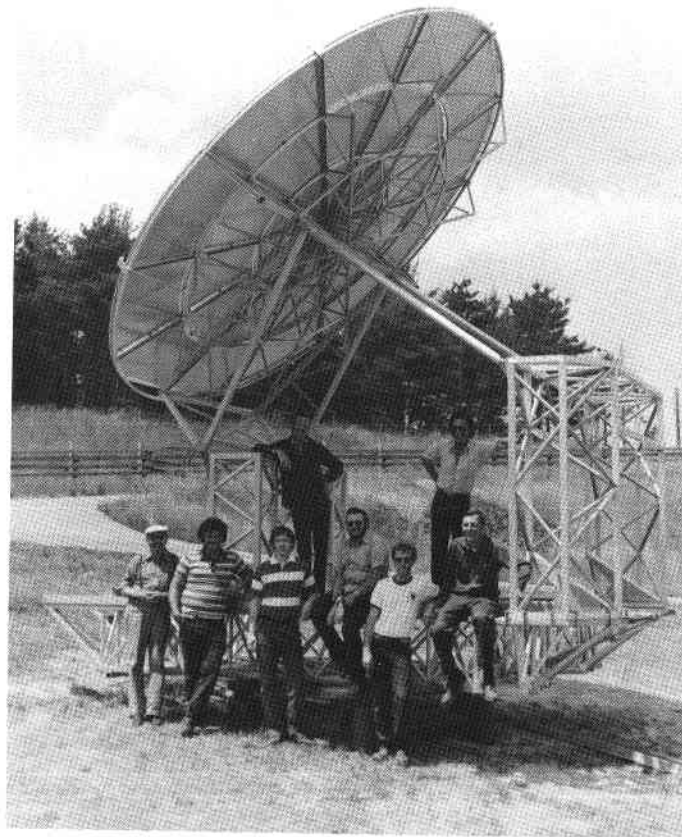


Figure 36. Heliostat with development team.

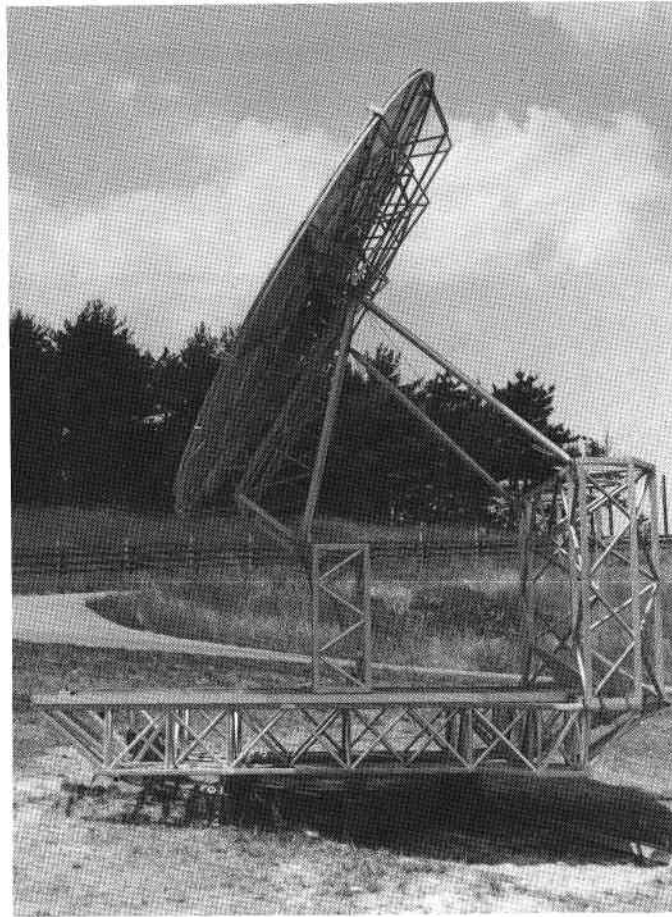


Figure 37. Heliostat in working altitude.

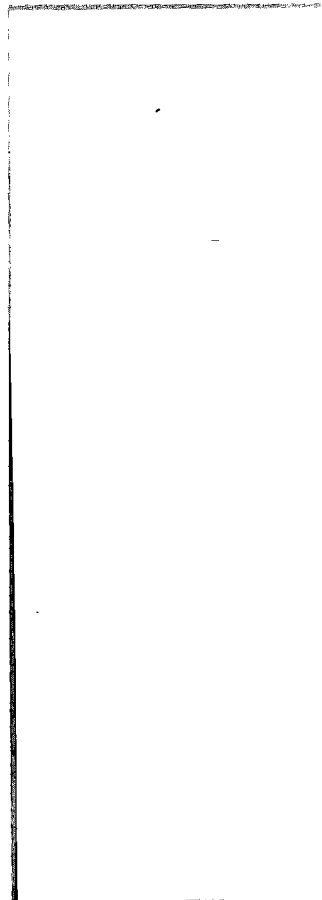


Figure 38. Heliostat prototype, front view.

Poor Quality
Original
Data Compromised
DISW



on.

Best Quality
Original
Data Compromised
DISW

SECTION IV
HELIOSTAT PERFORMANCE THERMAL ENERGY COLLECTION

Once the prototype heliostat was completed, preparation was initiated for a performance measurement. These preparations included the construction of an instrumented receiver located on top of a 20-foot tower. The receiver consisted of a 5-foot-diameter 1/4-inch-thick water-cooled copper disk. Copper constantan (type-T) thermocouples were located at the inlet and outlet of the water circuit on the receiver. These thermocouples were connected differentially at the receiver by connecting all the constantan terminals together. The copper leads were run down the tower via shielded wires and were used to measure water flow temperature differences. A six inch wide aluminum shroud was placed around the back of the receiver and filled with three layers of fiber glass insulation. The tower was hinged so that it could be raised and lowered for receiver modifications as needed. Water flow was measured by a calibrated flowmeter. The target was designed to control the temperature of the receiver to prevent degrading the absorptivity of the flat black paint on the receiving surface. The absorptivity of this black paint, Rustoleum, was measured on test samples to be 96%.

With no input from the heliostat, the receiver was calibrated for energy gain or loss to the ambient. This correction included conductive, convective, and radiation effects. Figure 40 shows the receiver gain-loss energy correction characteristic as measured. The following empirical relationship was derived for these data.

$$\text{Receiver Correction (watts)} = 24.59 (\Delta T) + 0.364 (I),$$

where ΔT is measured in $^{\circ}\text{F}$ and I in W/m^2 .

With the target calibration complete, heliostat performance measurements could be made. No automatic tracking was provided. The solar image was kept centered on the target manually. Measurements were made at 10-minute intervals with all readings taken simultaneously. The raw data taken included a normal incident radiation measurement with an Eppley Pyrheliometer.

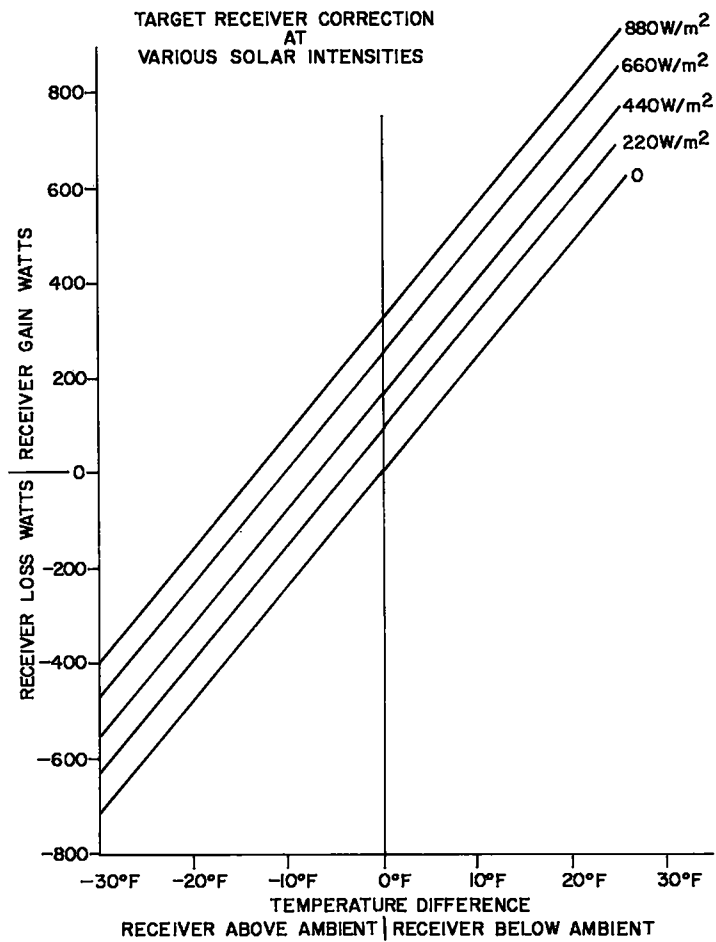


Figure 40. Receiver energy correction characteristic.

Figure 41 is a comparison of measured thermal energy collected by the receiver and the computed thermal energy directed to the receiver by the heliostat.

The computed thermal energy was based on the following:

1. Average reflectivity - 84%
2. Heliostat reflecting surface area - 165 ft² (4 outer panels were not in place during this experiment).
3. Receiver absorbability - 96%.
4. Computed cosine of the angle between the incoming solar ray and a normal to the heliostat.

The two curves of Figure 41 are in good agreement and differ by no more than $\pm 2-1/2\%$. Such measurements were conducted periodically from June 1978 to September 1978 at various solar intensities. The performance testing began in June with good agreement between measured and computed thermal values, but gradually a larger and larger discrepancy appeared. The computed value was always higher than the measured value and a difference of 25% was reached. Finally this discrepancy was traced to a number of mirror facets whose reflecting surface had delaminated, destroying their surface quality. Without the proper surface quality these mirror facets were not concentrating energy on the receiver. When these defects were corrected, good agreement was again obtained. The cause of the delamination is discussed in Section III.D.2. Figure 41 is a performance measurement made after all the defective mirror facets were identified.

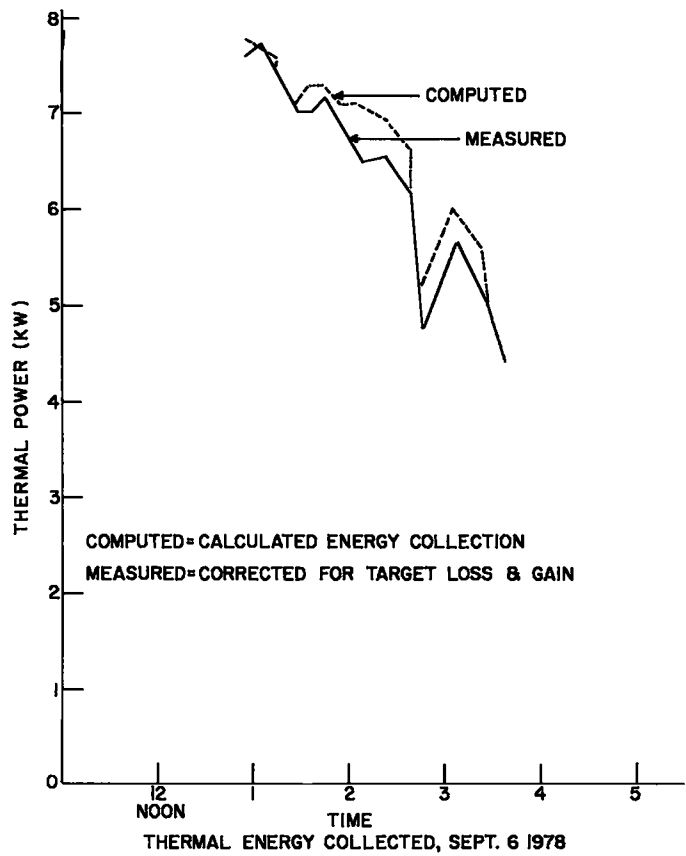


Figure 41. Heliostat performance confirmation experimental results.

SECTION V
REFLECTING FILM DEVELOPMENT

V.A. Why Plastic Reflecting Film?

A mirror facet that cannot flex must be supported on a mechanical structure which also does not flex, or the facet must be shielded from flexing motion through flexible fastenings. Both of these conditions are undesirable. A mechanical structure designed to limit flexure under wind force is massive and more costly than one allowed to flex. Alternatively, slip joints or other slide fastenings may freeze through the action of ice or other foreign contamination and fail to act. Thus the use of slip joints has a longevity uncertainty and therefore is also not attractive.

Flexible mirror facets can be made from plastic film or from thin laminated glass. Both have advantages and disadvantages. Some of these are listed as follows:

Laminated Glass

Advantages

Reflectivity
Specularity
Life

Disadvantages

Fragile to impact
High cost

Plastic Film

Advantages

Low cost

Disadvantages

Weatherability
Reflectivity
Specularity

From this listing it is clear that the laminated glass approach while more costly offered prospects for superior performance and contained less developmental risk. The plastic film path required that three major technical obstacles be overcome, namely, lower reflectivity, poor specularly when bonded to a supporting substrate, and relatively short life when exposed to the weather. The judgment of the Brookhaven research team was that the low cost possibility offered by the plastic film option justified the research effort necessary to solve the technical problems. Thus the higher risk path was chosen.

Early laboratory experiments produced a fabrication method for bonding plastic film to substrates yielding excellent specularly (less than 1 milliradian). This fabrication method is described in detail in Section III.D. and eliminated one of the technical obstacles to success.

V.B. Reflectivity and Weatherability - Dunmore Subcontract

A cooperative research project between Brookhaven and the Dunmore Corporation of Newton, PA. was initiated for the purpose of developing a plastic reflecting material with high solar reflectivity and good weatherable life. Dunmore supplied production materials that had been used in other applications and were mass produced at low cost. These materials were ICI America polyester films manufactured under the brand name Melinex 442 and were aluminized and given a protective overcoat by Dunmore.

One of these materials, 200 Dunchrome-393, proved to be interesting. As a first surface mirror it has an initial reflectivity of 84%. Brookhaven was able to fabricate this film into laminated packages with good specularly. Dunmore with help from Brookhaven would attempt to improve the life and reflectivity of this product. During the latter part of 1977, they produced 30 samples of film with various protective overcoats. These overcoats were applied with a granure process and included acrylics, polyesters, and crossed linked polyester-urethane materials. Table V.1 lists these materials.

Table V.1

Overcoating Materials List

<u>Dummore Product No.</u>	<u>Overcoat Generic type</u>	<u>External uv Stabilized</u>
393	Polyester	Yes
73X1	Polyester urethane	Yes
73X2	Acrylic	Yes
73X3	Urethane	No
73X4	Acrylic	No
73X5	Thermosetting acrylic	No
73X6	Vinyl acrylic	Yes
73X7	Acrylic	Yes
73X8	Thermosetting-modified PET	No
73X9	Thermosetting-modified PET	No
73X10	Thermosetting-modified PET	No
73X11	Vinyl acrylic	Yes
73X12	Acrylic	No
73X13	Waterborne aliphatic urethane	No
73X14	Polyester urethane	No
73X15	Vinyl urethane	Yes
73X16	Thermosetting vinyl	Yes
73X17	Thermosetting polyester	No
73X18	Thermosetting vinyl polyester	No
73X19	Polyester urethane	No
73X20	Thermosetting vinyl polyester	No
73X21	Modified oilfree alkyd	Yes
73X22	Cellulose modified acrylic	Yes
73X23	Aliphatic acrylic urethane	No
73X24	Acrylic (proprietary, vendor would not divulge)	No
73X25	UV-Cured acrylate	No
73X26	Polyester primer and polyester urethane topcoat	No
73X27	Acrylic primer and silicone topcoat	No
73X28	Waterborne acrylic lacquer	No
73X29	Thermoseting urethane	No
73X30	Silicone-modified polyester	No
DL-50	Polyester	Yes

The reflectivity of each virgin sample was measured at various sites on the sample and an average reflectivity obtained. Also the reflectivity of each sample was measured at various solar intensities. All the data taken for each sample were correlated relative to the solar intensity using a linear least squares fit.

It is interesting to note that the reflectivity of all the samples measured had a negative dependence on solar intensity similar to that shown in Figure 42. Two factors produced this result. At lower solar intensities more infrared is present in the solar spectrum and aluminum has a better coefficient of reflection for infrared than for visible light. Also the protective overcoats may be selective in their absorption spectra. The virgin reflectivity at solar intensities corresponding to typical air mass 1 and air mass 2 conditions for the 30 samples is summarized in Table V.2.

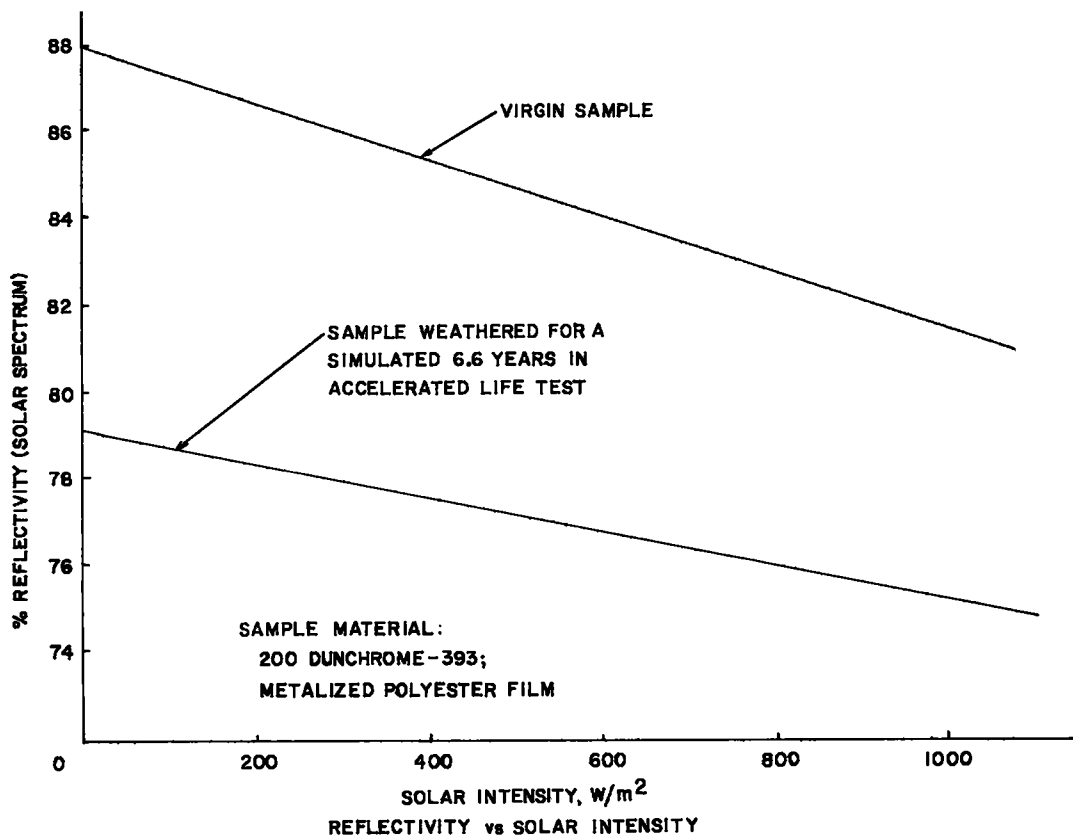


Figure 42. Reflectivity characteristic of Dunmore film 393.

Table V.2

Summary of Reflectivity of Virgin Samples

BNL sample No.	Dunmore sample No.	% Reflectivity		Slope % change per 1000 W/m ²	Overcoat thickness, in.
		Air mass 1	Air mass 2		
10 BNL Samples	393	82.6	83.6	5.62	0.00081
38B&38C	73X1	77.1	78.7	9.09	0.00081
39B&39C	73X2	76.9	79.2	9.09	0.00116
42	73X3	80.8	82.2	8.14	0.00038
43	73X4	81.3	82.2	4.92	0.00076
44	73X5	81.7	82.6	5.35	0.00060
50	73X6	81.0	82.0	5.10	0.00086
51	73X7*	-	-	-	-
52	73X8	80.6	81.0	2.20	0.00013
53	73X9	81.9	82.05	0.31	0.00042
54	73X10	76.7	77.9	-6.97	0.00021
55	73X11	82.1	81.8	-0.84	0.00025
59	73X12	82.0	82.2	-1.14	0.00037
60	73X13	78.8	80.2	-7.33	0.00078
61	73X18	78.8	77.9	-4.31	0.00052
62	73X15	81.5	84.0	-13.60	0.00021
70	73X16	81.1	82.2	-6.12	0.00021
71	73X17	79.2	80.5	-7.54	0.00009
72	73X18	79.2	79.5	-1.61	0.00015
73	73X19	77.8	79.5	-9.59	0.00015
74	73X20	84.1	84.6	-2.98	0.00015
77	73X21	83.5	84.1	-3.07	0.00010
79	73X22	81.6	82.7	-6.31	0.00004
80	73X23	82.2	83.3	-6.13	0.00017
88	73x24	85.3	86.1	-4.31	0.00015
89	73x25	84.1	84.6	3.05	0.00007
90	73x26	79.9	80.6	-4.24	0.00009
91	73x27	83.5	83.7	-1.07	0.00031
92	73x29	81.02	82.01	-5.59	0.00008
110	73x30	77.54	78.40	-4.85	0.00010
169	D1-50	74.6	78.9	-	-

(2nd surface mirror)

*Note both samples of 73x7 overcoat damaged at Brookhaven by a 1/3 ammonia and water solution while cleaning.

Of the 30 specially prepared samples, only 6 exceeded the original 393 material in reflectivity and only 1, sample 73X24, reached the reflectivity objective of 86%.

Other samples were exposed to an accelerated weatherability test. This accelerated life test consisted of an Atlas DMC twin arc weatherometer employing a duty cycle of 102 min of arc light, followed by an additional 18 min of arc light and water spray. This cycle was continuously repeated. The samples were visually examined daily during this exposure.

300 hours in the accelerated test is equivalent in ultraviolet exposure to 1 year of real time exposure in north-temperate latitudes. Each of the 30 overcoated samples was given a 300-hour accelerated life exposure as a first step in determining candidates for further work. Samples that had acceptable initial reflectivity and that satisfactorily survived the first 300 hours of accelerated exposure were subjected to additional exposure.

The original 393 overcoated material was also given additional exposure and became the reference sample for gauging improvement. Figure 42 plots solar intensity versus reflectivity for this 393 reference sample as measured before and after exposure to 1906 hours of accelerated life test. After this exposure, equivalent to 6.3 years, the reflectivity has dropped 8.4%. Table V.3 summarizes the solar reflectivity changes that occurred in the accelerated life test for the 393 material and certain promising alternates.

Only material 73X8 and 73X9 were subjected to the 6.3 year equivalent exposure. Material 78X8 showed the smaller loss in reflectivity but displayed a lower virgin reflectivity.

No clearly improved overcoat material could be identified.

The body film (Melinex) was not uv stabilized and therefore this film could not be used as a second surface reflector. Later Dunmore modified the body material to include a uv stabilizer and renamed this material DL-50. A second surface mirror made from this DL-50 material became a candidate. The resulting reflectivity was disappointing. A solar reflectivity below 78.9 was measured.

TABLE V.3

Summary of Solar Reflectivity With Exposure in Accelerated Life Tests

BNL No.	Dunmore Material no.	Reflectivity virgin	Reflectivity after accel. exp.	Reflectivity decrease	Hours accel. exp.	Equivalent years weather- ability
111,112	393	83.6	76.4	8.6	1906	6.3
43,115	73X4	82.2	74.9	8.9	1596	5.3
45,116	73X5	82.6	75.6	8.5	1596	5.3
52,114	73X8	81.0	75.4	6.9	1906	6.3
53,113	73X9	82.1	71.5	12.9	1906	6.3
74,174	73X20	84.6	74.5	11.9	1000	3.3
77,175	73X21	84.1	77.0	8.4	1000	3.3
79,176	73X22	82.7	77.5	6.3	1000	3.3
80,177	73X23	83.3	76.3	8.4	1000	3.3
88,178	73X24	86.1	75.7	12.1	1000	3.3
169	DL-50 (2nd Surface)	78.9	-	-	-	-
186	DL-50 (1st Surface)		78.2	6.4	1000	3.3

A finished mirror panel made from dunmore material 393 was sent to the San Albuquerque Laboratory for testing and evaluation. The tests were conducted through arrangements made with Mr. L. G. Rainhart. Reflectivity versus illumination wavelength was measured both upon arrival and after a 1000 hour exposure to ultraviolet light. The reported results are shown in Figure 43. The average total spectrum reflectivity did not change measurably as a result of the ultraviolet exposure although the reflectivity/wavelength distribution character was altered.

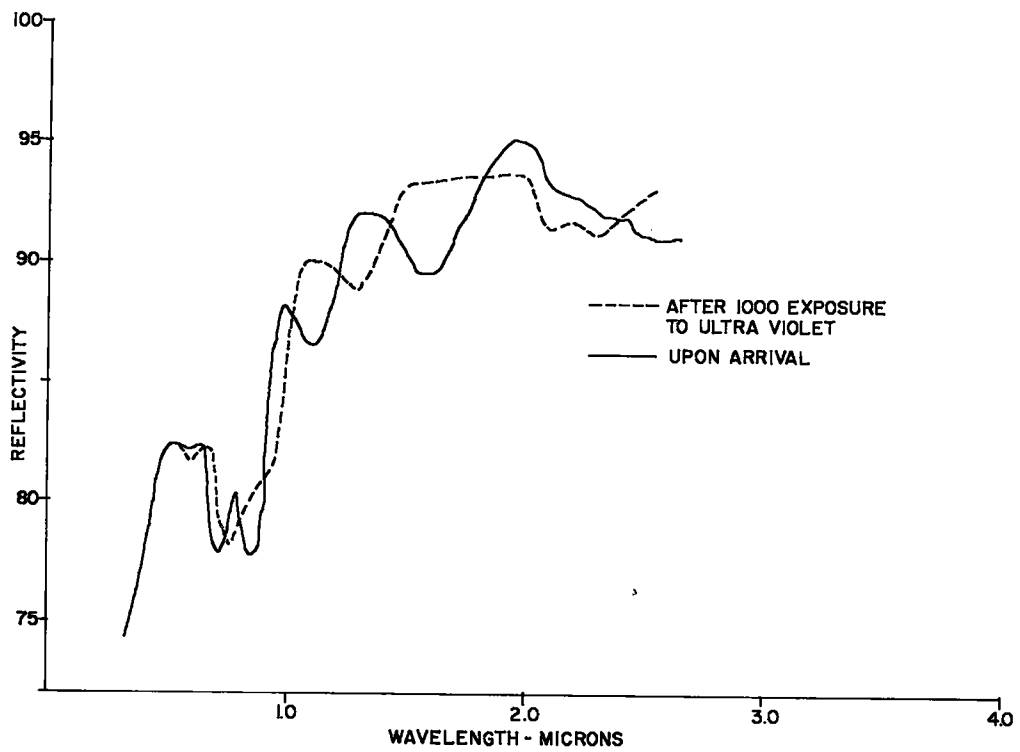


Figure 43. Reflectivity spectrum for Dunmore material 393 before and after exposure to ultra violet radiation.

SECTION VI
WIND-SOLAR INSOLATION STUDIES

VI.A. Analysis

The purpose of this wind-solar insolation correlation study is two-fold.

1. To test the validity of the wind-avoidance concept described in Section III.A.
2. To develop an operational scenario for the heliostat fold-down action to accomplish wind avoidance while maximizing solar energy collection.

Nine years of hourly climatology data for Upton, NY were studied as a first step. Hourly solar insolation as measured on a horizontal surface was summed to determine the quantity received at wind speeds below a specified value. This wind speed value was incremented from zero in 1 mph steps. The wind readings at 37 feet above the surface were used in this analysis. The result is displayed in Figure 44. The dashed lines show the extreme results for individual years, and the solid line is the computer-derived mean. The year 1970 was omitted from the analysis because a large block of data was missing as a result of instrument failure that year.

The results were encouraging and indicate that 95% of all solar energy received at Upton, NY, occurs with wind speeds below 15 mph for a typical year and during a worst case year 93% could be collected, if the heliostat were taken out of service and folded facedown for wind speeds above 15 mph.

To expand the scope of this wind-insolation correlation, SOMET tapes for 12 additional locations were obtained and similarly processed. These locations were:

Bismarck, ND,
Brownsville, TX,
Caribou, ME,
Dodge City, KS,
Fresno, CA,
Lake Charles, LA,
Miami, FL,
Nashville, TN,
Phoenix, AZ,
Santa Maria, CA,
Seattle, WA,
Washington, DC.

A map showing these locations is presented in Figure 45, and the expanded results are shown in Figures 46 and 47.

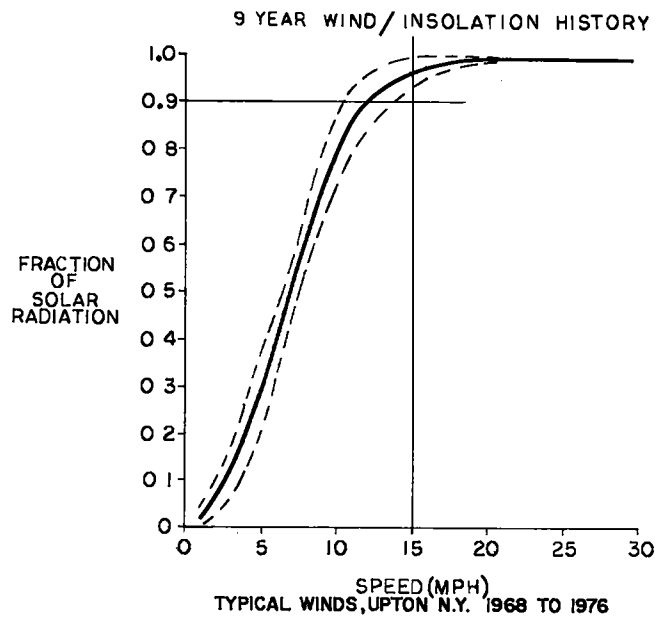


Figure 44. Wind-solar insolation correlation for Upton, NY.



WIND DATA LOCATIONS

Figure 45. Location of cities chosen for wind-solar insolation study.

Most of the new locations analyzed experienced more wind and the wind-speed limit for the wind-avoidance concept had to be increased. The 15-mph limit, satisfactory for Upton, NY, was not satisfactory for most other locations. A wind-speed limit of 20 mph was satisfactory for all locations in the East Coast steam technology area. Only the following locations analyzed were too windy to permit the 20 mph wind avoidance criteria:

Bismarck, ND,
Brownsville, TX,
Caribou, ME,
Dodge City, KS.

Caribou, Maine, is too far north to be an acceptable site for a solar steam installation. The other three locations are in the Great Plains for which a stronger heliostat must be developed. For these locations energy collection must occur at wind speeds up to 25 mph.

As a result of this analysis the heliostat prototype built at Brookhaven was designed to hold a solar image on target for wind speeds up to 20 mph. At this wind speed the image was allowed to be half-off target.

VI.B. Wind Gusts

The up-position heliostat damage limit is determined from wind gust studies. Once the wind speed exceeds the wind-avoidance limit (20 mph in the prototype case), a heliostat fold-down sequence is initiated. This process may require from 10 to 15 minutes. How strong will the wind gust be during this fold-down time?

One-year wind-gust data records from Upton, NY and from the nearby Brookhaven Airport were obtained and searched for periods of high wind (greater than 30 mph). The wind gust records for the worst of these periods are shown in Figure 48. In one case (3/19/75) the wind speed reached 40 mph 15 minutes after crossing the 20-mph criterion. A heliostat operating at this time could have experienced a 40-mph gust before reaching the safe fold-down position. This case occurred at night when the heliostat should be in the fold-down position and thus would have escaped exposure to this gust. Dr. S. Sethuraman, Brookhaven meteorologist, advised us to ignore this fact since there is no identifiable day-night preference for high wind storms.

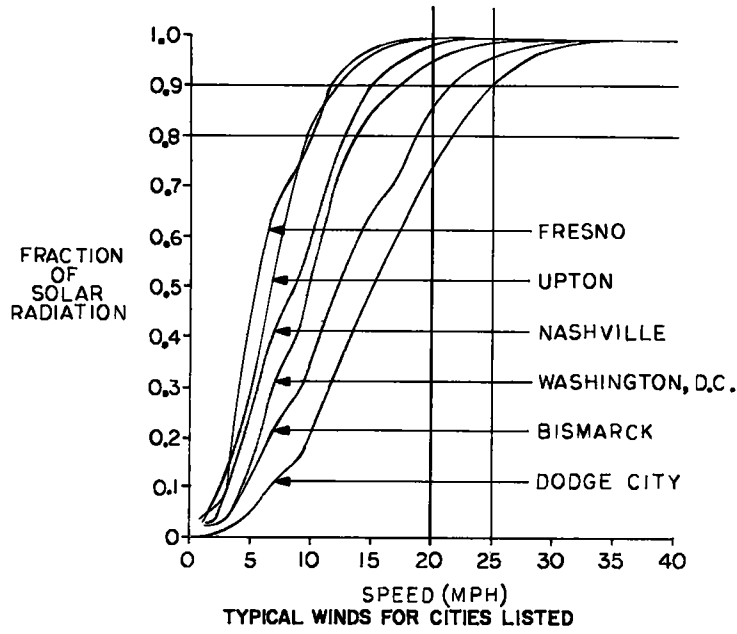


Figure 46. Wind-solar insolation history.

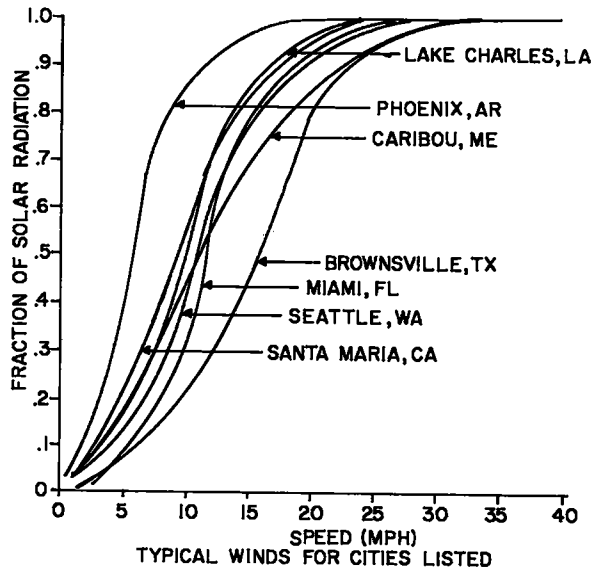


Figure 47. Wind-solar insolation history continued.

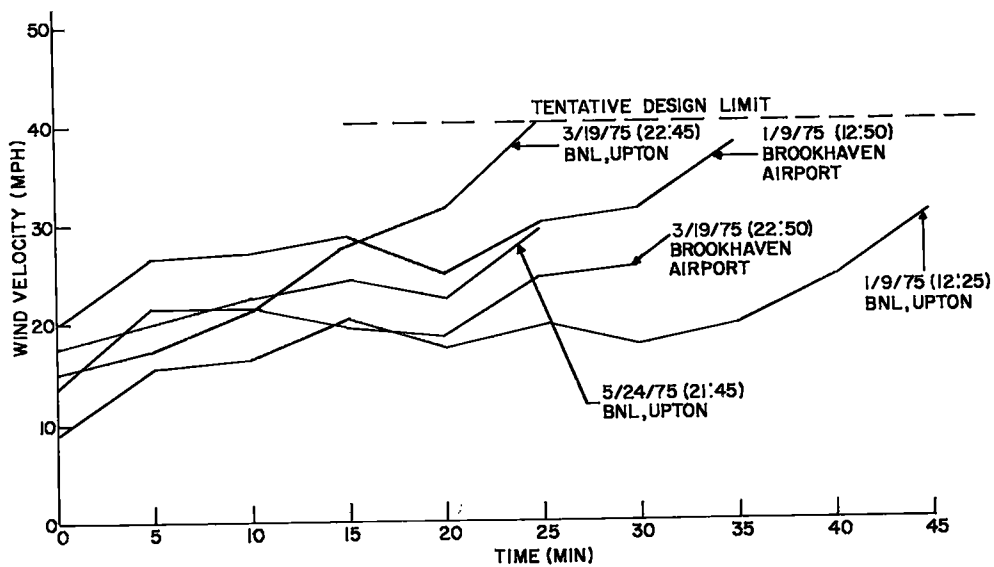


Figure 48. Wind gust record Upton, NY, and Brookhaven Airport.

In view of this wind-gust record, a heliostat damage wind velocity criterion of 50 mph was imposed for the up-position. This gave a 10 mph safety above the worst gust identified in the analysis described. Wind gusts of 50 mph are rare in this area and no record of such velocity could be found for sunlight conditions. In general, such wind velocities occur during or preceding hurricanes for which ample warnings are now given.

VI.C. Operational Scenario

The following operational scenario is recommended.

1. The heliostat is to be stored in the fully fold-down position during all nonsolar hours (night and cloudy).
2. The heliostat is to be raised and made to track during sunlight periods with wind speeds below 20 mph.
3. The fold-down sequence is to be initiated when the 5-min mean wind speed exceeds 20 mph.
4. The heliostat is to be held in fold-down position during periods of predicted hurricanes and other bad weather conditions.

SECTION VII
HELIOSTAT OPTICS AND FIELD CONFIGURATION

A heliostat can be built to produce a good image on-axis but as the image moves off-axis a distortion occurs which is a function of the off-axis angle and the f number of the optics. The f number is defined in the normal way and is the focal distance divided by the optical aperture, which in this case is the heliostat diameter. The f numbers are listed for each heliostat class in Table VII.1.

Heliostats near the target tower but not directly north of it encounter the greatest off-axis conditions. Off-axis distortion increases rapidly for heliostats located south of the tower. Because of this off-axis distortion of the image, a careful review of the optics is required to design the proper heliostat field for a small "power tower" solar energy collector.

To accomplish this analysis, a simple ray tracing computer program was written and used as a design tool. This simple program was made practical because of the relatively small number of heliostats planned.

Each heliostat was divided into an 11 x 11 faceted array (121 facets) and the ray from each facet of every heliostat was followed and results summed. The line of sight from each facet to the sun and to the target was tested for obstruction. This subroutine was useful as a separate routine for preliminary heliostat field design. In general, designs with optimum shadowing were also optimum overall and needed only to be performance evaluated.

A ray that was not shadowed was tested to see if it intersected the target. If so, energy from that facet was accrued with assigned weighting factors. Two weighting factors were used. One, proportional to the average of the facet area projected normal to the incident solar ray--namely, the cosine of the angle of incidence of that facet, and the second, proportional to the intensity of the normal incident solar irradiation for that hour and date. The solar intensity weighting factors were obtained from the ASHRAE Handbook of Fundamentals, 1972, Chapter 22, page 390. Values for 40 degrees

latitude were used. Only the relative values of these weighting factors are important since they were used only as weighting factors to make performance comparisons. No attempt was made to calculate total energy collections. The program used hourly steps and accrued monthly and annual energy sums. From these sums performance coefficients were derived and performance comparisons made.

Heliostats planned for different locations in the field require different focal lengths. This is accomplished by inserting shims under individual facets. All heliostat support structures and facets are identical and can be interchanged without altering the focal properties.

Analysis with the computer program described revealed that heliostat focal length could be grouped into four sets. These groups were given class nomenclature and focal length assignments as indicated in Table VII.1.

Table VII.1

<u>Class</u>	<u>Focal length,ft</u>	<u>f Number</u>
I	60	3.75
II	95	5.94
III	130	8.13
IV	165	10.31

An attempt to quantitize into only three classes was made but results were not satisfactory.

This computer analysis resulted in three optimum heliostat field designs of similar performance. The three designs contained 51, 53, and 55 heliostats respectively, and are described in Tables VII.3 to VII.5 and in Figures 49, to 51. Considerable information has been displayed in these figures and some explanation of the coding of this information is needed.

All designs are right-left symmetrical and the resulting coefficients for the two sides are the same. It is, therefore, convenient to use the left side of the figure to display one set of information, namely the heliostat class and shadowing coefficient, and the right side of the figure to display a second information set, namely, the projection or cosine coefficient and the total performance effectiveness. A symbol set at the top of each figure is a key to this display scheme. Note that heliostats on the north-south center line must contain all four items of information.

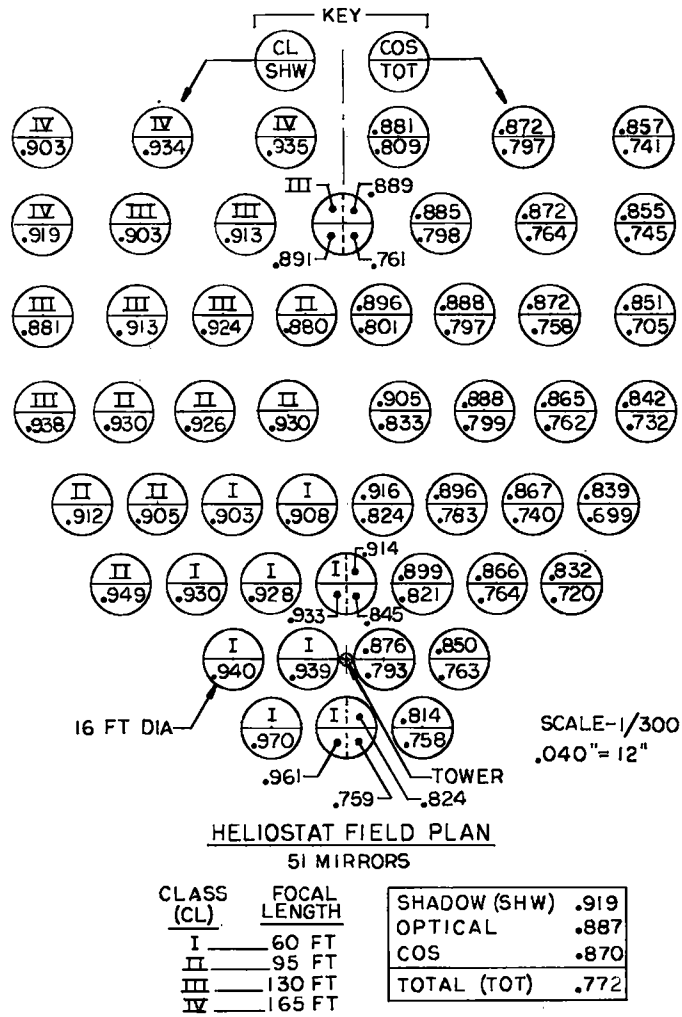
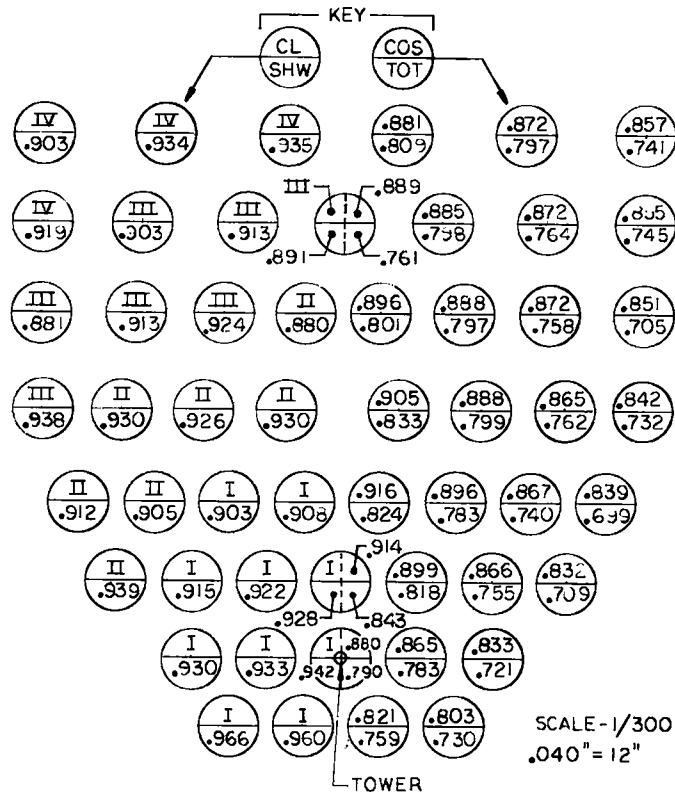


Figure 49. Heliostat field performance chart - 51 units design.



HELIOSTAT FIELD PLAN
53 MIRRORS

CLASS (CL)	FOCAL LENGTH	SHADOW (SHW)	OPTICAL
I	60 FT	.918	.885
II	95 FT	.868	
III	130 FT		
IV	165 FT		
		TOTAL (TOT)	.768

Figure 50. Heliostat field performance chart - 53 unit design.

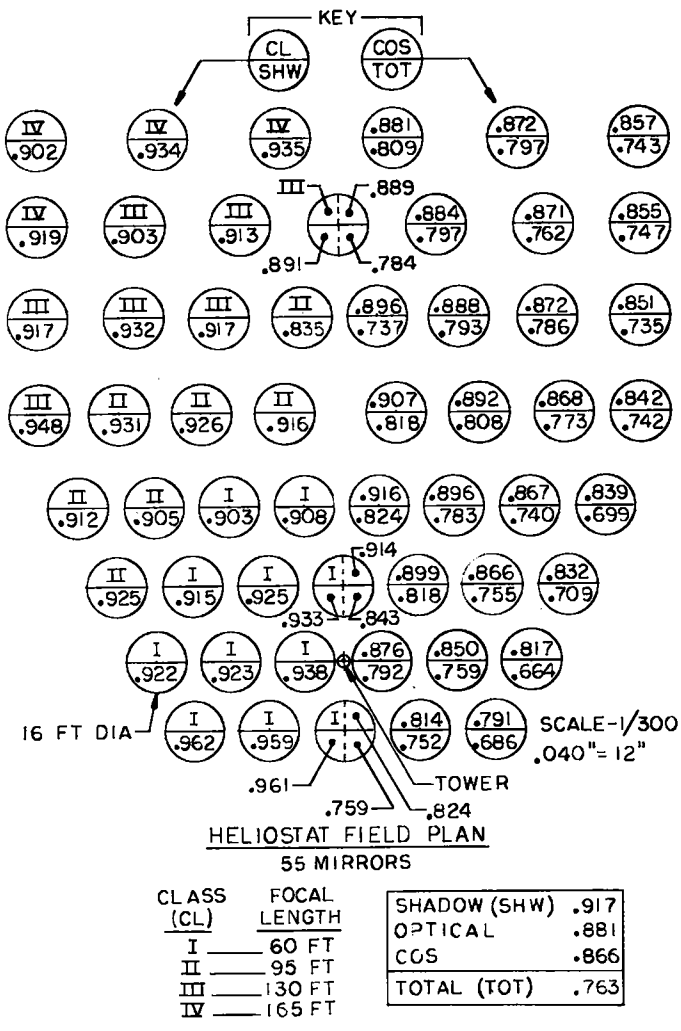


Figure 51. Heliostat field performance chart - 55 unit design.

Table VII.2

<u>Number of heliostats</u>	<u>Annual efficiency</u>	<u>Normalized solar energy collected</u>
51	0.772	1.0
53	0.768	1.034
55	0.763	1.066

Table VII.3

Heliostat Field Coordinates

51 Heliostat Field Design

<u>Row (south positive)</u>	<u>E-W location, ft</u>
+ 18	-20, 0, +20
0	-30, -10, +10, +30
- 20	-60, -40, -20, 0, +20, +40, +60
- 41	-70, -50, -30, -10, +10, +30, +50, +70
- 65.5	-80, -59, -37, -15, +15, +37, +59, +80
- 91	-80, -55, -32, -10, +10, +32, +55, +80
-115	-80, -54, -26, 0, +26, +54, +80
-138	-80, -48, -15, +15, +48, +80

Table VII.4

Heliostat Field Coordinates

53 Heliostat Field Design

<u>Row (south positive)</u>	<u>E-W location, ft</u>
+ 18	-30, -10, +10, +30
0	-40, -20, 0, +20, +40
- 20	-60, -40, -20, 0, +20, +40, +60
- 41	-70, -50, -30, -10, +10, +30, +50, +70
- 65.5	-80, -59, -37, -15, +15, +37, +59, +80
- 91	-80, -55, -32, -10, +10, +32, +55, +80
-115	-80, -54, -26, 0, +26, +54, +80
-138	-80, -48, -15, +15, +48, +80

Table VII.5
Heliostat Field Coordinates
55 Heliostat Field Design

<u>Row (south positive)</u>	<u>E-W location, ft</u>
+ 18	-40, -20, 0, +20, +40
0	-50, -30, -10, +10, +30, +50
- 20	-60, -40, -20, 0, +20, +40, +60
- 41	-70, -50, -30, -10, +10, +30, +50, +70
- 65.5	-80, -59, -37, -15, +15, +37, +59, +80
- 91	-80, -55, -32, -10, +10, +32, +55, +80
-115	-80, -54, -26, 0, +26, +54, +80
-138	-80, -48, -15, +15, +48, +80

SECTION VIII
NORMAL INCIDENT SOLAR RADIATION MEASUREMENT

The Northeastern part of the United States is not the sunniest part of the country, and for this reason much of the solar energy research and demonstration is planned and conducted in the Southwest. This is particularly true for energy-concentrating-type systems. These systems collect energy only from the normal incident beam and it is this energy form that is most affected by atmosphere scattering. Collecting systems that respond to scattered light re-collect some of the energy scattered from the direct beam.

Nevertheless, concentrating-type systems must not be eliminated from the Northeast region of the country since their high temperature output is essential to certain applications. Most cooling, mechanical, and electrical generating systems fall into this application set. The Northeast is also unique in that it has an in-place steam utilization technology with many building systems completely motivated by steam for both heating and cooling purposes.

As part of the heliostat development project at Brookhaven National Laboratory normal incident solar radiation measurements were made at Upton, NY, which is located on Long Island, 70 miles east of New York City. For this purpose an Eppley Normal Incident Pyrheliometer was mounted on the roof of the Atmospheric Science Building and operated by that group. Daily data were digitally recorded and processed by R. M. Brown. These data together with pyranometer readings giving the radiations received on a horizontal surface were processed by D. White and C. Henderson under the able direction of J. Tichler. This analysis is based on data collected over the 13-month period from June 1977 to June 1978.

In order that total incident energy be determined missing and erroneous data must be restored. Two principal causes of missing data are failure in the recording equipment and tracking errors. Mr. Paul Vosganian joined our staff in the summer of 1978 and addressed this data restoration problem. The normal incident readings were plotted versus the pyranometer reading for each

month. Plots thus made display a general smooth relationship. Data points far removed from this smooth curve were considered erroneous and were eliminated. The remaining data were fitted with a curve of the form $y = ax^n$ using a least squares method. Missing and erroneous pyrheliometer readings were replaced by values read used from the curve fit, if pyranometer readings were available. If no readings were available, the pyrheliometer value was assumed to be equal to the average for the month. Table VIII.1 summarizes these results. For comparison, long term values for solar radiation measured on a horizontal surface copied from ref. 1 are also included in this table.

It is clear from examining Table VIII.1 that the period over which these measurements were made was not typical and, in general, less solar insolation was received than the average reported for this location. Figure 52 plots the monthly average atmospheric transmission coefficient \bar{K}_H , the daily average ratio of solar energy received on a horizontal surface to that outside the atmosphere, for the long-term Lui and Jordan data¹ and for the months recently measured. The 1977 time period is notably below the average. Figure 53 shows the horizontal insolation as reported by additional references.^{2,3}

Figure 53 clearly shows changes in the averages measured for different time periods. It is believed that the Lui and Jordan work¹ is based in part on data from the 1950 time period and is therefore higher than indicated by later measurement.

In an effort to relate this brief set of normal incident solar insolation measurements to that of other time periods, two parameters were defined: \bar{K}_H , defined as before, and \bar{K}_\perp , the same ratio measured at normal incidence. These parameters were computed for each day for which good data was available and grouped into small bins and averaged. The resulting data set was fit with a third order polynomial. The result is shown in Figure 54 and the equation for the fit is

$$\bar{K}_\perp = 0.5548(\bar{K}_H)^3 + 0.9949(\bar{K}_H)^2 - 0.4218 \bar{K}_H + 0.0526.$$

Figure 55 shows the daily data superimposed on this polynomial.

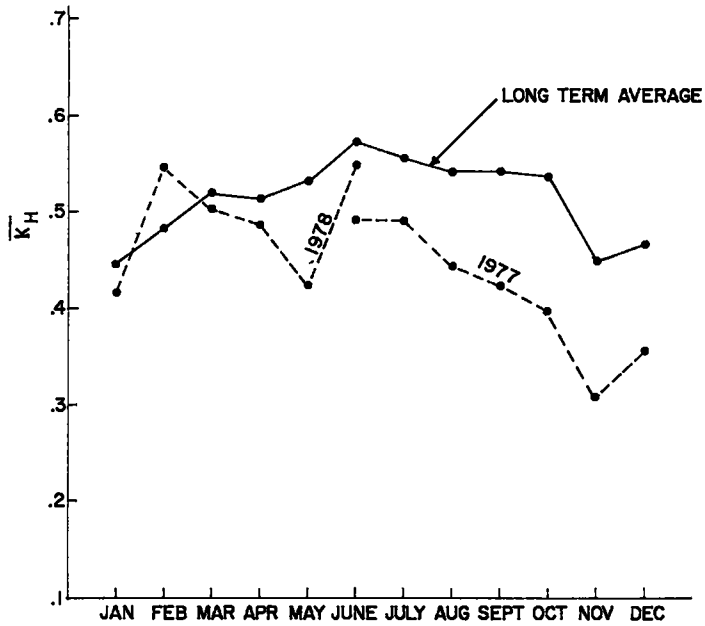


Figure 52. \bar{K}_H , the ratio of daily average radiation measured on a horizontal surface to that received outside the atmosphere, versus time.

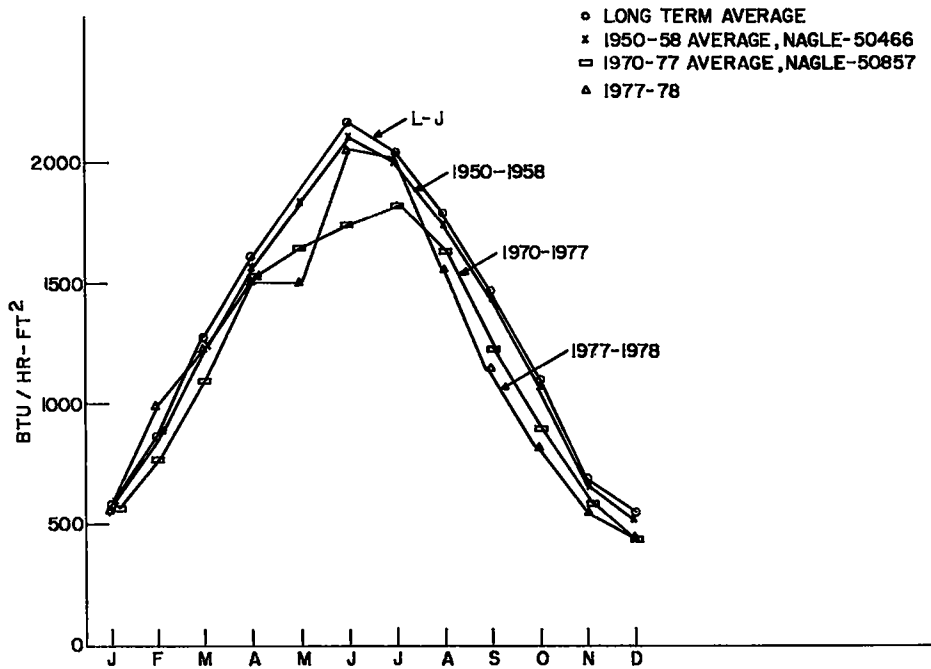


Figure 53. Solar radiation measured on a horizontal surface at Upton, NY, report by various authors and time periods.

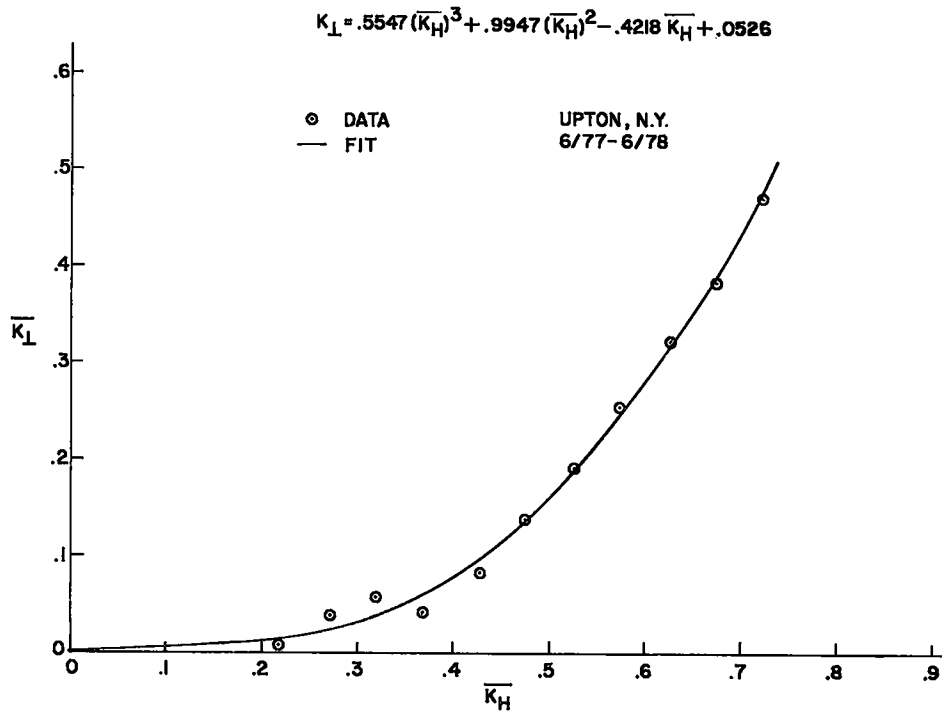


Figure 54. Measures values of \bar{K}_H versus \bar{K} grouped into bins and averaged for Upton, NY, 6/77 through 6/78 with least squares fit polynomial of 3rd order.

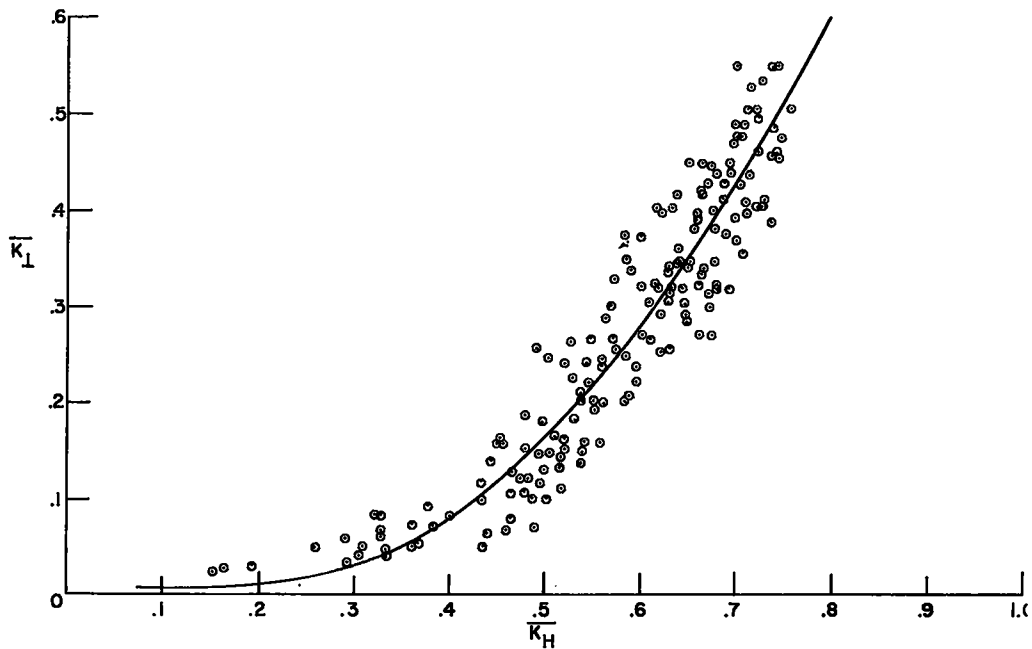


Figure 55. Daily values of \bar{K}_H and \bar{K} plotted against fit polynomial from Figure 3.

Table VIII.1

Solar Radiation Upton, NY (Btu/ft²)

<u>Total-horizonta! surface Upton, NY</u>				<u>Normal incident solar radiation</u>		
<u>Long-term</u> <u>Lui-Jordan</u>		<u>Measured</u> <u>daily average</u>	<u>Monthly</u> <u>total</u>		<u>Measured</u> <u>daily average</u>	<u>Monthly</u> <u>total</u>
2159.0	June '77	1856.0	55680	June '77	1270.0	38100
2044.6	July '77	2014.8	62459	July '77	1626.0	50406
1789.6	Aug '77	1467.5	45493	Aug '77	1022.5	31698
1472.7	Sept '77	1156.0	34680	Sept '77	914.6	27438
1102.6	Oct '77	820.4	25432	Oct '77	618.2	19164
686.7	Nov '77	473.1	14193	Nov '77	313.4	9402
551.3	Dec '77	439.0	13609	Dec '77	649.0	20119
583.0	Jan '78	547.6	16976	Jan '77	800.0	24800
872.7	Feb '78	993.5	27818	Feb '78	1517.2	42482
1280.4	Mar '78	1239.1	38412	Mar '78	1241.0	38471
1609.9	Apr '78	1526.9	45807	Apr '78	1279.5	38385
1891.5	May '78	1506.7	46708	May '78	1148.0	35588
2159.0	June '78	2067.1	62013	June '78	1624.4	48732

Yearly total 7/77-7/78, 4.34×10^5 Yearly Total, 7/77-6/78 3.87×10^5

This curve fit appears to be seasonally invariant. Data from widely spaced months are shown plotted superimposed with the curve of the polynomial in Figures 56 through 59 and no seasonal effects are evident. Time will test this invariant observation.

If the relationship between these two atmospheric transmission coefficients is seasonally invariant, it is reasonable to expect it to be invariant over the long term, since it is in major part a comparison between two methods of measuring the transmission of solar energy through the atmosphere. With the assumption of a fixed relationship between horizontally and normal incident measured transmission coefficient, estimations of normal incident radiation for other time periods are made possible using the existing horizontally measured data. The method proceeds as follows:

A_{\perp} , the annual total solar energy received at normal incidence, is given by

$$A_{\perp} = \sum_{\text{year}} I_{\text{Dn}} ,$$

where I_{Dn} = daily insolation received at normal incidence.

\bar{K}_{\perp} is defined as

$$\bar{K}_{\perp} = \frac{I_{\text{Dn}}}{I_{\text{on}}} ,$$

where I_{on} = daily insolation received at normal incidence outside atmosphere, and is given by

$$I_{\text{on}} = \frac{24}{\pi} w_s r I_{\text{sc}} ,$$

where

$$w_s = 1/2 \text{ daylight (radians),}$$

$$w_s = \cos^{-1} (- \tan L \tan \delta),$$

$$L = \text{latitude,}$$

δ = declination,

r = ratio solar intensity to mean solar intensity outside the atmosphere,

$$I_{sc} = 428.38 \text{ Btu-hr}^{-1} - \text{ft}^{-2} \text{ or } 1350 \text{ W/m}^2.$$

\bar{K}_\perp is related to \bar{K}_H through the polynomial, and is equal to

$$0.5548(\bar{K}_H)^3 + 0.9949(\bar{K}_H)^2 - 0.4218\bar{K}_H + 0.0526 = F(\bar{K}_H).$$

\bar{K}_H can be determined from existing data,

$$\bar{K}_H = \frac{H(\text{measured})}{H_0},$$

where H_0 = daily total solar radiations received on a horizontal surface outside the atmosphere and is given by

$$H_0 = (24/\pi) r I_{sc} [\cos L \cos \delta \sin w_s + w_s \sin L \sin \delta],$$

since

$$I_{Dn} = I_{on} \bar{K}_\perp = I_{on} F(\bar{K}_H) = \frac{24}{\pi} w_s r I_{sc} F(\bar{K}_H).$$

Then

$$A_\perp = \frac{24}{\pi} I_{sc} \sum_{\text{year}} r w_s \times F(\bar{K}_H).$$

The \sum_{year} can be evaluated in segments, where each segment is made small enough to approximate a straight line. Within a segment $F(\bar{K}_H) = C_i$, where C_i is a constant that varies from segment to segment and is determined from the polynomial. The contribution to A_\perp from any segment becomes

$$\frac{24}{\pi} I_{sc} \sum_{\text{year}}^{\text{segment}} r w_s C_i = \frac{24}{\pi} I_{sc} C_i \sum_{\text{year}}^{\text{segment}} r w_s.$$

The term $\left[\sum_{\text{year}}^{\text{segment}} r w_s \right]$ is a weighted count of days occurring in the chosen \bar{K}_H segment with $r w_s$ used as the weighting factor. With this weighted count, the contribution of this segment to the quantity A_\perp can be determined. Summarizing over all segments yields the total A_\perp result.

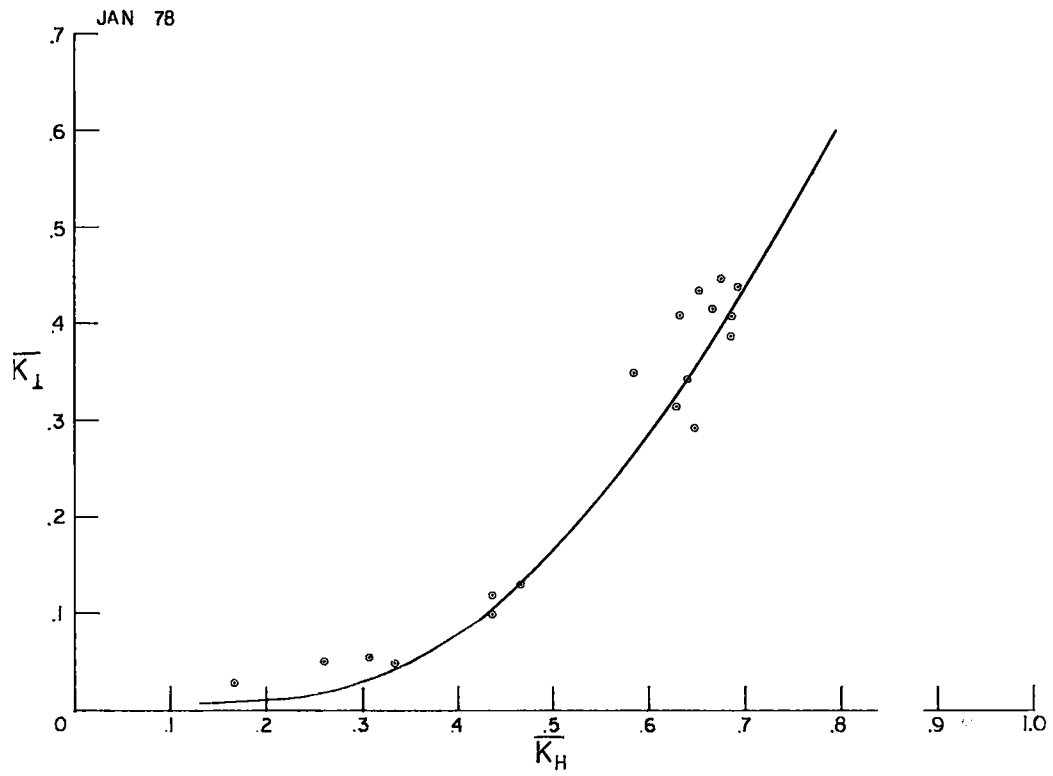


Figure 56. Curve fit versus data from January 1978

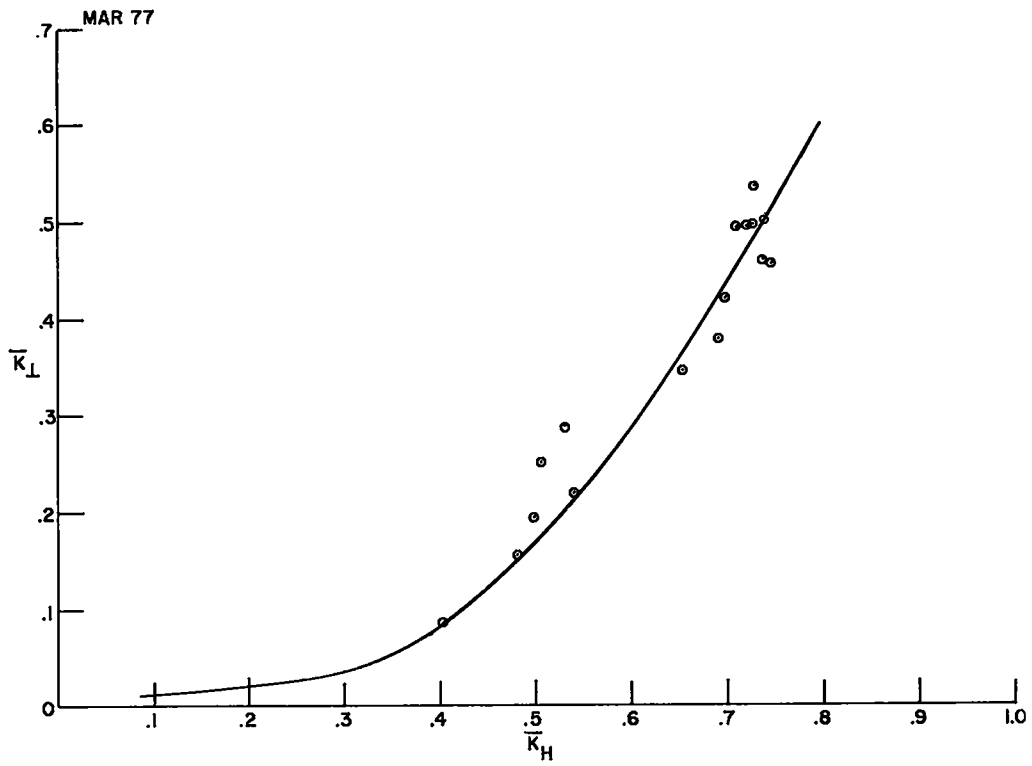


Figure 57. Curve fit versus data from March 1977.

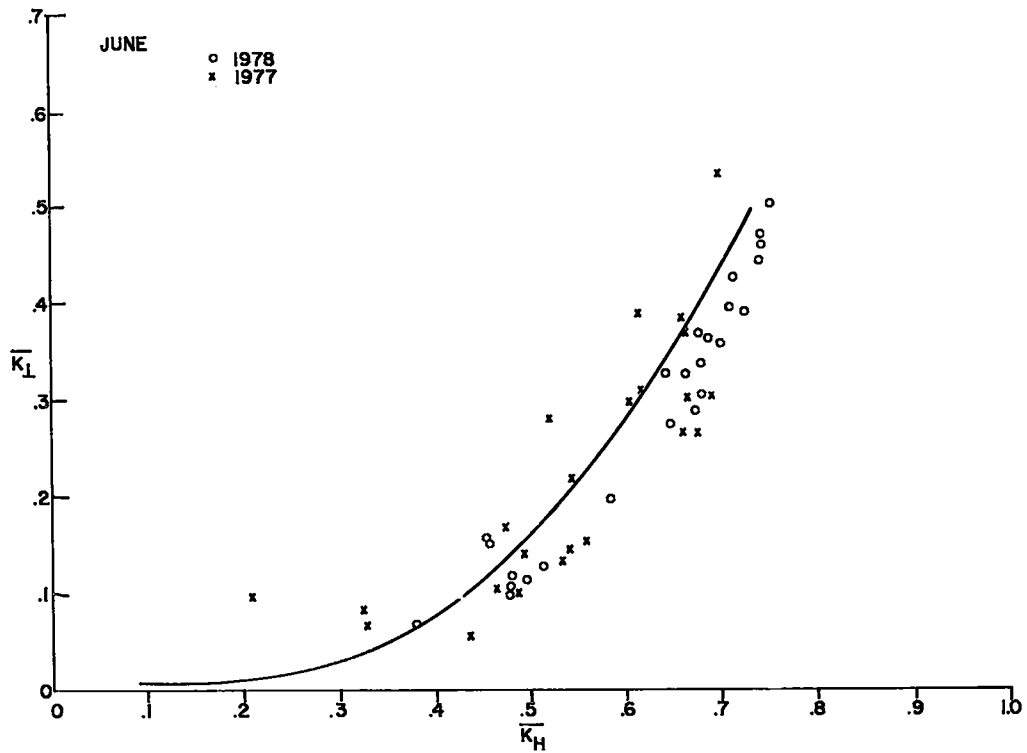


Figure 58. Curve fit versus data from June 1977 and 1978.

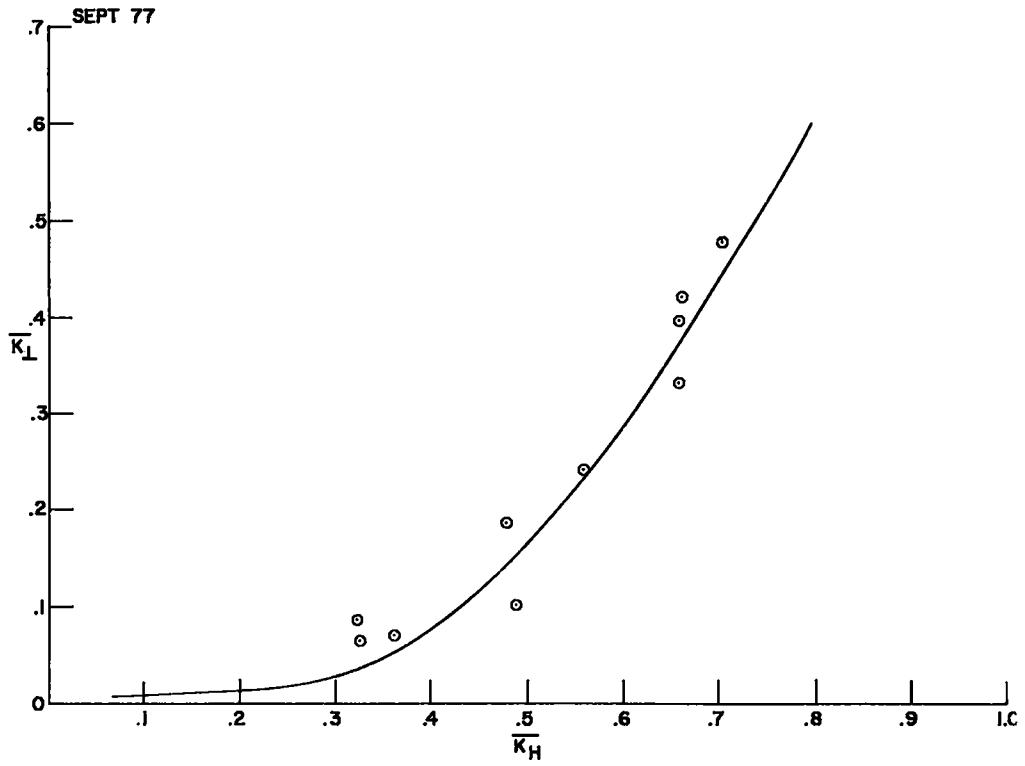


Figure 59. Curve fit versus data from September 1977.

Figure 60 shows the weighted \bar{K}_H occurrence frequency for Upton for two different time periods and illustrates the effect of climatic changes upon this weighted sum. Figure 61 shows the long-term occurrence frequency of \bar{K}_H for four other locations and the variation in this parameter with location along the Eastern Seaboard.

Using this method for computing A_{\perp} and measured \bar{K}_H occurrence frequency values for A_{\perp} can be determined for other locations. The results are summarized in Table VII.2. Table VIII.3 shows values of A_{\perp} as computed by William Dickinson.⁴

Table VIII.2

<u>Locations</u>	<u>Long-term annual solar energy received at normal incidences</u>
Boston, MA	3.51×10^5 Btu-ft ⁻² -yr ⁻¹
New York, NY	3.27
Sterling, VA	3.63
Cape Hatteras, NC	4.49
Greensboro, NC	4.29
Charleston, SC	3.95

Table VIII.3

<u>Locations</u>	<u>Long term annual solar energy received at normal incidences (ref. 4)</u>
Phoenix, AZ	7.98×10^5 Btu-ft ² -yr ⁻¹
Albuquerque, NM	8.19
Fort Worth, TX	5.45
Omaha, NB	5.17
Nashville, TN	4.17
Blue Hill, MA	3.78

Annual normal incident solar radiation received at Upton, NY, can also be computed for each year for which good horizontal data are available. Figure 62 presents these results. Data for the 1960's are missing. A smooth curve

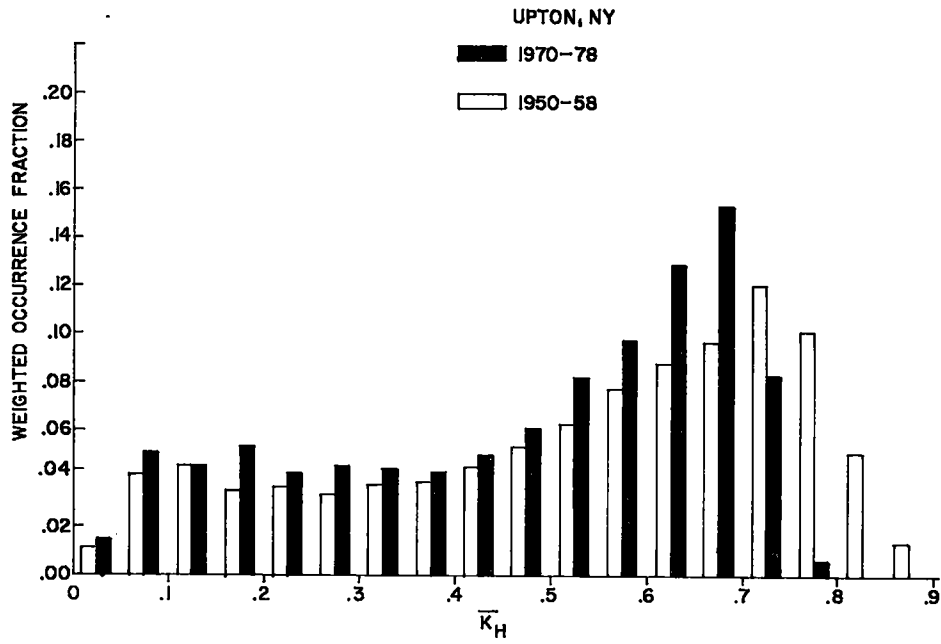


Figure 60. Weighted \bar{K}_H occurrence frequency for Upton, NY, for time period 1950-58 and 1970-78.

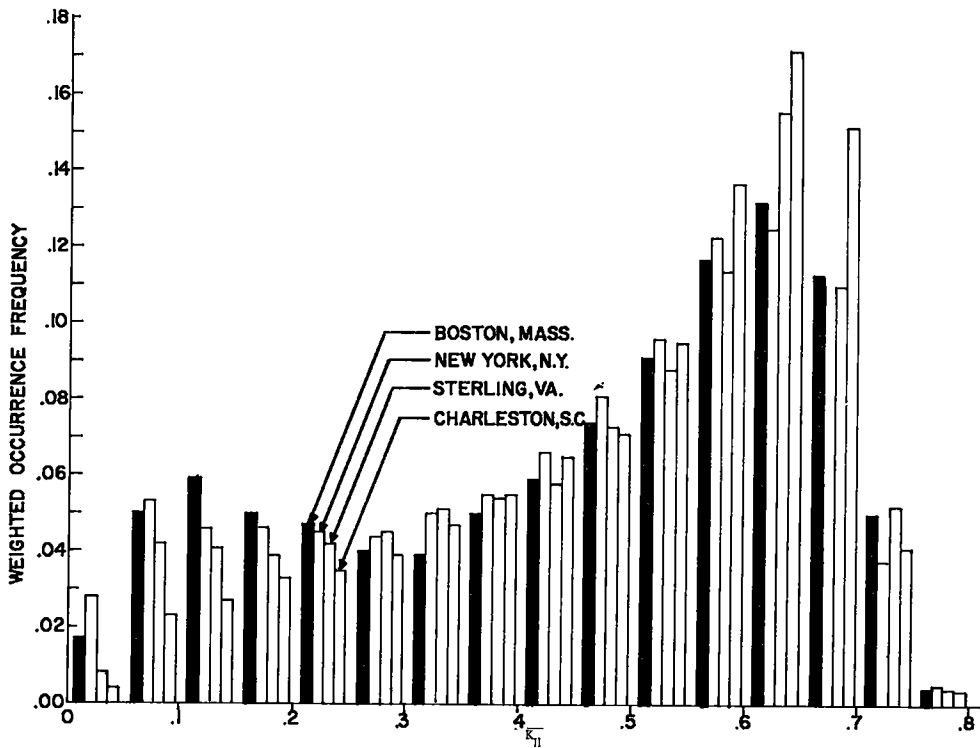


Figure 61. Long term weighted \bar{K}_H occurrence frequency for Boston, MA; New York, NY; Sterling, VA; Charleston, SC.

has been passed through the data of Figure 62 suggesting long-term seasonal changes. During the next decade, Upton, NY, might anticipate receiving an average of 5.0×10^5 Btu-ft²-yr⁻¹ solar radiation at normal incidence, if extrapolation from Figure 62 is valid.

Computed values of A_1 for three other sites, Greensboro and Cape Hatteras NC and New York City, were also examined for long term effects and none was found. These results are shown in Figures 63, 64, and 65.

ACKNOWLEDGMENTS

The author wishes to acknowledge the invaluable assistance and enthusiastic cooperation which he received from the meteorology group under the direction of Dr. Paul Michaels. The computer analysis by J. L. Techler, and the data reduction by Robert M. Brown and Paul Vasgianian were essential to this work.

REFERENCES

1. B.Y.H. Lui and R. C. Jordan, A rational procedure for predicting the long-term average performance of flat-plate solar-energy collectors, Sol Energy 7, No. 2 (1963).
2. Constance M. Nagle, Climatology of Brookhaven National Laboratory 1949 through 1973, BNL 50466, November 1975.
3. Constance M. Nagle, Climatology of Brookhaven National Laboratory 1974 through 1977, BNL 50857, May 1978.
4. William C. Dickinson, Annual available radiations for fixed and tracking collectors, Sol Energy, 21, No. 3 (1978).

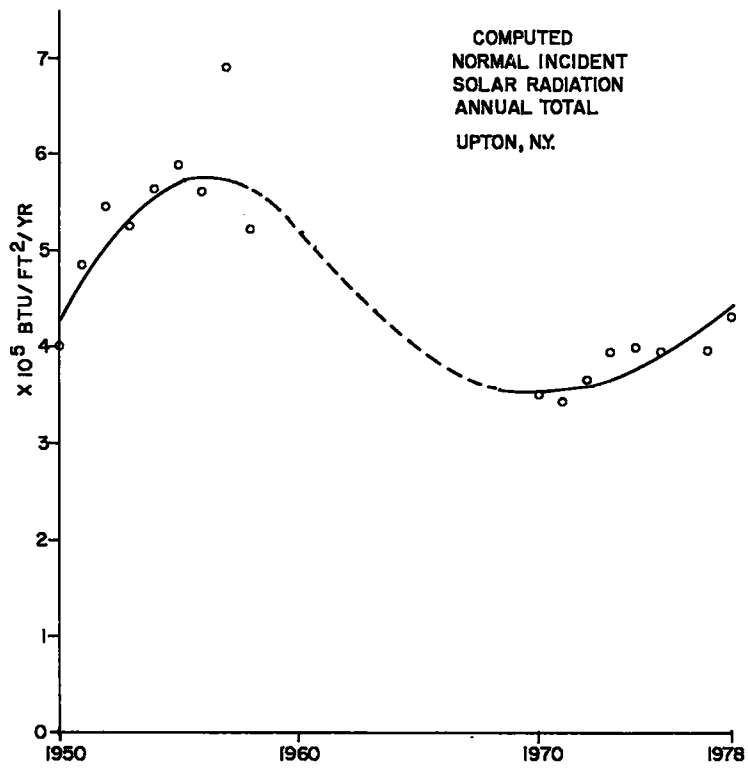


Figure 62. Computed annual normal incident solar radiation received at Upton, NY.

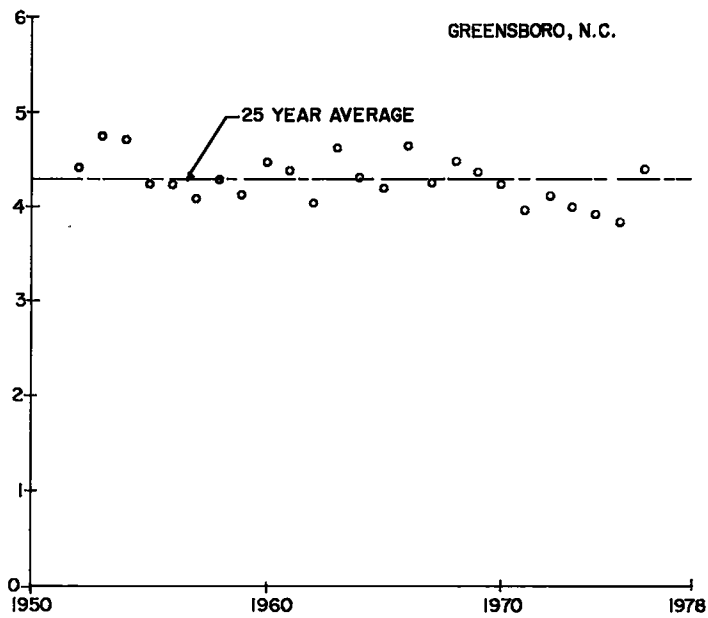


Figure 63. Computed annual normal incident solar radiation received at Greensboro, NC.

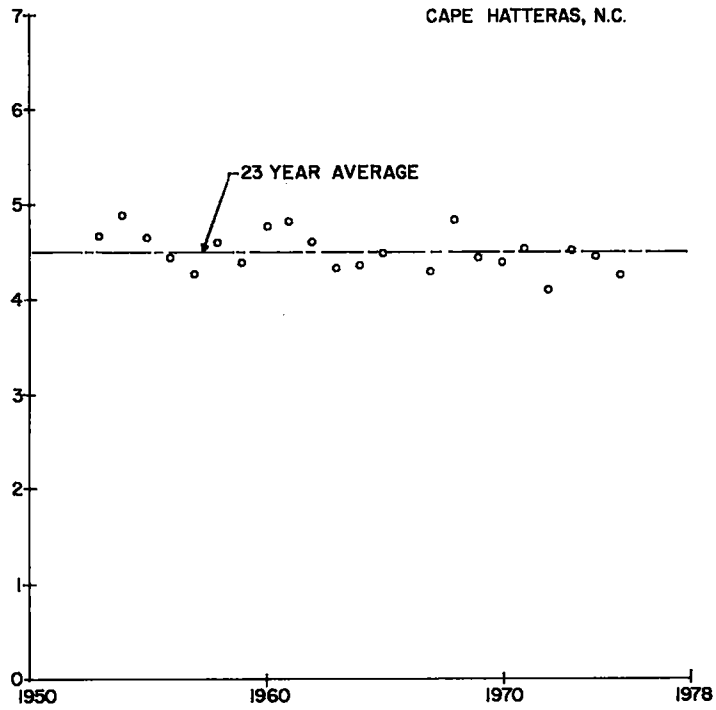


Figure 64. Computed annual normal incident solar radiation received at Cape Hatteras, NC.

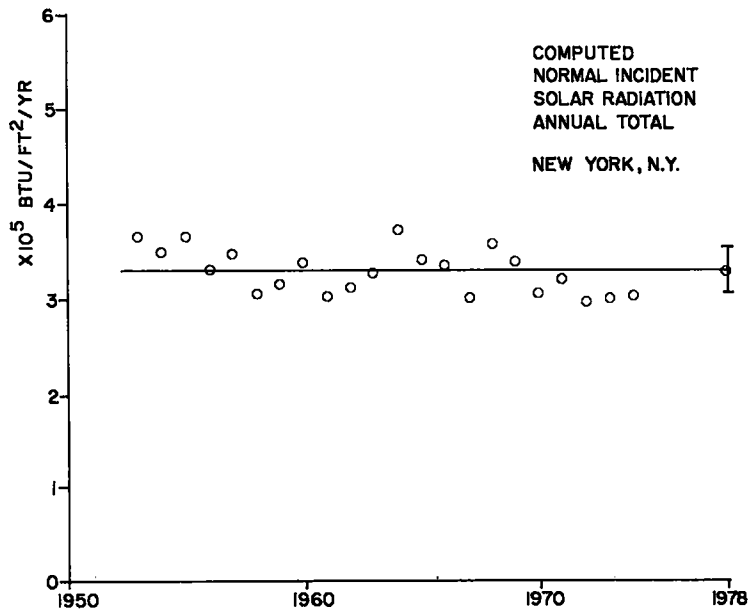


Figure 65. Computed annual normal incident solar radiation received New York, NY.

SECTION IX
HELIOSTAT PRODUCTION COST ANALYSIS--WESTINGHOUSE REPORT

Brookhaven issued a subcontract to the Advanced Energy Systems Division of the Westinghouse Electric Corporation to conduct a production cost analysis of the possible heliostat designs. Three designs were considered:

1. The Brookhaven design described in Section III of this report.
2. The same design modified for production.
3. A proprietary design under development at Westinghouse.

The description and cost estimates that follow are copied from Westinghouse's report on their work.

IX.A. Description of Westinghouse Proprietary Design

The Westinghouse heliostat design features an externally braced beam matrix reflector panel support structure borne by large-diameter elevation and azimuth rings. These large-diameter rings provide a stable platform for reflector panel positioning while translating wind-induced overturning moments into longitudinal reaction forces in the heliostat foundation.

The baseline heliostat reflector panel support structure is predicated on the use of 5- by 10-ft reflector panels arranged in a 4 by 3 array, providing an assembly having a 30- by 20-ft reflector surface. Each 10 ft-wide reflector panel is supported by two hat-shaped beams bonded to the back of the reflector panel. The support hats are located on the reflector panel in positions that create the minimum deflection of the panel for any uniform loading condition. The baseline heliostat also includes four reflector panels, mounted on the elevation wheel spokes, which provide an additional reflective area of approximately 30 square feet, bringing the total reflective surface to approximately 630 square feet without affecting the overall heliostat envelope or structure.

The reflector panel support hats are connected to transverse beams in the reflector panel support structure. The longitudinal spacing of the transverse beams has been chosen to minimize the bending moments and deflections of the reflector panel assemblies. The transverse beams are supported by two longitudinal beams which carry the reflector panel loads to the elevation wheels. The transverse pitch of the longitudinal beams has been chosen to minimize both bending moments and deflections in the transverse beams.

The reflector panel support hats are connected to transverse beams in the reflector panel support structure. The longitudinal spacing of the transverse beams has been chosen to minimize the bending moments and deflections of the reflector panel assemblies. The transverse beams are supported by two longitudinal beams which carry the reflector panel loads to the elevation wheels. The transverse pitch of the longitudinal beams has been chosen to minimize both bending moments and deflections in the transverse beam.

Geometric considerations preclude optimization of the incidence of the load and support points on the longitudinal beams, but deflection of these two members is limited by use of a diagonally disposed beam in each reflector panel bay and by the external support rods attached to the end of each longitudinal beam.

The single-spoke elevation rings are integral parts of the reflector panel support structure as well as the means for providing elevation adjustment. The longitudinal reflector panel support beams are attached directly to the spokes of the elevation wheels, and the external support rods are connected to the rings. The pattern of external rod routing serves to support the ends of the longitudinal beams and to stabilize the elevation rings against relative lateral and rotational motion.

The entire support structure, comprised of transverse, longitudinal and diagonal beams plus external support rods and the elevation rings, provides a stiff, stable, lightweight platform for mounting the reflector panels.

The elevation rings are cradled in four rollers supported by pillars mounted on the azimuth ring, which in turn is supported by wheels mounted atop three support columns. This arrangement provides a broad, stable base for the heliostat. The elevation drive train is carried on the azimuth ring while the azimuth drive is mounted on one of the heliostat support columns. The elevation drive consists of the motor and speed reduction gearing plus a sprocket and fabricated ladder cable. The ladder cable consists of two wire ropes connected by cross members (rungs) swaged in place on a carefully controlled pitch. The drive cable assembly passes under the drive sprocket and around the periphery of one of the elevation rings. A similar pair of cables, but without the cross rungs, passes under an idler sheave and around the other elevation ring. The ends of each cable are fastened to the

elevation rings at a position that will not inhibit necessary elevation assembly movement. Tensioning of the drive and idler cables produces the necessary hold-down restraint to counteract wind forces and obviates elastic cable reaction to elevation movement forces.

The azimuth drive train is identical to the elevation drive except that a shorter ladder cable assembly is required because the azimuth ring has a smaller circumference than the elevation ring. Lift-off protection is provided by catcher hooks mounted on the azimuth ring support columns, which interact with the lower face of the azimuth ring belt track recess.

All structural elements are formed of sheet, strip, or tube steel, press formed or roll formed to the desired configuration. The gussets on the elevation-roller-support pillars will be press formed while the remaining structural component cross sections will be roll formed. These forming processes permit the selection of element designs possessing the stiffness required to support the reflector panel modules while keeping structural weight to a minimum.

The reflector panel structural support components will be roll-formed sections. The transverse beams will be "Z" sections with reentrant beads at the outer edges of the flanges to increase the buckling resistance of these members. The longitudinal beams are rectangular box sections while the diagonal beams and elevation wheel spokes are square box sections. Both the elevation and azimuth rings are rectangular box sections with provisions for belt tracks and, on the azimuth ring, catcher beads formed integrally into the cross section. The basic rectangular sections will be formed into arc sections for elevation and azimuth ring assembly after roll forming.

The heliostat weighs 4430 pounds, or 7.4 pounds per square foot of reflector surface. The breakdown of this weight in terms of the functional entities of the heliostat is given in Table XI.1.

Table IX.1

Westinghouse Heliostat Design Weight

(W) Design (630 ft²)

<u>Support structure</u>	<u>1166 (1.851 lb/ft²)</u>
Azimuth ring assembly (1)	495
Azimuth ring (1)	375
Pillars (4)	120
Elevation ring assembly (2)	671
Elevation rings (2)	586
Spokes (2)	85
<u>Mirror Support Structure</u>	<u>697 (1.106 lb/ft²)</u>
Longitudinal beams (2)	159
Transverse beams (6)	181
Diagonal beams (3)	64
Tie rod system (1)	83
Mirror hats (24 + 8)	210
<u>Mirrors (12 + 4)</u>	<u>2100 (3.33 lb/ft²)</u>
<u>Drive train & miscellaneous</u>	<u>467 (0.741 lb/ft²)</u>
Motors	38
Gearboxes	236
Encoders	18
Belts & cables	70
Pulleys, rollers, mounts	105
Total	4430
Unit weights: Gross	7.03 lb/ft ²
Mirror assembly only:	4.44 lb/ft ²
Foundation: 3 @ 3785 =	11,355 (18.02 lb/ft ²)

Although the present heliostat is designed for a total reflector area of 630 square feet, smaller heliostats can be produced using the same design concepts. If the total reflector area of a smaller heliostat were within approximately 75% (475 to 630 ft²), it would probably be economical to use the same beam sections as employed in the present design in order to preclude tooling costs. For heliostats smaller than approximately 475 ft², different structural components could be attractive from a weight savings viewpoint.

In either event, the basic structure would remain an externally braced beam matrix with in-plane diagonal stiffeners. Support and positioning would continue to be provided by elevation and azimuth rings of a size commensurate with the area and external loading parameters of the heliostat and its installation site.

IX.B. Cost Estimate for Heliostat Manufacture

IX.B.1. BNL Heliostat Cost Estimate (for design see Section III)

The manufacturing cost of the BNL heliostat reflector support and tracking mechanism as defined on BNL drawings D10-M-410-5 was estimated by Westinghouse manufacturing personnel. The estimate was based on large-volume production rates (say 50,000 units per year) and presumed use of jigs and tooling to reduce labor costs.

The estimate utilizes the following basis:

- Raw material pricing.

Current price per pound x single unit quantity x 80% (reduction for mill run purchase approximately 20%). Estimated cost plus outside services (bending and forming) = total materials and services.

- Labor hour estimate.

Fabricating truss members - Quantity of structural supports x 2 hours each =

2 hours estimated breakdown is as follows:

Machinist	20%
Helper	15%
Welder	40%
Material handling	25%

- Additional assembly hours are estimated based on in-house manufacturing and the judgment of the manufacturing engineer.

The above approach resulted in the following costs:

Material	\$ 3086.00
Labor (2142 hr)	<u>49986.00</u>
Total	\$52072.00

protect your cost

The high cost is predominantly the result of the labor intensive nature of the truss structures and complex joints as designed. A lesser, but in our opinion significant, cost penalty accrues from the use of aluminum rather than carbon steel members.

IX.B.2. BNL Design Adapted for Production

We offer for design consideration the following suggestions to achieve substantial cost reductions.

- Utilize standard extruded aluminum shapes rather than a formed channel, this could result in a possible 15% reduction of materials and services; however, we do not consider use of aluminum cost effective.
- Reduce the number of supports by using higher-strength materials (carbon steel). This reduces labor cost in proportion to number removed.
- Redefine the subassembly structures to show smaller subassemblies that will increase the use of fixturing. Simplify the joints within the subassemblies to permit automatic welding.
- Consider adjustable pivots to relax fabrication tolerance requirements.

Our judgment is that exploitation of these modifications would offer major savings as follows:

- Use of carbon steel could eliminate about 60% of the truss members and 33% of the material cost
- Use of simplified joint designs to permit automatic welding could eliminate about 90% of the labor on 80% of the joints

Implementation of these features would result in a cost estimate of

Material	\$2086
Labor	<u>5487</u>
Total	\$7573

Savings from adjustable pivots cannot be estimated without a specific design. Further savings may well be possible, if commercial truss members (i.e., roofing beam structures) or optimum deep-channel roll-form sections were applied to the basic structure. We would recommend investigation of these approaches in any redesign effort.

IX.B.3. Westinghouse Heliostat Cost Estimate

Westinghouse has pursued a heliostat design for the large central power-tower application described in Section IX.A. For several months attention has been centered on this design to achieve low manufacturing costs. As a result, a design to carry 638 ft² of reflective glass has been cost reduced to an installed cost estimate of about \$3300.00 without the mirror panels.

The cost estimates are based on a fifth-year level of 50,000 heliostat units per year with labor extended on experience curves to the tenth year. The fifth year was assumed to be the first year to obtain the 50,000 level, allowing time to design, plan, procure, install, and debug the manufacturing equipment and processes. The tenth year represents a cumulative production of 400,000 units with the main factory on a 90 percent experience curve and each site factory on an 80 percent curve.

Outside suppliers were used to produce as many items as possible, thus maintaining a minimal level of plant/machine tool facilities. This approach should insure adequate production capabilities even at higher production levels. The heavy use of roll-form shapes is typical for this type of planning.

Labor cost rates were taken from DOE report SAN-1108-8 which is based on low side national average; G&A represents AESD factors.

Material costs were obtained from quotations, catalog listings of similar items, and material indices from Iron Age, Oct. 30, 1978, issue. It is assumed that material handlers and production clerks are part of overhead expense and are not factored as direct labor.

Labor hours were established by Manufacturing Engineering estimates. The cost analysis reflects the use of standard, developed, high production systems with modern methods employed for material handling.

Understandably, the unit cost will be higher during a production buildup period, considering the disadvantages of reduced-volume purchasing, increased machine setup and tear-down frequency, and nonoptimized material-handling techniques. It is estimated that the heliostat unit cost might be approximately 25 percent higher at a production rate of 25,000 units/year compared to 50,000 units/year. Similarly, the unit cost would decrease further as the rate increases over 50,000 units/year, although the decrease would not be as dramatic.

The unit area cost of this heliostat is $\$5.17/\text{ft}^2$ without the reflecting panels. BNL has estimated the production cost for the light weight panels shown in Figure 9 to be $\$1.25/\text{ft}^2$. This estimate is based on material cost using production tooling to minimize labor content. We have assumed that all tooling costs have been written off on prior sales. Thus the total heliostat purchase price is $\$6.42/\text{ft}^2$.

SECTION X
SYSTEM COST AND PAYBACK

The economic value of a small power-tower-type solar energy collector is dependent on many factors. However, the system cost, solar insolation and cost of competing fuel are the dominant parameters.

The application analyzed by Brookhaven is limited to the building heating and cooling loads found in the Northeastern stream technology area of the United States although other applications exist.

The system cost is dominated by the heliostat cost. The Westinghouse Advanced Energy System Division working under a subcontract from Brookhaven has conducted a production cost estimate of the heliostat and this work is summarized in Section IX. The best production design was found to cost \$6.42/ft² of reflector surface. This unit-area cost will be used in the system cost analysis which is summarized in Table X.1.

Table X.1
Power-Tower System Costs

Heliostats	\$70,972
Boiler	12,000
Tower	15,000
Controls	1,500
Installation - checkout	<u>7,500</u>
	\$106,972

When used as an energy supplement, this system is expected to displace 20,354 gallons of fuel oil when deployed in the Northeast where the mean annual incident input is 3.36×10^5 Btu/ft². The details of this determination are shown in Table X.2.

Table X.2
Fuel Displacement

Collector area	11,055 ft ²
Solar input per year	3.36 x 10 ⁵ Btu/ft ²
System efficiency boiler losses, reflectivity	70%
Geometry factor shadowing, optics, cosine 0	76.3%
Energy yield (1 gal #6 oil burned at 75% eff.)	2.24 x 10 ⁹ Btu
Annual fuel savings	20,354 gal

The economic relationship between the invested sum and the operating saving is user dependent. Two balance sheets have been prepared and are shown in Tables X.3 and X.4. One balance sheet is for a tax exempt user such as a school, hospital, municipal, or other nonprofit institution, and the second for a profit-making user in the 50% tax bracket. It is interesting to note that a shorter payback period exists in the 50% tax case because of allowable write-off for capital investment.

This analysis is based on the assumption that the first commercial system will be installed in 1985. This allows time for further development and field testing of this solar energy collection system before its introduction into a competitive energy market. Using a 7% inflation rate the system cost in 1985 will become \$160,500. The balance sheet analysis will be based on this cost.

Table X.3

Balance Sheet - Tax Exempt

	Price of oil #6, \$/gal	Fuel savings, \$ (20,354 gal)	\$160,500 Amortized 8%-12 yr, \$	Maintenance 7% inflation, \$	Net savings per year, \$	Gross savings, \$
1979	0.60	-	-	-	-	-
1985	0.95*	19,379	20,852	2,000	-3,473	-3,473
1986	1.02	20,930	↓	2,140	-2,062	-5,535
1987	1.11	22,604		2,290	- 538	-6,073
1988	1.20	24,412		2,450	+1,110	-4,963
1989	1.30	26,366		2,622	2,892	-2,073
1990	1.40	28,477		2,805	4,820	+2,749
1991	1.51	30,753		3,001	6,900	9,649
1992	1.63	33,213		3,211	9,150	18,799
1993	1.76	35,870		3,436	11,582	30,381
1994	1.90	38,740		3,677	14,211	44,592
1995	2.06	41,839		3,934	17,053	61,645
1996	2.22	45,186	20,852	4,210	20,124	81,769
1997	2.40	48,801	0	4,504	44,297	126,066
1998	2.59	52,705	0	4,820	47,885	173,951
1999	2.80	56,921	0	5,157	51,764	225,715
2000	3.02	61,475	0	5,518	55,957	281,672

*Assumed 8% increase per year.

Table X.4

Balance Sheet - 50% Tax Bracket

	Price of oil, #6 \$/gal	Fuel cost savings after tax credit, \$ (20,354 gal)	\$160,500 Amortized 8%-8 yr, \$	Return from interest credit, \$	Return from capitol write-off, \$	Maint. cost after tax, credit, \$	Net savings per year	Gross savings, \$
1979	0.60	-	-	-	-	-	-	-
1985	0.95*	9,690	27,223	6,120	10,031	1,000	- 2,382	- 2,382
1986	1.03	10,465	↓	5,532	↓	1,070	- 2,265	- 4,647
1987	1.11	11,302	↓	4,819	↓	1,145	- 2,216	- 6,863
1988	1.20	12,206	↓	4,087	↓	1,225	- 2,124	- 8,987
1989	1.30	13,183	↓	3,293	↓	1,311	- 2,027	-11,014
1990	1.40	14,239	↓	2,435	↓	1,402	- 1,920	-12,934
1991	1.51	15,377	↓	1,502	↓	1,500	- 1,813	-14,747
1992	1.63	16,607	27,223	493	10,031	1,605	- 1,697	-16,444
1993	1.76	17,935	0	0	0	1,718	+16,217	- 227
1994	1.90	19,370	↓	↓	↓	1,838	17,652	+17,425
1995	2.06	20,920	↓	↓	↓	1,967	18,953	36,378
1996	2.22	22,593	↓	↓	↓	2,105	20,486	56,864
1997	2.40	24,401	↓	↓	↓	2,252	22,145	79,009
1998	2.59	26,353	↓	↓	↓	2,410	23,943	102,952
1999	2.80	28,460	↓	↓	↓	2,578	25,882	128,834
2000	3.02	30,738	0	0	0	2,759	27,979	156,813

*Assumed 8% increase per year.

SECTION XI
CONCLUSIONS AND RECOMMENDATIONS

XI.A. Conclusions

XI.A.1. Wind-Avoidance Design

Solar energy, in general, is received during hours of low wind velocity. Therefore, a heliostat design to operate in a wind-avoidance mode is viable and confirmed by analysis (see Section VI for details).

This fold-down wind avoidance concept results in a lightweight heliostat design. The present first-generation prototype heliostat has a weight-to-area ratio of 6.5 lb/ft². This was a conservative design and considerable weight reduction is obtainable through an iterative design process. The design effort was insufficient to drive to lowest cost (see recommendations item 1).

XI.A.2. Normal Incident Solar Insolation

The quantity of normal incident solar insolation was measured at Upton, NY for 13 months and an improved method of estimating this normal incident insolation generated. The resulting yearly sums of normal incident insolation for the Northeastern steam-powered space-conditioning region were disappointingly low (see Section VII). These low insolation values adversely affected the economic analysis and resulted in a longer than desired payback period.

XI.A.3. Reflecting Film Development

The Brookhaven-Dunmore cooperative search for acceptable reflecting plastic film was not successful in that it failed to identify a better reflecting film than the standard Dunmore product 393. Neither reflectivity nor life was improved over those of the 393 product which are 84% and 6.3 years, respectively.

XI.A.4. Reflecting Film Support Package

A large fraction of the development effort was devoted to developing a reflecting film support system which is inexpensive to manufacturer, has good weatherability, and preserves good specularly. All of these objectives were

achieved and two satisfactory structures developed. These are shown in Figures 10 and 11. The design shown in Figure 10 has the poorer specularly, but it is acceptable and will be the least expensive to manufacture.

XI.A.5. Small Power-Tower Concept

The small power-tower solar energy collecting concept was studied in great detail and found to be technically viable with an economic potential. The space-conditioning market in the Northeastern part of the U.S. appears to represent a viable market although other interesting applications exist. A further reduction in the heliostat production cost is necessary to meet competition from fossil fuels in the identified market. A recommendation addressing this need is given in item 1.

The power-tower configuration is more cost effective than other system configurations because the freedom of the two axis motion systems allows more energy to be collected per unit area of reflector and the stationary energy receiver reduces energy collection losses. This configuration should ultimately dominate the solar energy market once the hard facts of economics become clear.

XI.A.6. The lifting of a 6-inch snow load is a serious design consideration and should be reexamined.

XI.B. Recommendations

XI.B.1. Heliostat Cost Reduction

Because of the short time schedule of this development, the planned iteration in the heliostat design was cancelled. As a result, only the first heliostat prototype was built. This design was of necessity conservative and at least one design iteration is required to reduce its weight and cost.

A two-year design effort using modern 3-dimensional computer stress analyzing techniques should result in a major reduction in weight and production cost. The interaction with snow should be carefully studied. This action is strongly recommended.

A carefully planned cost-reduction program with adequate time for good engineering will result in the development of a heliostat that is price competitive with other energy sources in the market.

XI.B.2. Plastic Film Development

In spite of the disappointing results of the Brookhaven-Dunmore reflecting film development program (see conclusions, item 3), the need to develop an inexpensive, nonfragile, flexible reflecting surface still exists. This necessity should eventually force a solution to the problem and our failure does not mean that no solution exists. Efforts to develop a plastic reflecting surface should continue.

SECTION XII
PROJECT PERSONNEL

During this two-year development many people contributed services, some for short periods of time, others for longer.

Mr. Peter A. Montemurro, serving as project coordinator, was invaluable. Through his diligent and industrious efforts, the diverse tasks of this program were collectively brought to successful conclusions.

I would also like to make special note of the aid and encouragement received from the late Dr. George Kenneth Green in the concept and planning phase of this program. His wisdom and invaluable insight were critical to this and many other activities at Brookhaven. Brookhaven lost a cherished leader in his passing.

The following is a listing of those people who worked hard and faithfully to make this solar energy collecting concept successful and whose services were greatly appreciated. Brookhaven wishes to take this opportunity to thank each and every one.

<u>Name</u>	<u>Function</u>	<u>Comment</u>
Michael Acker	Mechanical Technician	Heliostat Laboratory
Bob Brown	Meteorologist	Part time, Insolation Measurement
Larry Bruno	Mechanical Design	Heliostat Design
Joe Considine	Mechanical Technician	Reflector Fabrication
J. G. Cottingham	Principal Investigator	
Felix Cruz	Mechanical Design	Heliostat Design
Brendon DeMilt	Engineering Writer	Gross Summary Report
Frank DiCresco	Electronic Technician	Heliostat Laboratory
Ted Faust	Electrical Technician	Testing
G. Kenneth Green	Physicist	Concept Generation
David E. Gumm	Machinist	Structure Fabrication
Jim Long	Mechanical Design	Heliostat Design
Edgar McKenna	Technical Specialist	Laboratory Foreman
Peter A. Montemurro	Engineer	Reflector Surface

<u>Name</u>	<u>Function</u>	<u>Comment</u>
Harry C. Moore	Student Engineer	Heliostat Laboratory
Michael Peragine	Mechanical Design	Heliostat Design
John Reany	Mechanical Technician	Heliostat Laboratory
Bob Roosa	Mechanical Technician	Reflector Fabrication
Ronald Segal	Student Engineer	Heliostat Laboratory
Robert Scheverer	Mechanical Technician	Heliostat Laboratory
Kevin Scoles	Reflectivity Measurements	Summer student
S. Sethuraman	Meteorologist	Part time, Wind Analysis
Kathryn Szabat	Mathematics	Summer employee
Joyce Tichler	Meteorologist, Programmer	Part time, Data Analysis
Bill Wilhelm	Electrical Engineer	Part time, Instru- mentation and Test

★ U.S. GOVERNMENT PRINTING OFFICE: 1979-614-036/37